1-1-2002

Particle speed distribution in an electrostatic suspension

Chad Evertt Eimers
Iowa State University

Particle speed distribution in an electrostatic suspension

by

Chad Evertt Eimers

A thesis submitted to the graduate faculty

in partial fulfillment of the requirements for the degree of

MASTER OF SCIENCE

Major: Mechanical Engineering

Program of Study Committee:
Gerald Colver, Major Professor
Ron Nelson
Balaji Narasimhan

Iowa State University

Ames, Iowa

2002

Graduate College
Iowa State University

This is to certify that the master's thesis of

Chad Evertt Eimers

has met the thesis requirements of Iowa State University

Signatures have been redacted for privacy

_____

_____

TABLE OF CONTENTS

LIST OF FIGURES

LIST OF TABLES

ABSTRACT

Particle speed distribution in an electrostatic particulate suspension (EPS) has been measured by suspending and leaking copper and aluminum particles (63-149 μm) from a small hole from the top plate of a parallel plate test section. Different speed ranges were determined by capturing particles on epoxy-coated glass slides located at different heights above the test section. Assumed Maxwell speed distribution curves, by two different approaches, were fit to the data. Experimental values of particle speed (average, most probable, rms) were compared to theoretical speed of a single particle. Calculations based on experiment were used to determine the particle number density of the suspension. Three methods were used to verify particle number density: laser beam intensity, count (weight), and particle mass flux. Values between the three methods appear to be in agreement, within experimental error. Experimental values of particle flow rate were compared to theoretical values. Recommendations are suggested for further study.

1. INTRODUCTION

1.1 Background

An electrostatic particulate suspension (EPS) is a method used to lift small particles against gravity using a dc high voltage electric field (~ kV/cm) applied between parallel-plate metal electrodes. The resulting suspension is both uniform and steady-state. The suspension is maintained by charging and discharging of individual particles during contact with the parallel electrodes. The uniformity of the suspension is maintained by the dynamic state wherein collision processes produce random motion, similar to that of molecules, by colliding with both the plates and each other. Different methods for measuring particle concentration in a suspension include the following: scanning the suspension by laser beam attenuation [1-4], current density measurement [5], and by count (weight) of particles [2]. The EPS method has been used to study in various applications including heat transfer [6, 7], particle dynamic processes (diffusion and charge transfer) [4, 8], and combustion [1, 6].

1.2 Present Study

A current study is being conducted using the EPS method for evaluating quenching effects of powders in microgravity. The EPS may be a benchmark for design of quenching flames which could create a new fire safety standard [9] for the National Aeronautics and Space Administration (NASA). This study is a contribution to the dynamic state of particle in an electrostatic suspension in normal gravity (1-g) for combustion modeling.

The present study is an investigation of the dynamic nature of the particles and their speed distribution in an EPS. This phenomenon was first investigated by Colver and Ehlinger [2]. The present study extends their experiment and provides additional analysis of the nature of a two-dimensional speed distribution. Particles are contained by cylindrical

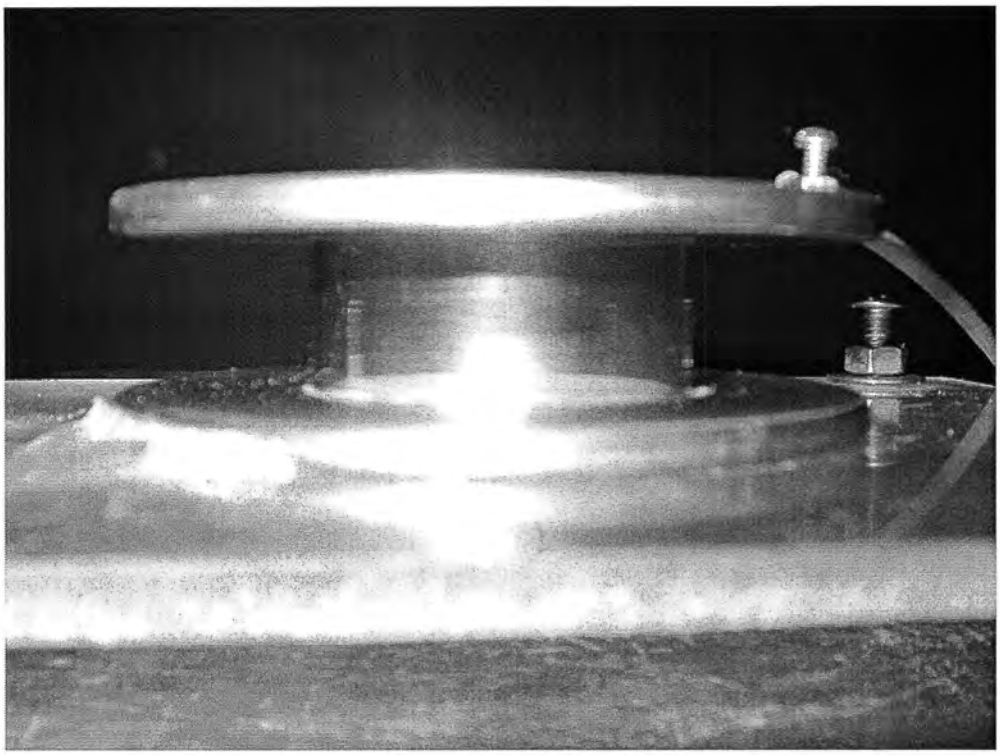

Figure 1.1. Two metal electrodes (brass) separated by a 2-cm Pyrex cylinder. The bottom electrode is connected to a high voltage power supply. The top connected to a ground source.

Pyrex glass and parallel electrodes in a closed system as shown in Figure 1.1. Using the EPS method, particles are then leaked from a small hole in the top plate electrodes and captured above the test section on glass sides containing an epoxy resin. This coating is formulated to remain tacky over time periods necessary to sample 5-7 slides. The following variables were investigated: (1) particle species (copper, glass, and aluminum), (2) particle size (20μm-149μm), (3) electric field strength (7-14 kV/cm), and (4) test section height (1-2cm). Results from Colver and Ehlinger [2] give reason to suggest particle speed behavior is governed by the Maxwell speed distribution of gaseous molecules.

Suspended particles contain both x- and y-components of velocity. With the vertical and horizontal displacements of particles recorded on glass slides, the equations of motion (of a single particle) can be employed to back calculate the initial velocity of a particle leaving the sampling hole. This gives a direct indication of the speed of the oscillating particles inside the test section. An analysis of all the captured particles gives the desired particle speed distribution.

In the present study the particle speed distribution of copper and aluminum particles in an EPS is measured and fit to an assumed Maxwellian in the direction of the applied electric field. The off-axis distribution is also measured and discussed. Stratification effects in the particulate cloud itself are expected due to gravity. Recommendations and an error analysis are discussed.

2. LITERATURE REVIEW

2.1 Electrostatic Particulate Suspension

Colver [10] characterized the electrostatic particulate suspension (EPS) method as a cloud containing charged particles, which is formed or sustained with an applied electric field as a direct result of field induced charging at an interface. He studied dynamic and stationary charging of metallic and dielectric particles charged by contact with a parallel-plate capacitor from an externally applied dc field [10]. He suggested particles are charged as a result of the "capacitance" effect of the particles themselves when in electrostatic contact with the wall. While in contact, the particle becomes part of a larger capacitor, the wall, and is charged to the same sign and potential. For a large enough dc electric field, charged particles are lifted against the force of gravity. Particles tend to oscillate as a result of impact, discharging, and recharging at the particle-wall interface. The applied electric field (in the absence of contact effects) is entirely responsible for the lifting force on a particle since it alone specifies the field strength E and also controls the amount of charge Q accumulated on the particle.

2.2 Single Particle Theory

The magnitude of the charge on a sphere is in contact with a infinite flat plate in the presence of a uniform electric field is the Maxwell [12] charge

$$Q = \pi \varepsilon_0 d^2 E K \tag{2.2.1}$$

where ε_0 is the permittivity of free space, d is the particle diameter, and E is the apparent electric field strength. Colver experimentally gives K = 1.64 for copper spheres [10]. The natural independent variable controlling the motion is the externally applied electric field. If the electric field is unchanged in sign, a force of the type

$$F_E = QE \tag{2.2.2}$$

will tend to drive the particle away from the wall against attracting particle forces of the kind

$$F_q = \frac{Q^2}{4\pi\varepsilon_0 S^2} \tag{2.2.3}$$

and opposed by a viscous air drag force

$$F_D = \frac{\pi\rho d^2 v^2}{8} C_D \tag{2.2.4}$$

where S is the particle separation distance from the surface, C_D is the drag coefficient, and d and v are the particle diameter and velocity, respectively. The theoretical equilibrium force required to lift a single sphere from a plane in a uniform electric field was expressed by Lebedev and Skal'skaya [13] as

$$F_E = \pi\varepsilon_0 d^2 E^2 (1.37). \tag{2.2.5}$$

A particle confined between two oppositely charged parallel plates of and possessing sufficiently large charge (once set in motion) will continue in a cyclic motion, oscillating between the parallel walls, resulting from impact, discharging and recharging with each wall in the presence of a dc electric field. Body forces such as gravity, inelastic collisions with the walls, and viscous air drag limit the maximum velocity of the particle. Particle-wall-gas properties, which affect the dynamic discharging process, such as surface conductivity, dielectric constant, relative humidity, and geometry will limit maximum charge transfer to the particle. Figure 2.1 shows the driving forces on a single particle in an electric field.

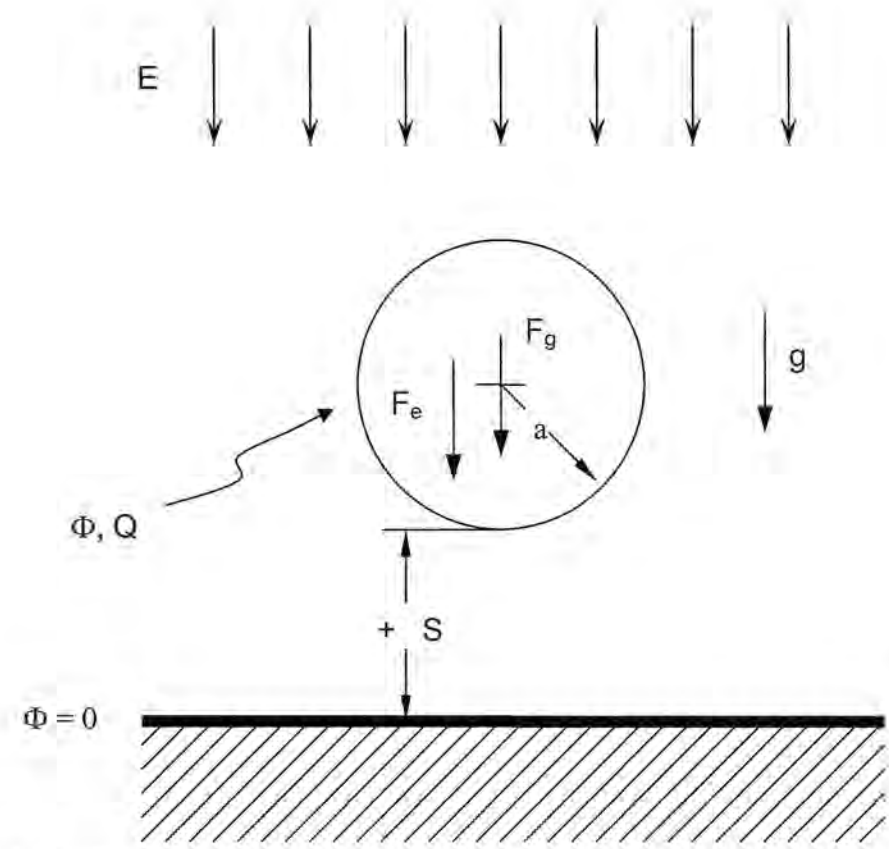

Figure 2.1. A single particle of charge Q of radius a in the presence of an applied electric field E, gravity g, and separation distance S from an infinite conducting wall at ground potential $\Phi = 0$.

The motion of oscillating particles can be determined from the differential equation of particle motion under the influence of an electric field (E), charge (Q), gravity (g), particle viscous drag (v/τ), and image charge force (F_q), is given by

$$\frac{dv}{dt} = \frac{QE}{m} - \left(\frac{v}{\tau} \pm g + \frac{F_q}{m}\right) \tag{2.2.6}$$

where the intertia-viscous drag relaxation time τ is given by

$$\tau = \left(\frac{m}{3\pi\mu d}\right)\left(\left(1 + \frac{3Re_d}{16}\right)^{-\frac{1}{2}}\right) \tag{2.2.7}$$

where m is the particle mass, and Re is the particle Reynolds number based on diameter ($Re_d = \rho vd/\mu$); ρ and μ are the air density and viscosity, respectively, at room temperature. Equation 2.2.7 characterizes the modified Stokes drag for a sphere through a fluid. The drag coefficient, C_D, for modified Stokes drag becomes

$$C_D = \frac{24}{Re}\left(1 + \frac{3Re}{16}\right)^{\frac{1}{2}} \tag{2.2.8}$$

and the viscous drag force in Equation 2.2.5

$$F_d = 3\pi\mu dv\left(1 + \frac{3Re}{16}\right)^{\frac{1}{2}} \tag{2.2.9}$$

This is valid for particle Reynolds numbers up to 100 [14].

Colver and Cotroneo [5] derived the average speed of a single particle oscillating between parallel plates, given by

$$\bar{v}_s = \left[\frac{L}{8\left(1 - e_t^2 e_b^2\right)}\right]^{\frac{1}{2}} \left\{ \begin{array}{l} \left[(1 + e_t^2)\left(\frac{QE}{m}\right) + (1-e_t^2)g\right]^{\frac{1}{2}} (1 + e_b) + \\ \left[(1 + e_b^2)\left(\frac{QE}{m}\right) - (1-e_b^2)g\right]^{\frac{1}{2}} (1 + e_t) \end{array} \right\} \tag{2.2.10}$$

where L is the plate separation, and e_t, e_b are the coefficients of restitution of the particle collision of the top and bottom walls, respectively. Image charge forces were negligible compared to charge, gravity, and viscous drag. Viscous effects can be accounted for by substituting $QE-F_d$ for QE in Equation 2.2.10.

Colver and Ehlinger [2] determined the maximum speed of particles by considering a particle traveling through an inviscid fluid (again neglecting image charge forces) and equating the kinetic energy of the particle to the work done on the particle from the electric field, given by

$$v_{max} = \sqrt{\frac{2QEL}{m}} \tag{2.2.11}$$

When a particle is in contact with the upper plate, its velocity is zero. A lower limiting condition of the electrostatic force, QE (from Equation 2.2.3), below which particle motion cannot be sustained is obtained from Equation 2.2.8, that is

$$QE_{L.L.} = \frac{1 - e_b^2}{1 + e_b^2} mg\,. \tag{2.2.12}$$

Combining Equations 2.2.1 and 2.2.12, the limiting electric field strength and average velocity for a given electric field are given respectively by

$$E_{L.L.} = \left[\left(\frac{1 - e_b^2}{1 + e_b^2}\right)\left(\frac{mgE}{Q}\right)\right]^{\frac{1}{2}} \tag{2.2.13}$$

$$\bar{v}_{L.L.} = \left[\left(\frac{gL}{4}\right)\frac{(1+e_b)^2}{(1+e_b^2)}\right]^{\frac{1}{2}} \qquad (2.2.14)$$

Assuming that particle motion is one-dimensional in either the upward or downward direction, the particle number flux, i.e. in the direction of the applied electric field, J_n, is given by

$$J_n = \frac{n\bar{v}}{2} \qquad (2.2.15)$$

where n is the particle number density and $\bar{v}$ is the average particle velocity.

Single particle theory can be considered a representation only of the dynamics of the electrostatic suspension. It is only an approximation in predicting multiple particle dynamics resulting from particle-particle collisions and other effects such as irregularities in particle shape, and charge distribution on the particles.

2.3 Multiple Particle Theory

Particle-particle collisions form two important effects: to reduce velocities and absolute charge. From Equation 2.2.10, it is evident that average particle velocity decreases with decreased charge. Generally, the effect of random collisions is to decrease velocity compared to a single particle with no collisions.

Colver and Howell [4] studied the diffusion process in an electrostatic suspension. They electrostatically suspended copper particles against gravity and diffused them horizontally in a rectangular duct. Particle number densities were experimentally measured by three independent methods: (1) electrical current density, (2) laser beam attenuation, (3) and by count (weight measurement). They showed in an electrostatic suspension the diffusion

process is significant and can be isolated particles in the absence of fluid dynamic driving forces.

Diffusion of copper particles in the ranges of 74-81 μm and 125-147 μm was observed under the influence of an electrostatic suspension. The self diffusion coefficient is given by

$$D = \frac{-\text{number flux}}{dn/dx} \tag{2.3.1}$$

where the number flux is number of particles per square meter (of duct) per second, and dn/dx is the change in number density (number of particles per cubic meter) measured along the duct (position x). Experimental data suggested that the self-diffusion coefficient increases with increasing electric field strength or with decreasing particle size (other variables held constant).

Moreover, since diffusion is a randomization of motion, Colver and Howell [4] hypothesized that the origin of diffusion due to electrostatic suspension is a result of one or more of the following processes: (1) gradients in the electric field strength along the duct as a consequence of spatial variations in net charge concentration, (2) random motion due to particle-particle collisions and particle-wall collisions. They also noted that since diffusion coefficients are independent of concentration, particle-wall collisions are significant. Quantitatively, Colver and Howell [4] experimentally determined that the diffusion force,

$$F_{diff} = mD^2\left(\frac{\Delta n}{n\Delta x}\right)^3 \tag{2.3.2}$$

to be $\sim 10^{-11}$ Newtons per particle. This force is a result of particle concentration and is negligibly small compared to gravity and viscous drag forces.

For a uniformly distributed suspension of non-interacting particles between parallel-plate electrodes, the vertical direction current density J is given by

$$J = nQ\bar{v} \tag{2.3.3}$$

Colver and Cotroneo [5] derived a more realistic expression accounting for collision phenomena as

$$J = fnQ\bar{v}\left[e^{-n\sigma L} + \gamma\left(1 - e^{-n\sigma L}\right)\right] \tag{2.3.4}$$

$$\approx nQ\bar{v}e^{-n\sigma L} \tag{2.3.5}$$

where the parameter, f (<1), accounts for the irregular particle bounces (e.g., due to rotation of particles) at the wall, and σ is the particle cross-sectional area (πd^2). The first exponential term is the probability of a particle traversing a distance L without collision, and the second term represents the remaining fraction of particles traversing over L with a collision.

2.4 Particle Speed Distribution

Colver and Ehlinger [2] measured particle speed distribution in an electrostatic suspension by leaking spherical copper particles (44-53 μm, 63-75 μm, and 105-125 μm) from a small sampling hole on the top parallel-plate electrode. Particles were acquired on epoxy-coated glass slides located at various heights above the sampling hole. The sampling hole was chosen large enough to allow particles to pass but small enough to create a minimal disturbance in the electrostatic suspension. This leads to

$$\lambda \gg d_{hole} \gg d \tag{2.4.1}$$

where λ is the particle mean-free path, d_{hole} is the leak hole diameter, and d is the particle diameter. The particle mean-free path was estimated from gas kinetic theory (adjusted to one-dimensional electrostatic suspension theory) and given by

$$\lambda = \frac{1}{\sigma n} \tag{2.4.2}$$

where σ is the particle collision cross section (πd^2), and n is the particle number density (10^3-$10^4/cm^3$). Typical numerical values for particle-particle mean-free path for a 115-μm copper particle were λ = 0.9 cm, d_{hole} = 0.161 cm, and d = 0.0115 cm. This gives a ratio λ:d_{hole}:d = 78:14:1.

Particle mean speed $\bar{v}$ and root mean square (rms) speed v_{rms} were defined as

$$\bar{v^m} = \frac{1}{n}\int_0^\infty v^m \left(\frac{dn_v}{dv}\right) dv \tag{2.4.3}$$

where m=1 for mean speed and m=2 for rms speed. The rms speed was calculated as $v_{rms} = (\bar{v}^2)^{1/2}$. These values apply to the distribution speed. The mean speed $\bar{v}$ was used to calculated particle number density based on particle mass flux.

Using the equation of motion for a vertically decelerating particle (similar to Equation 2.2.6), a particle's initial velocity, i.e. a particle's velocity as it left the sampling hole, could be determined as a function the particle's height, expressed by

$$\frac{dv}{dt} = -\left(\frac{v}{\tau} + g + \frac{F_q}{m}\right). \tag{2.4.4}$$

Figure 2.2 shows numerical solutions for maximum height attained by particles with initial speed v(t=0). Only one-dimensional particle motion was studied due to the relatively strong force due to electric field compared to diffusion force [4]. Particle number density was

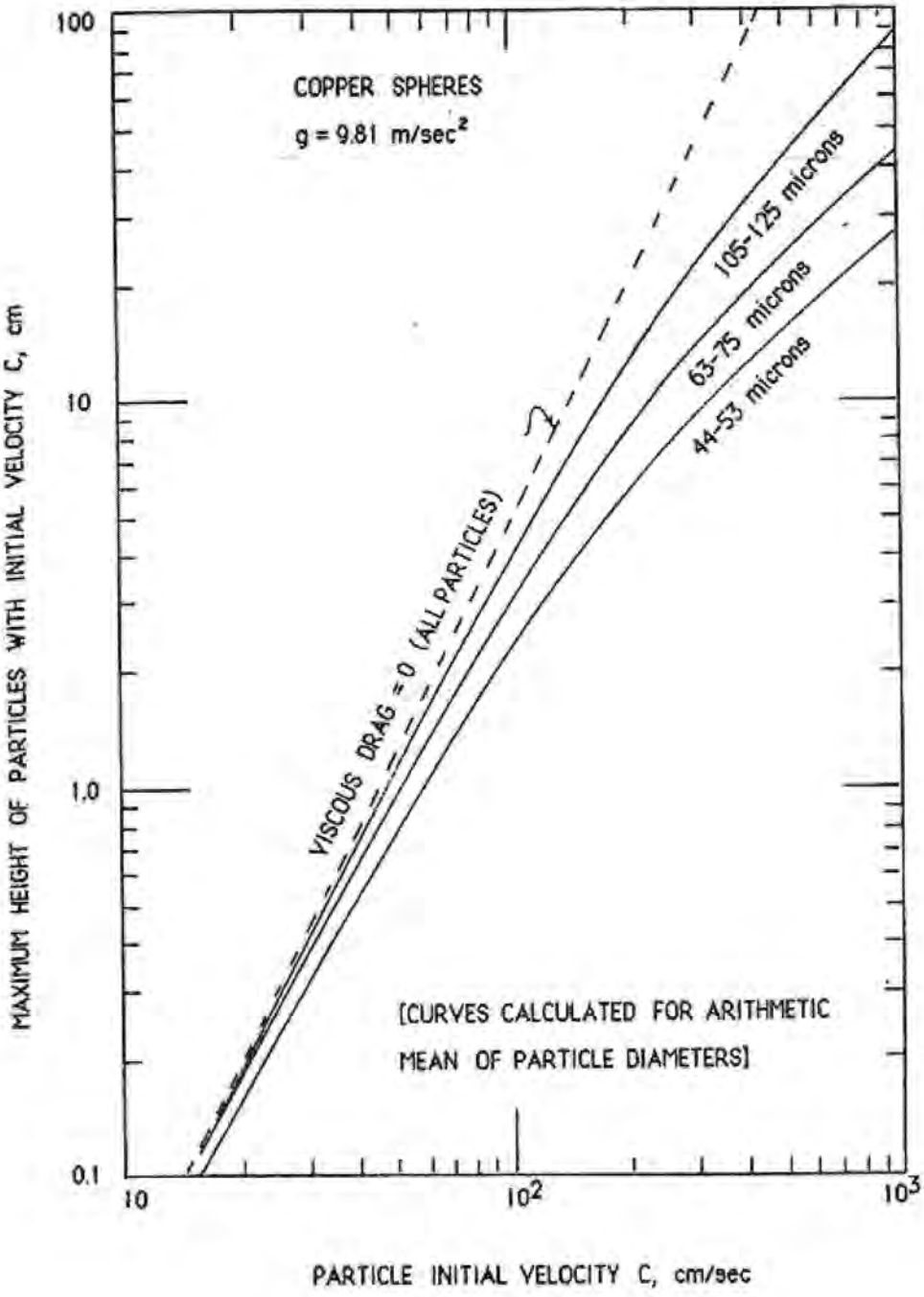

Figure 2.2. Numerical solutions for maximum height h attained by particles with initial speed C(t=0)*, including viscous drag, gravity, and image charge force attraction (always negligible.

*C was used as the variable for speed by Colver and Ehlinger [2].

verified experimentally by laser beam attenuation. Curve-fitting experimental data suggested a Maxwell speed distribution for gaseous molecules applies to particle motion in the direction of the applied electric field.

The Maxwell speed distribution for particles is given by

$$\frac{dn_v}{dv} = \frac{4n}{v_0\sqrt{\pi}}\left(\frac{v}{v_0}\right)^2 e^{-\left(\frac{v}{v_0}\right)^2} \tag{2.4.5}$$

where dn_v is the number density of particles in the speed range v to v + dv, and v_0 is the most probable speed (determined experimentally). The most probable speed is substituted into the Maxwell speed distribution for $(2kt/m)^{1/2}$, the random motion of molecules in kinetic theory related to temperature [15,16]. Equation 2.4.4 was normalized to the particle number density of the suspension by

$$n = \int_{\text{all } v} dn_v = \int_0^\infty \left(\frac{dn_v}{dv}\right) dv\,. \tag{2.4.6}$$

The number of particles N exiting the sample hole per unit time (flow rate) was calculated by multiplying A_e, the area of the sampling hole by Equation 2.2.15, expressed as

$$\frac{dN}{dt} = A_e J_n = \frac{A_e n \bar{v}}{2} \tag{2.4.7}$$

where A_e is the area of the sampling hole, J_n is the particle number flux, n is the particle number density, and $\bar{v}$ is the distribution mean speed. Experimental data was compared to an assumed Maxwell-type speed distribution by adjusting the most probable speed, v_0.

Using Equations 2.2.15 and 2.4.5, the fraction of total particles leaving the leak hole which reach a height h on a glass slide is given by

$$\frac{N}{N_0} = \frac{J_n(v \to \infty)}{J_n(0 \to \infty)} = \frac{\int_v^\infty v(dn_v/dv)dv}{\int_0^\infty v(dn_v/dv)dv} \tag{2.4.8}$$

$$= \left[(v/v_0)^2 + 1\right] e^{\left[-\left(\frac{v}{v_0}\right)^2\right]} \tag{2.4.9}$$

where N is the number of particles reach height h, N_0 is the total number of particles (sum of all particles collected on glass slides), dn_v/dv is the Maxwell speed distribution for particles, and v_0 is the most probable speed.

An independent test using laser beam attenuation theory verified the number density of the suspension. A laser beam was directed through the test section and could be seen in the test section, as the suspended particles attenuate the laser. A laser power meter was placed at the opposite end of the laser to record the initial laser intensity I_0 and the intensity of the attenuated beam, I. The Lambert-Beer [17] law associates the laser intensity ratio with number density, given by

$$I = I_0 e^{(-nzA_p\varepsilon)} \tag{2.4.10}$$

where I is the attenuated laser beam intensity due to suspension, n is the number density, z is the path length the laser travels within the test section, A_p is the projected area of the particle ($\pi d^2/4$), and ε is the extinction coefficient. For particles larger than 35 μm, the Mie theory [17] predicts the extinction coefficient becomes stable at $\varepsilon = 2.0$.

3. EXPERIMENTAL SETUP

3.1 Overall Experimental Setup

The apparatus used for experimentation was a modification of that used by Colver and Ehlinger [2]. Figures 3.1a and 3.1b show the apparatus and all measurement devices, respectively. Figure 3.2 shows a circuit diagram for the system. A rectangular section of acrylic (32 cm X 32 cm) provided the base. Another acrylic section platform (23 cm X 17 cm) with three threaded bolts provided a triangle stand used to adjust the platform to ensure the test section was level. Two nuts on each bolt, below and above the platform, secured the platform once it was leveled. The test section was placed on the platform and could be leveled with the platform to ensure that a uniform suspension was produced with respect to the gravitational field. A three-sided acrylic rack placed above the test section consisted of several rectangular steel inserts spaced approximately 0.65 cm apart from each other on two opposite sides of the rack to hold square glass slides (5.08 cm to a side). The rack could be positioned in the vertical direction above the test section and leveled by two bubble levels placed at right angles. The rack could hold up to 25 glass slides.

The (negative) high voltage potential power supply (Hipotronics HV DC) was attached to the bottom plate of the parallel-plate system. The upper plate was connected to an electrometer (Keithley Instruments 602) and then connected to a ground source. A voltmeter (Keithley 175 Autoranging Multimeter) was used to record voltage across the test section. A laser (Metrologic Neon Laser 617J-1106) was placed to one side of the apparatus (see Figure 3.1b) and a laser power meter (Metrologic 45-540) was placed opposite of the laser such that

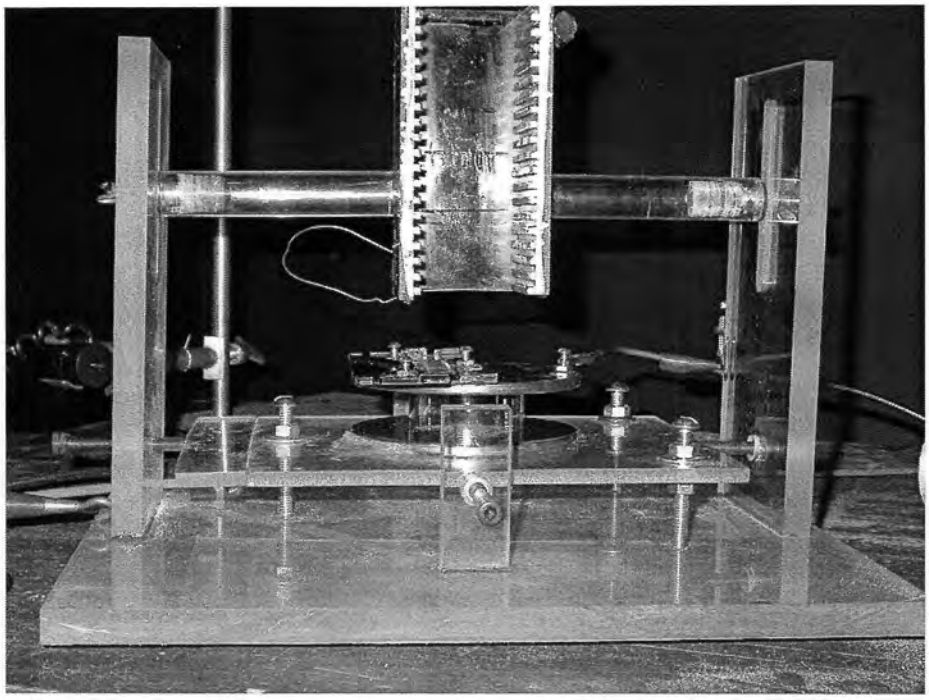

Figure 3.1a

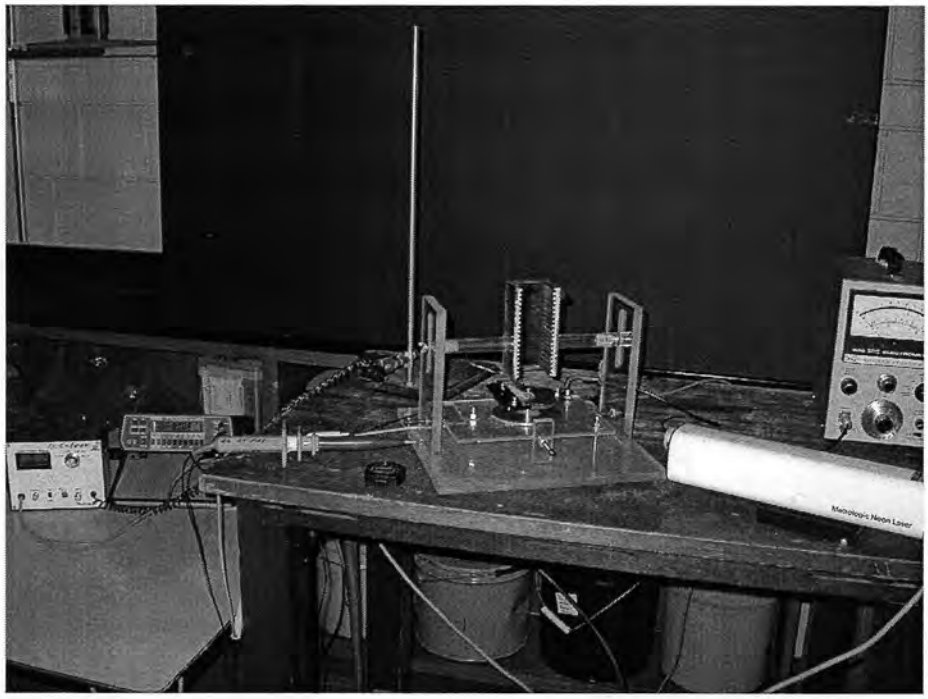

Figure 3.1b

Figure 3.1. (a) The EPS test section inside the acrylic apparatus. (b) Apparatus and all testing devices from left to right: laser power meter, voltmeter, apparatus, laser, and electrometer (behind laser).

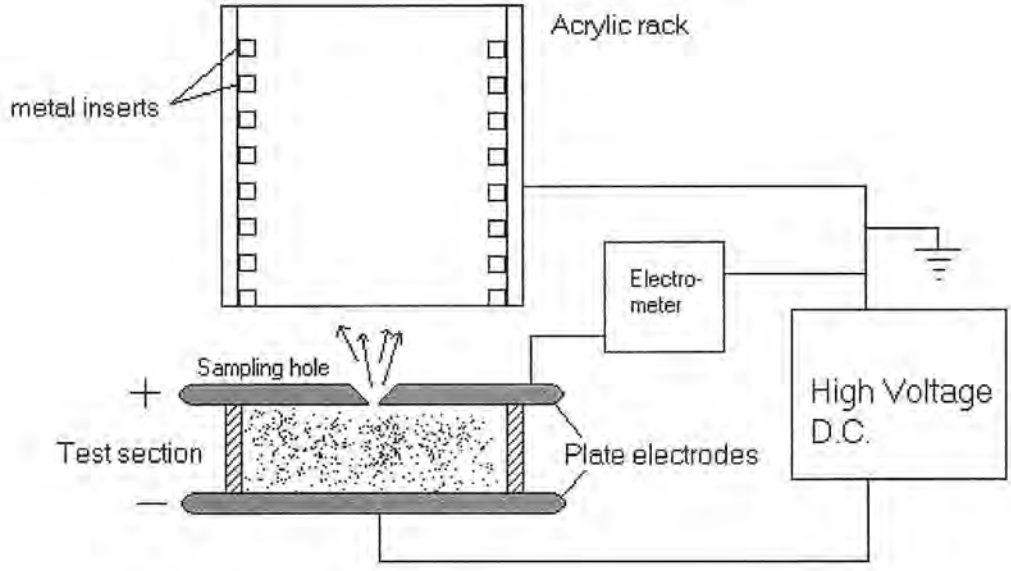

Figure 3.2. Circuit diagram of experimental setup. A negative dc high voltage lead was connected to the bottom plate electrode.

the beam traversed through the center of the Pyrex containment cylinder and half way between the top and bottom plates.

3.2 Test Section

The test section consisted of two circular brass plates (0.5 cm thick, 9.16 cm diameter) separated by a Pyrex glass cylinder. The Chemistry Machine Shop in Gilman Hall (Iowa State University) machined the plates and a conic leak hole on the top plate. The cone opening measured 1 cm at the top side of the plate decreasing to a 1.91 +/- .05 mm opening at the bottom. This is referred to as the leak hole of diameter d_{hole} = 1.91 +/- .005 mm. These proportions are utilized to minimize the disturbance effect of the sampling hole in the electrostatic suspension. A Pyrex glass cylinder was inserted between the plates to contain the particles. Two different cylinders (1.993 +/ .008 cm height, 4.793 +/- .006 cm inside diameter and 1.020 +/ .005 cm height, 4.788 +/- .008 cm inside diameter) were used in experimentation. The cylinders were aligned along the center of the glass sampling slides and marked on the base plate to facilitate re-centering following a run.

The leak hole on the top plate was sealed by a movable a rubber plug fixture during the time when a voltage was applied to the test section. This allowed the suspension to reach steady-state conditions before sampling particles. The plug fixture was fastened to the top plate utilizing a "swivel" piece. The conical silicon plug was attached to an adjustment screw. Figures 3.3a and 3.3b show the hole-plugging system for the leak hole.

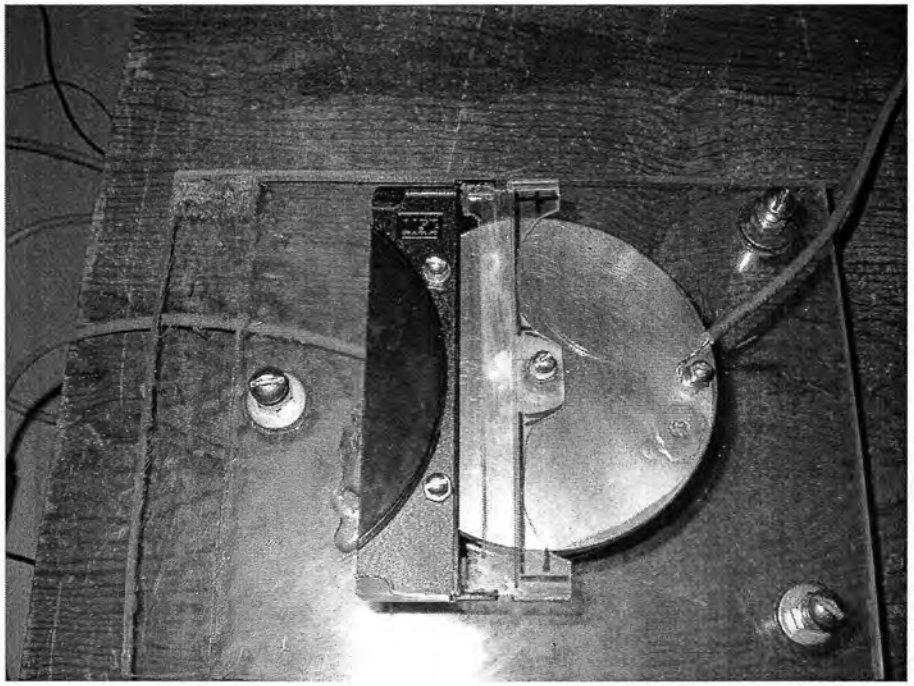

Figure 3.3a

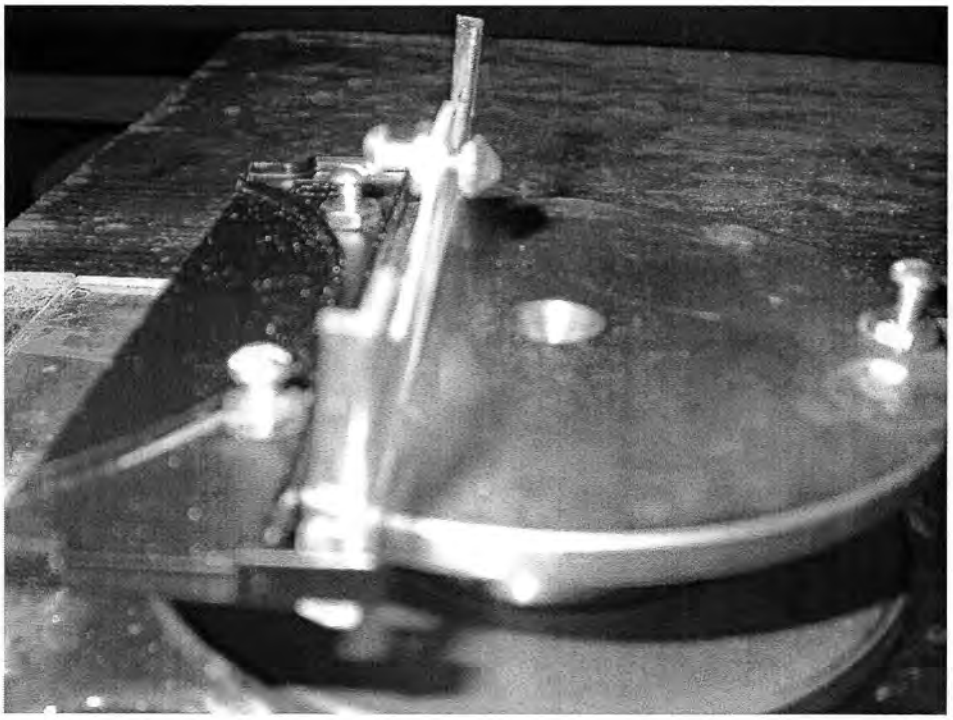

Figure 3.3b

Figure 3.3. (a) Top view of hole-plug design. (b) Front view of hole-plug design.

A special particle collection plate electrode (.175 cm thick, 11.74 cm diameter) was used to experimentally measure particle leakage rate from the test section (see Section 5.1). The plate was constructed from copper-plated PC board. A separate external plug was used to permit the outward flux of the particles. The design of the second plate facilitated the capture of leaked particles (see Section 5.1). Figures 3.4a and 3.4b show the copper plate electrode.

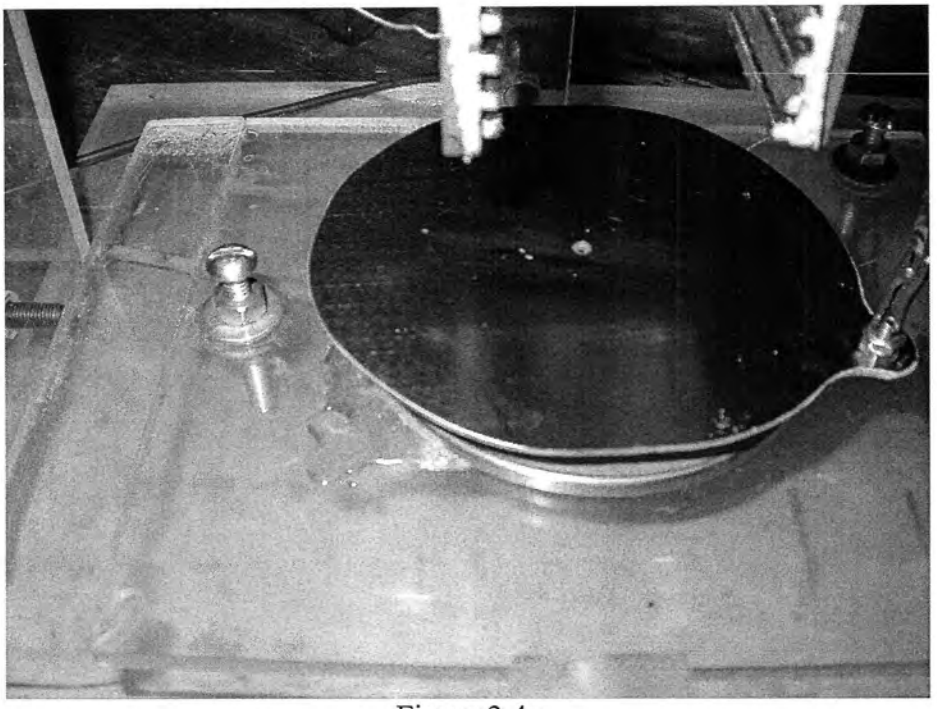

Figure 3.4a

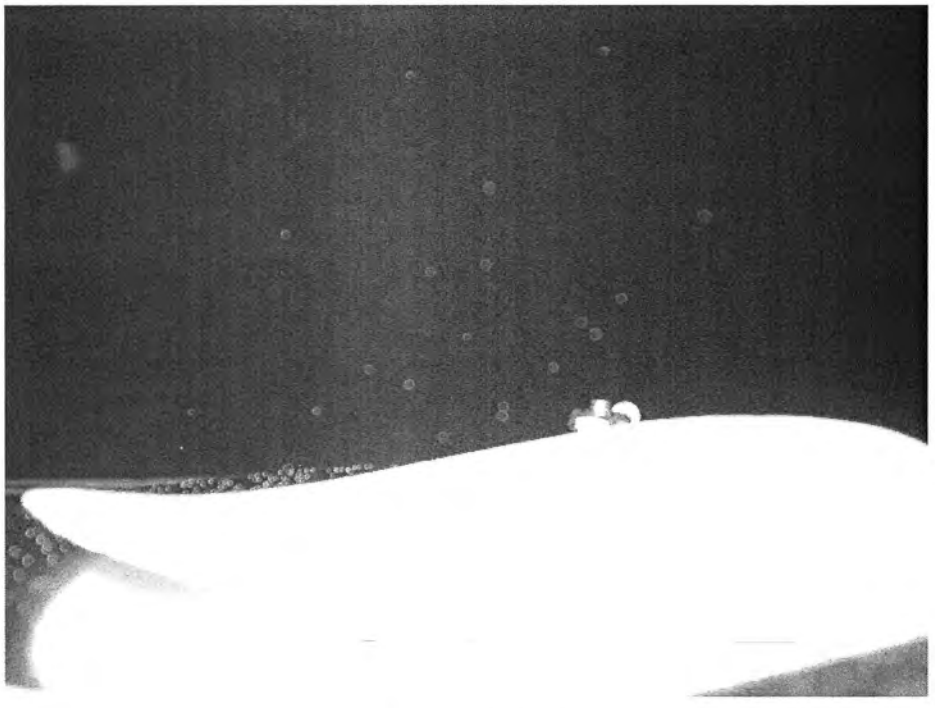

Figure 3.4b

Figure 3.4. (a) Copper collection plate electrode in place of original plate electrode. (b) Particles are leaked from the plate onto filter paper.

4. PROPERTIES OF PARTICLES

4.1 Copper

Copper particles (U.S. Bronze) of different sizes (aforementioned) were used for experimentation. The copper particles were assumed to be spherical. Calculations involving copper assumed a density of 8.94 g/cm^3. Figures 4.1a and 4.1b are photographs taken by a scanning electron microscope (SEM, Ames Laboratory) of sieved copper particles which were used in experimentation. Copper particles were be shown to be non-spherical in some instances using the SEM, and other small "satellite" particles were attached to larger particles.

4.2 Glass

Glass microbeads were also investigated. The glass was also assumed to be spherical. Calculations involving glass assumed a density of 2.27 g/cm^3. Figures 4.2a and 4.2b are SEM photographs of glass particles used in experimentation. These particles appear to be consistently spherical.

4.3 Aluminum

Aluminum (Alfa-Aesar) particles were also investigated. Particles were assumed to be spherical. Calculations involving aluminum assumed a density of 2.7 g/cm^3. Figures 4.3a and 4.3b are SEM photographs of glass particles used in experimentation. These particles were observed to be non-spherical.

4.4 Particle Sieving

The particles (copper, glass, and aluminum) were sieved using a sonic sifter (ATM Corp. L3 P) and precision sieves (ATM Corp.) ranging in the following sizes: 20-25 μm, 63-75 μm, and 125-149 μm.

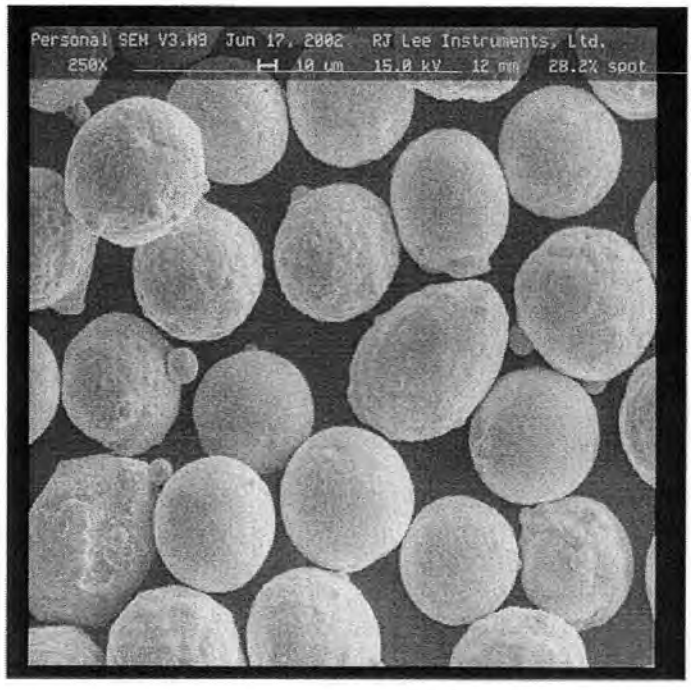

Figure 4.1a

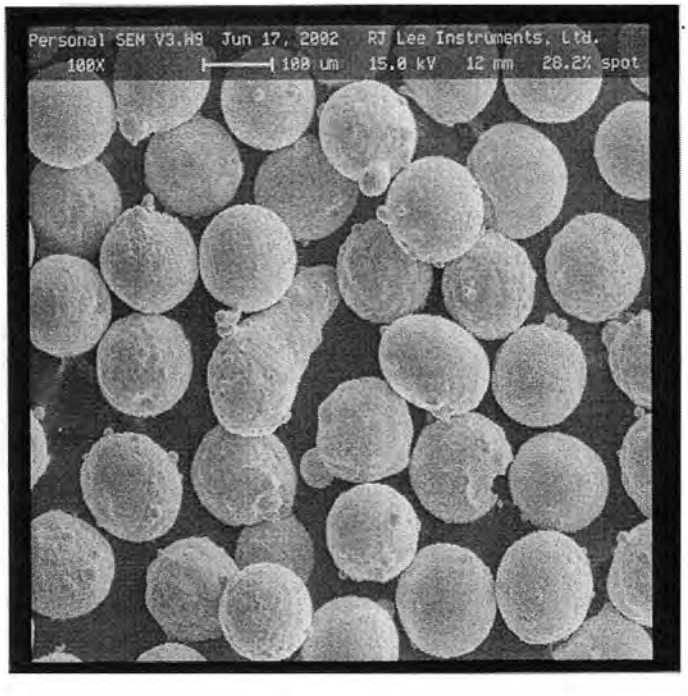

Figure 4.1b

Figure 4.1. SEM photographs of copper particles, in the following size ranges: (a) 63-75 μm, (b) 125-149 μm.

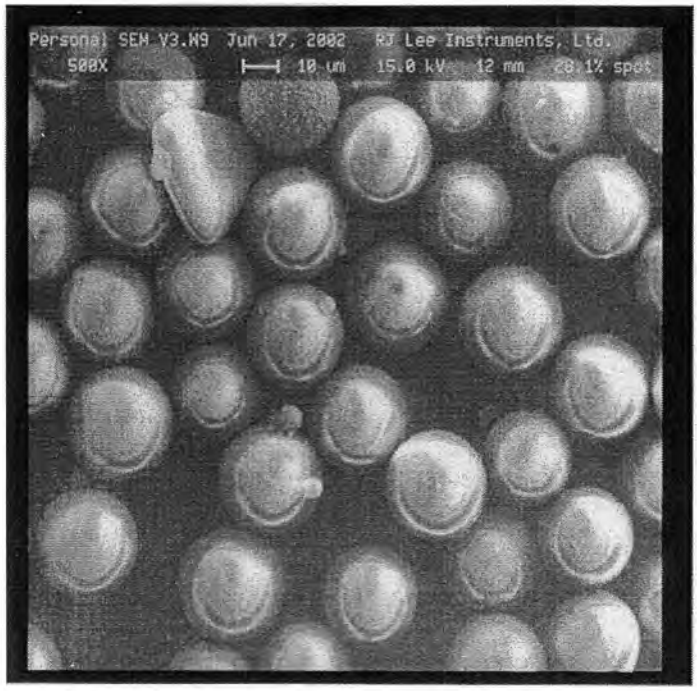

Figure 4.2a

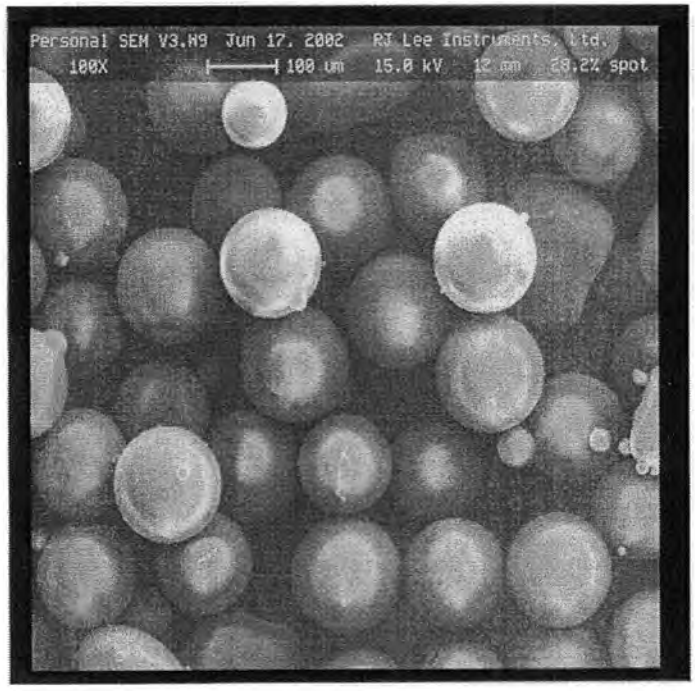

Figure 4.2b

Figure 4.2. SEM photographs of glass particles, in the following size ranges: (a) 20-25 μm, (b) 125-149 μm.

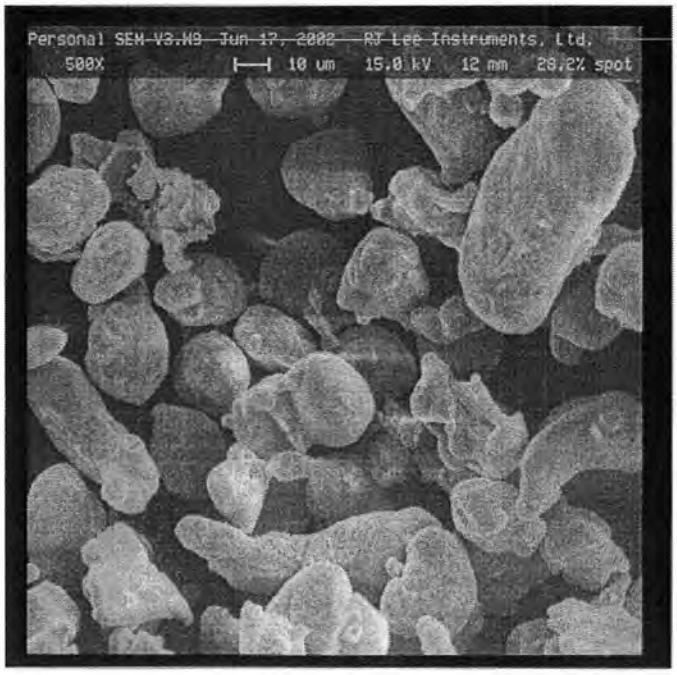

Figure 4.3a

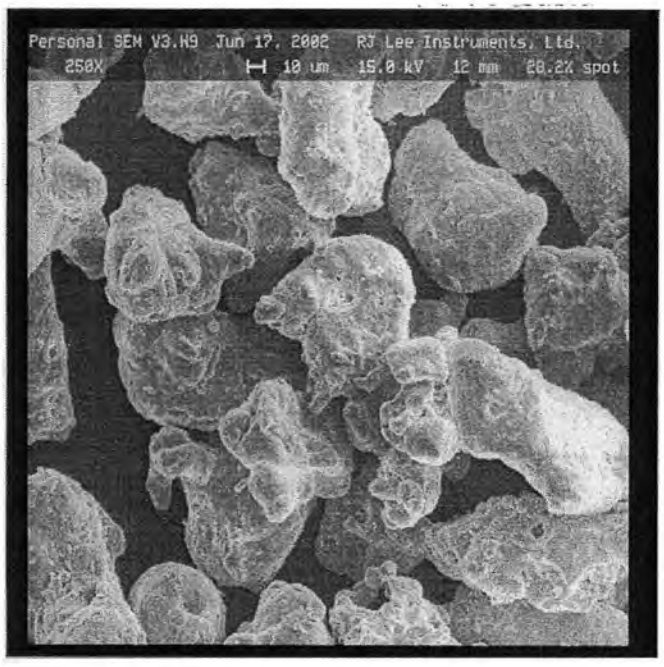

Figure 4.3b

Figure 4.3. SEM photographs of aluminum particles, in the following size ranges: (a) 20-25 μm, (b) 63-75 μm.

5. EXPERIMENTAL PROCEDURE

5.1 Particle Image Velocimetry

The author's first attempt for data collection involved the use of Particle Image Velocimetry, PIV. LaVision, Inc. (Germany) developed a system of hardware and software that consist of a dual lasers and CCD camera controlled by computer. The user inputs a time delay, dt (~μs), for the laser to send a pulse. The CCD camera acquires refracted intensity of any displaced objects, one from each laser pulse. When the CCD camera is calibrated, the distance an object is displaced is known and since the time delay is specified, a velocity is established. The PIV system has the capability to analyze several particles at a time to develop a velocity field.

The PIV system was used on the test section used in the experiment. The laser pulses passes through an optical lens that directed the beam into a laser "sheet." This "sheet" was directed over the leak hole of the test section. When an electrostatic suspension was established the hole was unplugged and computer-controlled system fired two rapid successive laser pulses over given time dt. The DaVis5.2 (LaVision) software can calculate the velocities of the particles exiting the leak hole. LaVision's Particle Tracking Velocimetry, PTV, software counts the number of particles present. In the same manner as the present study, the particles' initial velocities could be calculated by the equation of motion. Thus, the particle speed distribution could be experimentally determined.

Figures 5.1a and 5.1b show images of the PIV hardware and a close-up of the CCD camera, respectively. Figures 5.2a, 5.2b, 5.2c, and 5.2d, contain an image of projectile particles (a), and their corresponding vector fields (only one image of the projectile is shown; another was taken by system to create vector field). Difficulties arose in using the system

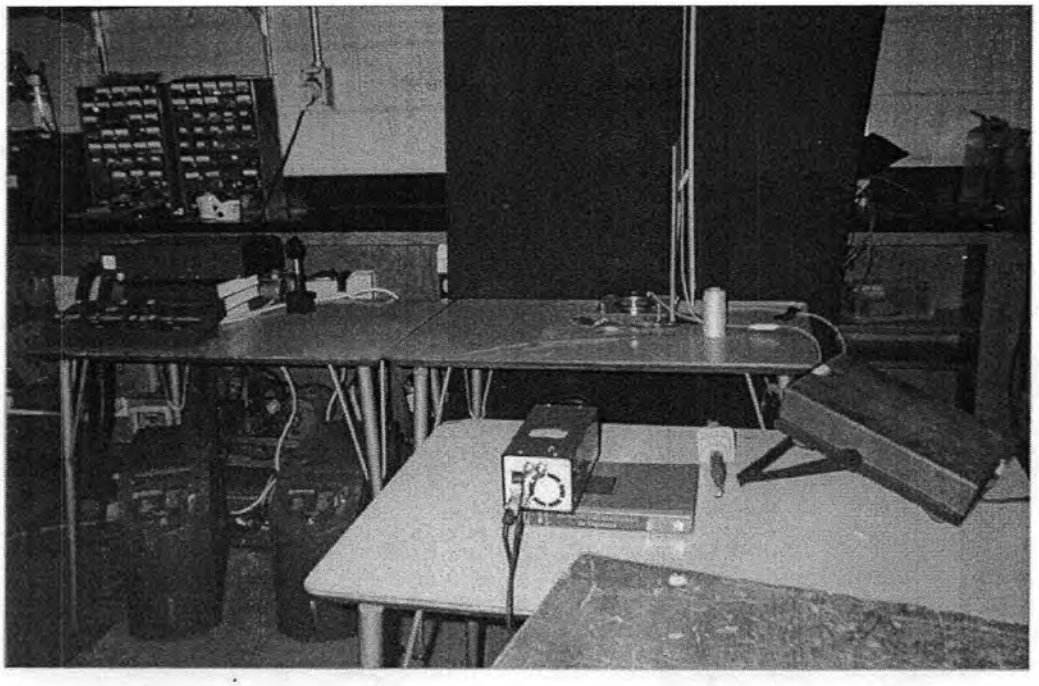

Figure 5.1a

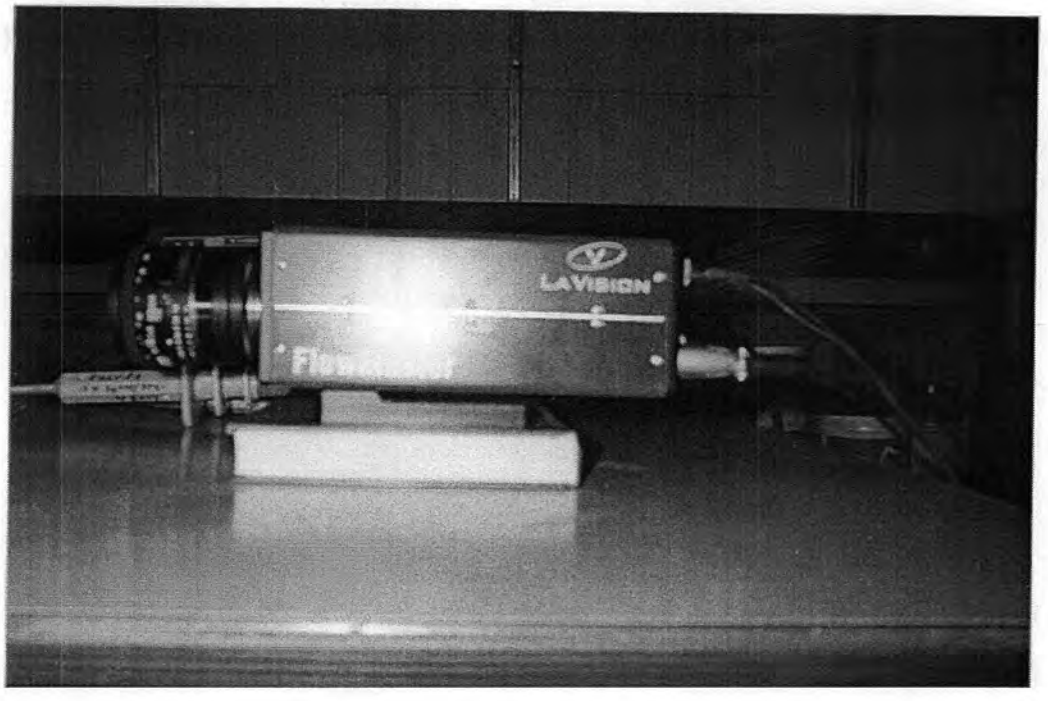

Figure 5.1b

Figure 5.1. (a) From left to right: dual lasers, optical lens (produces laser sheet), test section, and CCD camera (front, right). (b) Close-up of CCD camera.

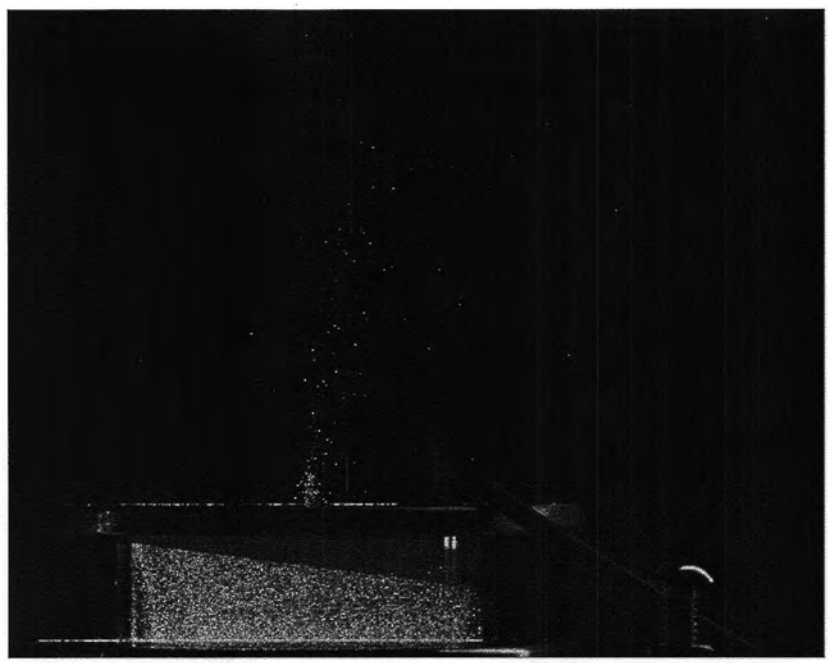

Figure 5.2a

Figure 5.2b

Figure 5.2. (a) CCD image of 20-25 μm aluminum particles leaked from test section. (b) Velocity vector field of particles calculated by PIV software.

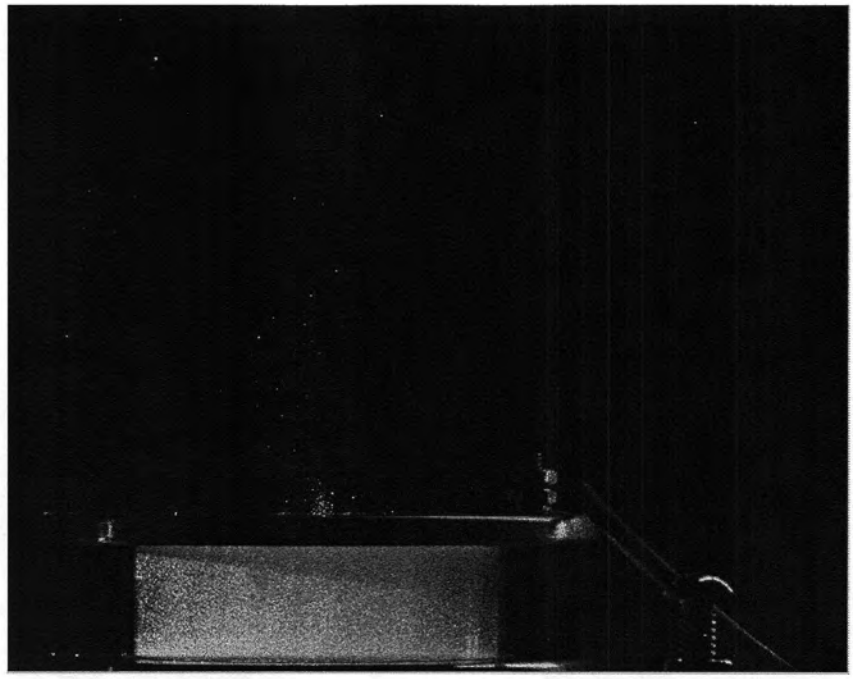

Figure 5.2c

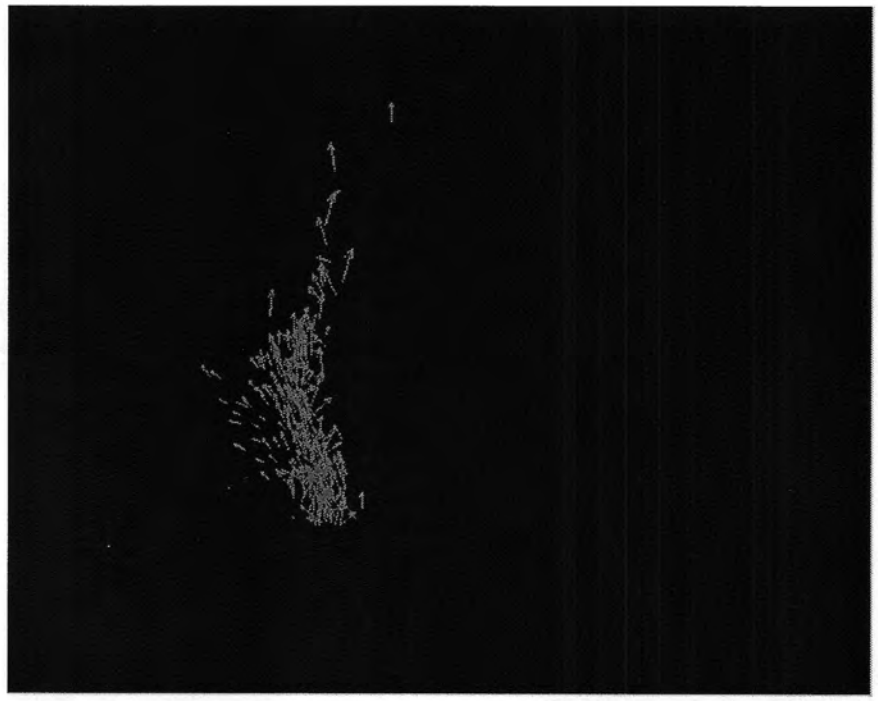

Figure 5.2d

Figure 5.2. (c) CCD image of 20-25 μm glass particles leaked from test section. (d) Velocity vector field of particles calculated by PIV software.

because of the relatively short time the system was available for use and also an experienced consultant was not available in the laboratory. In an attempt to improve parameters of the system, the author contacted technicians from the manufacturing company. The acquisition and results were much improved, but inconsistencies between the number of particles counted by the software and the number of vectors produced by the software were substantial. If improvements were made to the system, the images suggest that the PIV system could provide a more accurate representation of particle speed distribution.

5.2 Data Collection

Table 5.1 shows the variables investigated (particle material and diameter, electric field strength and plate separation) together with the range tested. The experiment was designed with the intention that particles of various size ranges were subject to a range of electric field strengths. Using a sling psychrometer, the relative humidity in the room was measured before proceeding with data collection. Particles were placed the Pyrex cylinder by removing the top plate (Figure 5.3). Samples were run with an excess of particles, i.e. particles not suspended by electric field, in the test section to provide makeup of particles leaked through the leak hole, to keep particle number density n consistent. These excess particles were deposited on the bottom electrode as shown in Figure 5.4. Seven glass slides coated with epoxy (LocTite 90-Minute Epoxy) were placed in every other slot on the rack, beginning with the open slot nearest to the test section (2.92 cm from 2-cm glass test section, 3.86 cm from 1-cm test section). The rack was lowered so that it would not interfere with movable hole-plugging system. The initial laser power reading, I_0, was measured. The power supply was set to predetermined values necessary for suspension (based on Equation 2.2.5 for a single particle). Laser power and current measurements were measured. The

Table 5.1. Summary of variables investigated

Material	Diameter (μm)	*Electric Field (103 kV/cm)	Plate Separation (L, cm)	Cylinder diameter (z, cm)
Copper	20-25	6.82, 8.93, 13.2	1.993 +/- .008	4.793 +/-.006
	63-75	6.82, 9.43, 13.0	1.993 +/- .009	4.793 +/-.006
	125-49	7.58, 9.43, 13.3	1.993 +/- .010	4.793 +/-.006
Aluminum	63-75	7.58, 12.5	1.993 +/- .010	4.793 +/-.006
	125-49	7.45, 13.5	1.020+/- .005	4.788 +/- .008
Glass**				

*names in parentheses indicates trial name. Names given to organize data (see Appendix B).
**not investigated (see Section 5.3)

Relative humidity: 45-52 %

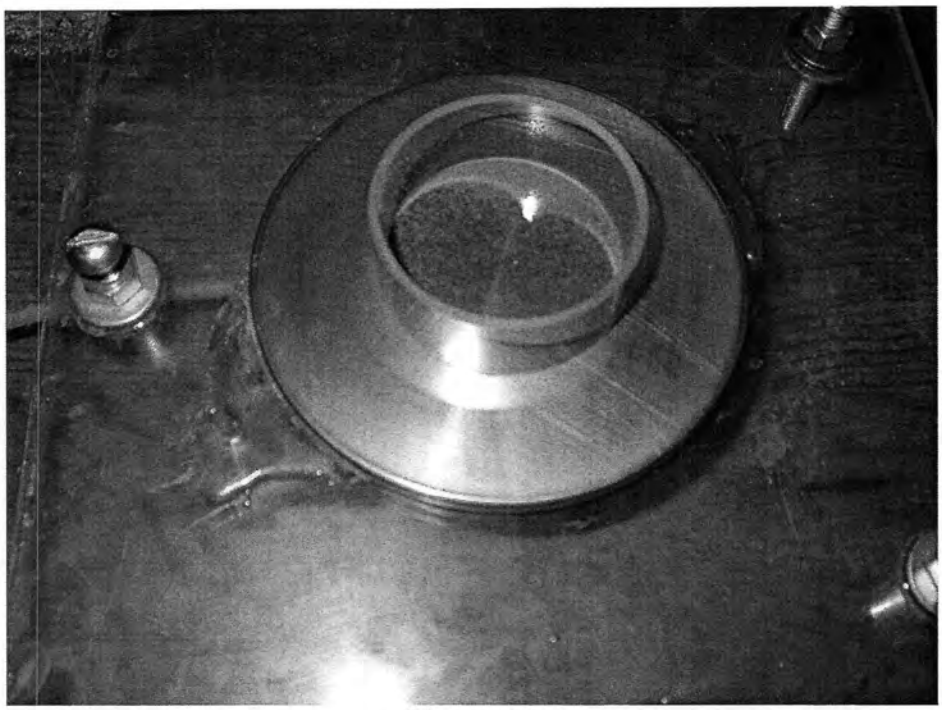

Figure 5.3

Figure 5.4

Figure 5.3. The top plate is removed from the test section for insertion of particles.

Figure 5.4. A small layer of 125-149 μm copper particles rests on the bottom electrode (deposition) during suspension.

leak-hole plug was opened manually for approximately 2 seconds (assisted with a stopwatch). Once leakage of particles was established, the first glass slide (nearest to leak hole) was removed. With the particle suspension still running, the leak hole was again opened for approximately 2 seconds; then, the next glass slide was removed. This process was repeated until the last slide was exposed. After sampling with the glass slides was completed, the power supply was removed and the copper plate (Section 3.2) was substituted into the test section to measure flux rate of particles. A piece of filter paper with small hole in the middle was placed over the top plate to collect the total number of particles over known time (a verification test). This filter paper was weighed with a precise scale (Ainsworth 24N) before and after particle collection. The leak hole was plugged and the power supply was reset to the previous values. The plug was released for 5 seconds and particles were leaked from the system onto the paper. The paper was again weighed and recorded. This procedure gives an experimental value and check of the particles exiting the test section per unit time. The entire procedure was repeated for investigated particles. The test section was thoroughly cleaned after each sample using Trichloroethylene.

5.3 Glass Particle Filaments

Colver [10, 11] investigated charging dynamics of glass particles. The charge per particle was experimentally lower than the predicted theory. He experimentally determined that the charge per particle had a clear dependence on relative humidity (surface conductivity) [10]. He observed clouds of particles (rain) that form into "funnels" and then into "filaments" due to current saturation. In his study [9], spontaneous formation of filaments from an electric suspension was not observed for glass at high relative humidity (>40%).

Current density measurements were also lower for a confined test section (using glass or Teflon) than for an unconfined test section [10].

Glass particles used in the present study also formed filaments in an electrostatic suspension (Figures 5.5a, b). The relative humidity in the test section was measured to be approximately 45%. A humidifier was used in the laboratory (closed vents, all doors shut) for 30 minutes. The relative humidity rose to approximately 52%. The electric field was again applied to copper particles of sizes 63-75 μm and 125-149 μm. Glass filaments were again observed and particle suspension was limited. Due to formations of filaments, data collection for glass particles was not carried out.

5.4 Particle Counting

Epoxy applied to glass slides was allowed to dry overnight after particle sampling. Slides were then placed under a stereo microscope (National 420T-430PHF-10, 120X) connected to a camera (Nikon COOLPIX4500) to be counted. The Nikon camera allowed the microscope viewing area to be projected onto a monitor (monitor) for particles to be counted. A 5.08-cm equal-area grid was designed to aid in counting the particles. The grid contained eleven concentric rings, divided into eight sections; it was attached underneath of the slide by rubber cement. Figures 5.6a and 5.6b show the microscope-camera-monitor system and a digital camera image of particles under microscope, respectively. Figures 5.7a and 5.7b show the equal-area grid (with dimensions) and the grid superimposed under a 63-75 μm aluminum particle slide, respectively.

The equal-area grid was not useful when counting aluminum 63-75 μm and 125-49 μm particles of slides nearest to the leak hole, i.e. the first two slides, due to irregularity of the

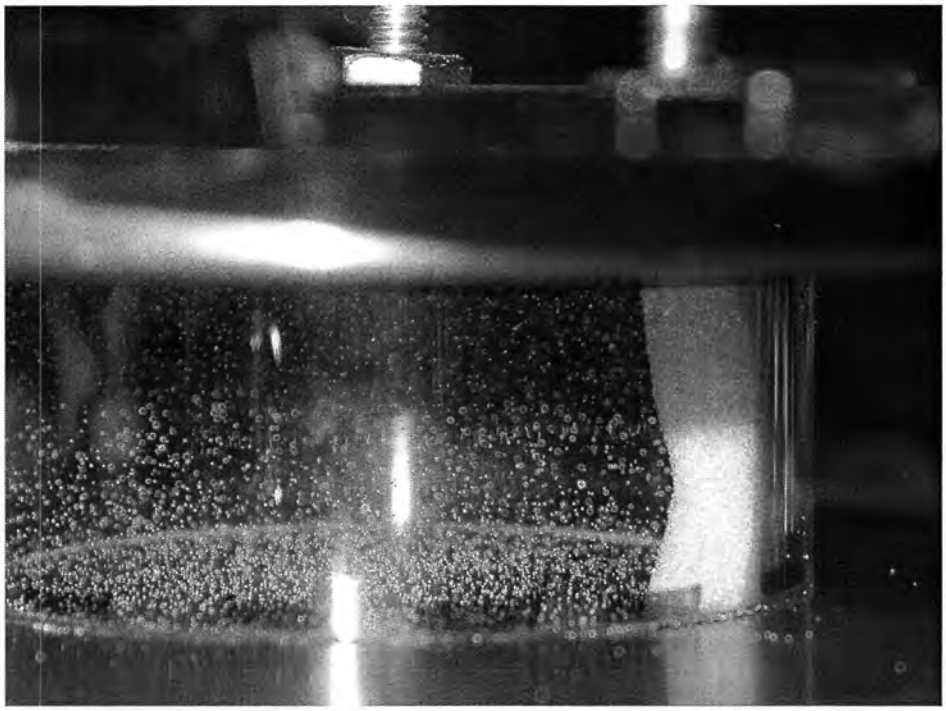

Figure 5.5a

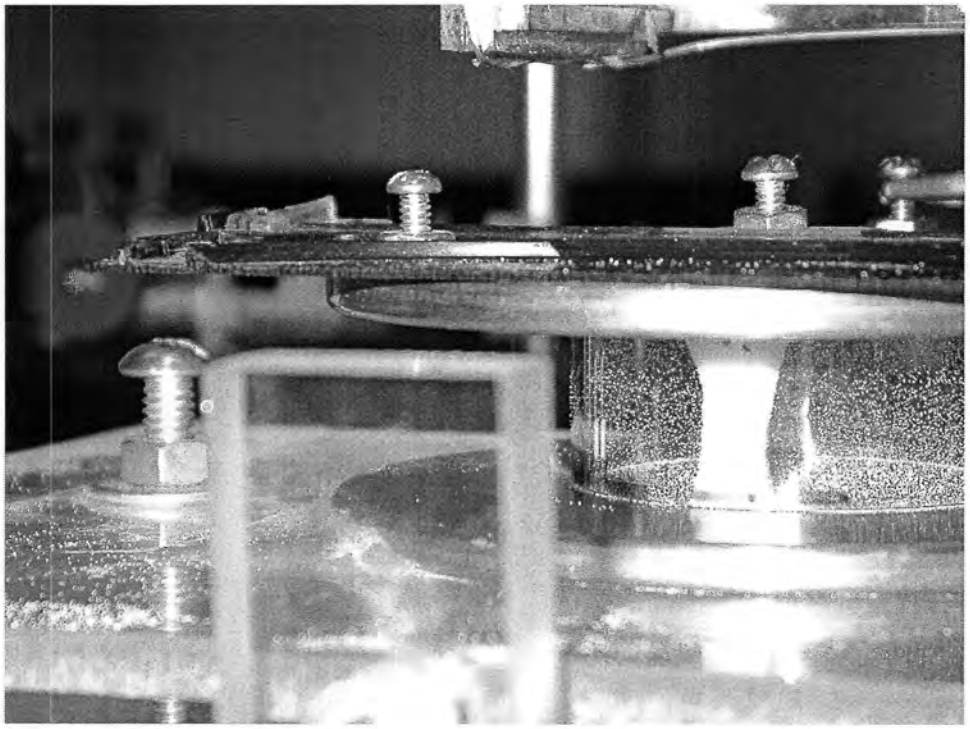

Figure 5.5b

Figure 5.5. (a),(b) Glass filament forming against the glass cylinder.

Figure 5.6a

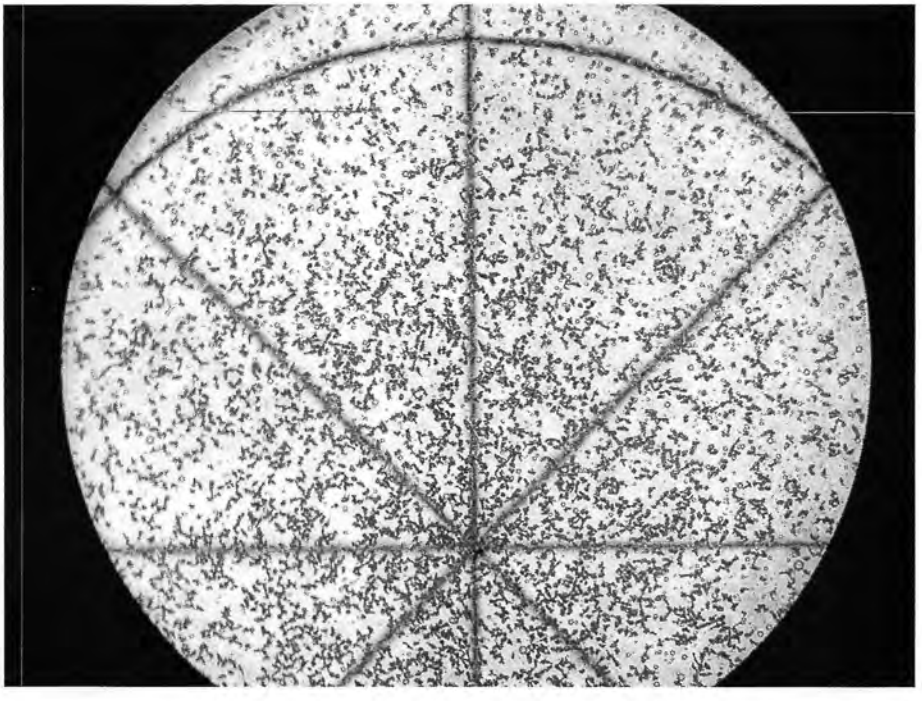

Figure 5.6b

Figure 5.6. (a) From left to right: monitor, camera (attaches to microscope), and microscope. (b) Digital camera image of 63-75 μm aluminum particle slide under microscope.

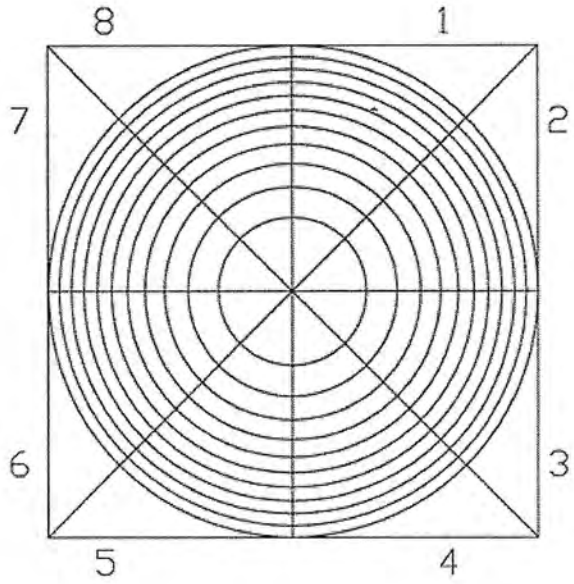

Sectors 1-8 are labeled

Ring	Radius (cm)
1 (inner)	0.7658
2	1.0831
3	1.3265
4	1.5317
5	1.7125
6	1.8759
7	2.0262
8	2.1661
9	2.2975
10	2.4218
11	2.5400
Outer:	>2.5400

Figure 5.7a

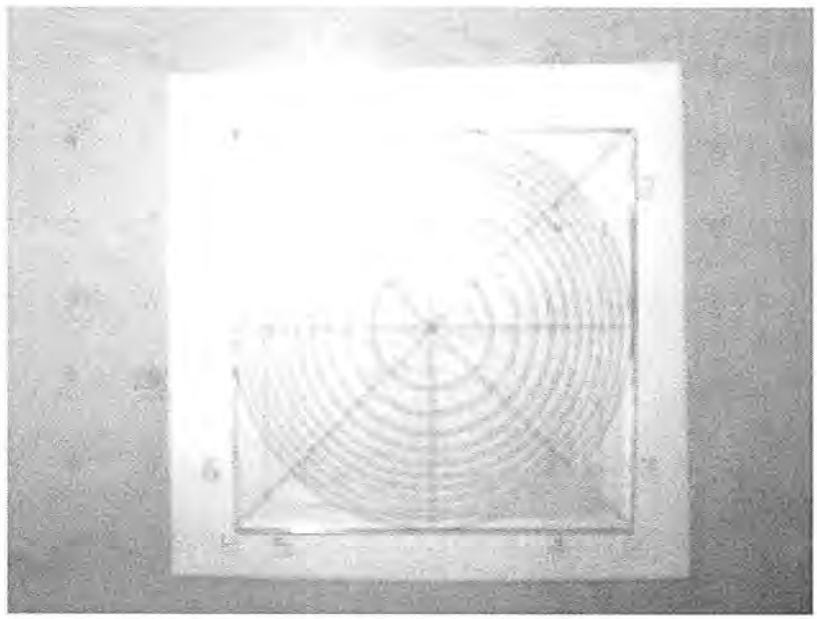

Figure 5.7b

Figure 5.7. (a) Equal-area grid designed with individual sections containing the equal area. (b) Grid superimposed under a 125-149 mm aluminum particle slide.

particles themselves and the large number of particles collected on the first two slides. The grid was modified with two concentric circles inscribed in the first circle. A magnifying lens (1.5X) could be mounted under the microscope to zoom in on the particles to distinguish one particle from another. An entire section of the grid could be seen under the microscope. Thus, erroneous counting was more limited. Small copper particles (20-25 μm) were determined to be too small for counting. Once focused under the microscope, a full grid section could not be seen under the microscope. An even more improved counting grid, with more concentric circles and subdivided into more sections, would be required to obtain an accurate count. This was considered a more extreme and time-consuming process; data collection for 20-25 μm copper particles was abandoned. Similarly, 20-25 μm aluminum particles were not collected.

6. RESULTS

6.1 Particle Initial Speed-Height Relationship

A particle's initial speed v(t=0) when exiting the leak hole was the assumed speed of the particle in the test section. Initial speed was related to the glass slide height h in which it was captured by the equation of motion

$$\frac{dv}{dt} = -\left(\frac{v}{\tau} + g + \frac{F_q}{m}\right) \tag{2.4.4}$$

for a vertically decelerating particle. Using Mathematica, a program was written to numerically solve for particle height vs. initial velocity. The program was written using the fact that a particle reaches its maximum height when velocity is zero. It allowed the user to input the particle and air properties, and accounts for gravity and viscous drag (image charge forces are neglected). Table 6.1 gives velocity related to particle height calculated for copper and aluminum particles in sizes ranges of 63-75 μm and 125-149 μm. Figures 6.1a and 6.1b show a graph of height vs. initial velocity for copper and aluminum particles, based on values in Table 6.1. If no drag is present, the height achieved by any particle size is the same. It is evident that the drag on a smaller particle (63-75 μm) is larger than for a larger particle (125-149 μm). Values obtained from Figures 6.1a and 6.1b were used to find a particle velocity based on height obtained. If a particle reached a given height, then its initial velocity is greater than (or equal to) the initial velocity calculated.

6.2 Maxwell-Type Speed Distribution

Figures 6.2a and 6.2b show data collected for number of copper particles collected at different heights over a 2-second interval. The total number of particles at height h = 0 is the

Table 6.1. Initial velocity (cm/s) to reach glass slide height h

Calculated using Mathematica

a. Drag = 0

b. Velocity of copper particles, diameter d = 63-75 μm

c. Velocity of copper particles, diameter d = 125-149 μm

d. Velocity of aluminum particles, diameter d = 63-75 μm

e. Velocity of aluminum particles, diameter d = 125-149 μm

Slide Height h (cm)	a. Drag = 0	b. Copper	c. Copper	d. Aluminum
2.920	75.691	95.432	81.146	152.034
4.230	91.101	121.296	99.455	212.393
5.515	104.022	145.210	115.404	274.934
6.845	115.888	169.162	130.572	343.692
8.170	126.608	192.594	144.734	416.543
9.505	136.561	216.002	158.296	494.489
10.860	145.971	239.707	171.504	578.370

Slide Height h (cm)	e. Aluminum
3.860	113.862
5.170	139.041
6.455	163.049
7.785	187.607
9.110	212.03
10.445	236.754
11.800	263.962

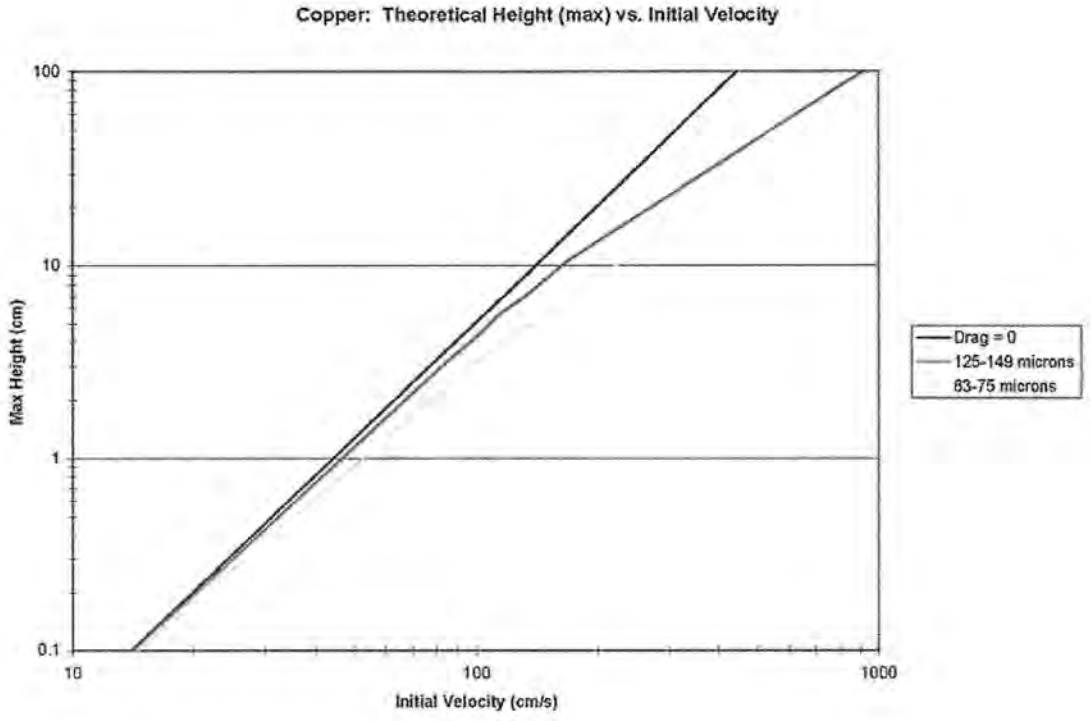

Figure 6.1a

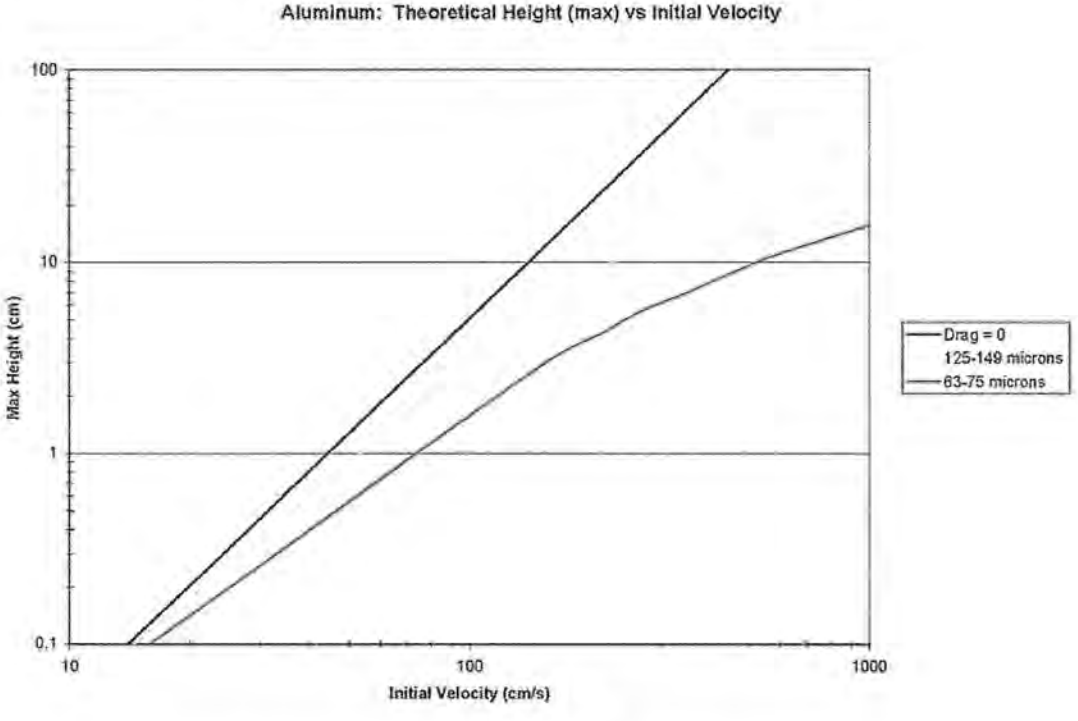

Figure 6.1b

Figure 6.1. Initial velocity v(t=0) required to reach vertical height h for (a) copper and (b) aluminum. A particle traversing through medium with drag = 0 is the same for any diameter.

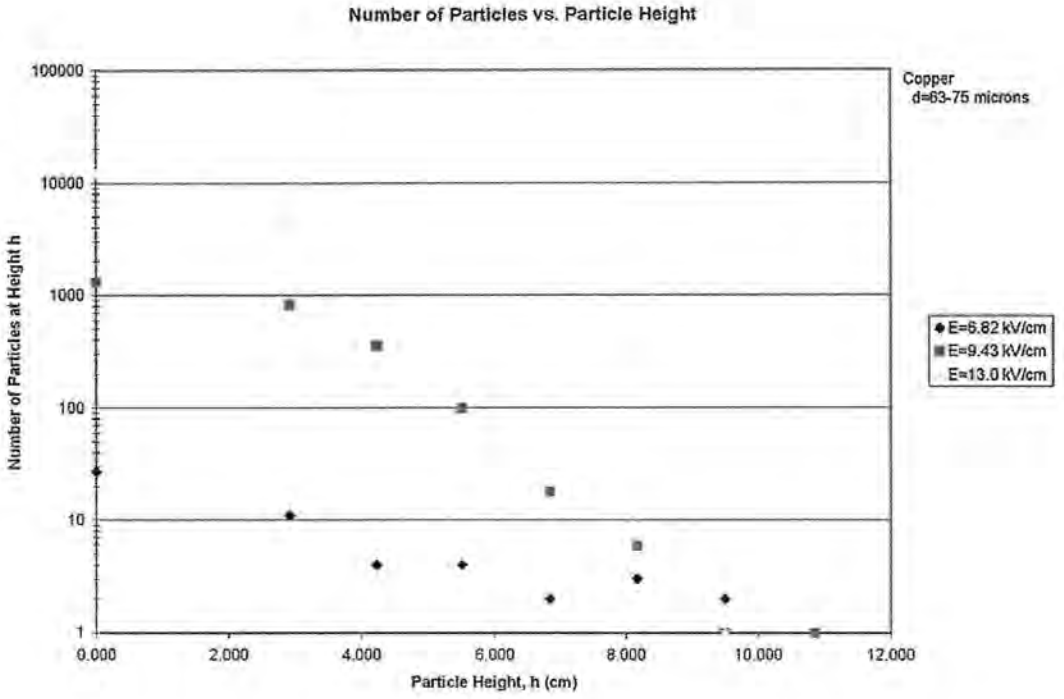

Figure 6.2.a

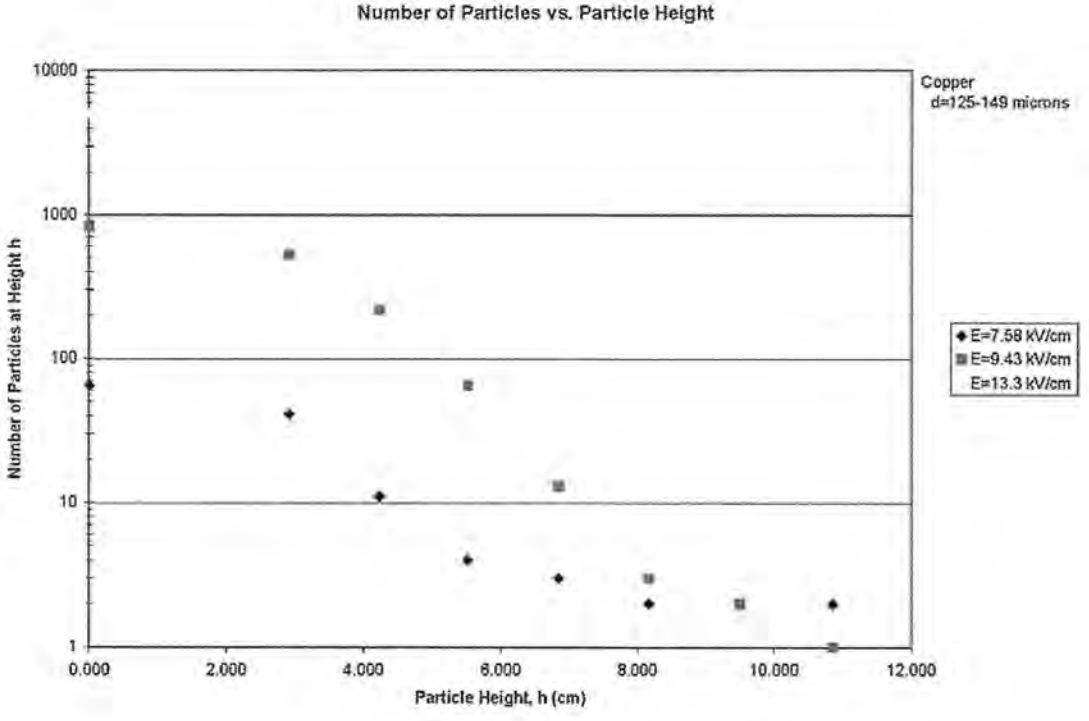

Figure 6.2b

Figure 6.2. Number of copper particles collected at different heights above leak hole for (a) 63-75 μm and (b) 125-149 μm.

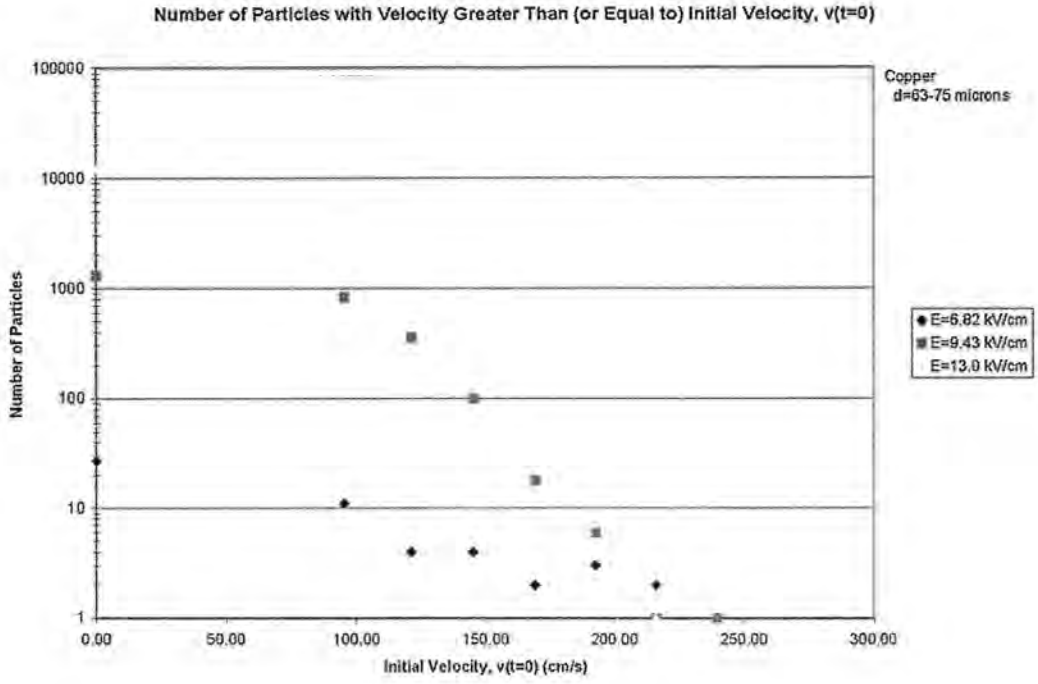

Figure 6.3a

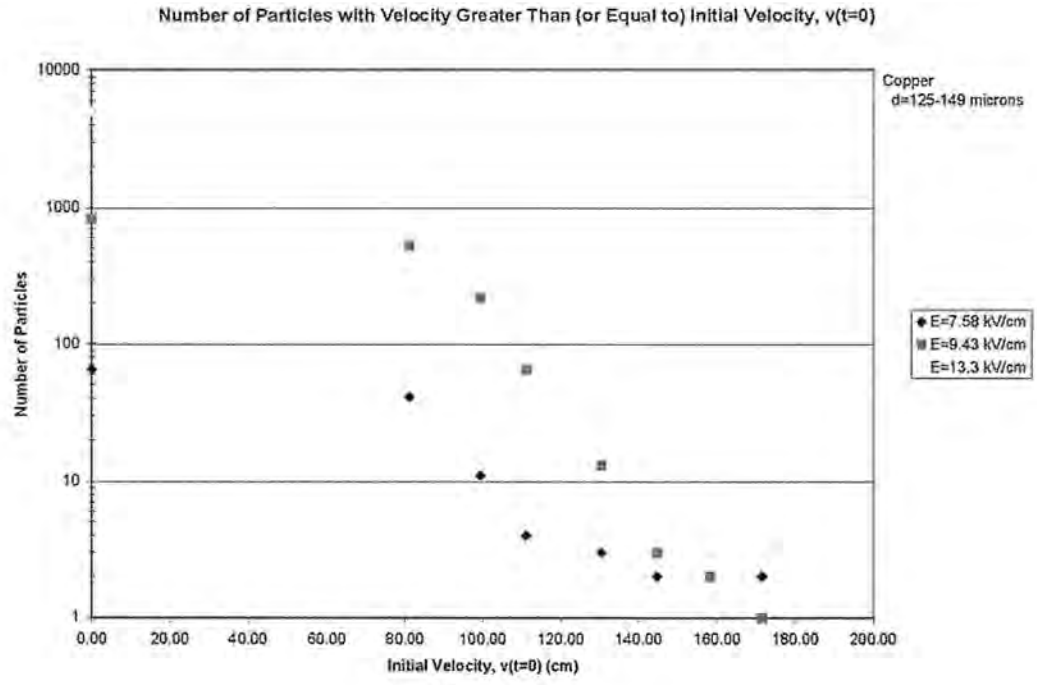

Figure 6.3b

Figure 6.3. Number of copper particles at different speeds by applying Table 6.1 to Figures 6.2a and 6.2b for particle sizes (a) 63-75 μm and (b) 125-149 μm.

total number of particles collected for a particular sample. Using Figures 6.2a and 6.2b and theoretical results from Table 6.1, Figures 6.3a and 6.3b show the number of copper particles that reached a speed greater than the initial velocity calculated from equation of motion (see Appendix C for data for all samples). To fit a Maxwell-type speed distribution curve to the data, Equations 2.4.7 and 2.4.8 were equated to give

$$\frac{N}{N_0} = \left[\left(v/v_0\right)^2 + 1\right] e^{\left[-\left(\frac{v}{v_0}\right)^2\right]} \qquad (6.2.1)$$

where, v and v_0 are respectively the particle speed and most probable speed, N is the number of particles at a height h and N_0 is the total number of particles collected for a particular sample (sum of all particles on glass slides, h = 0). The most probable speed v_0 was calculated from experimental data using two methods. Method I compared the error terms of experimental data (Equation 6.2.1, L.H.S) to an assumed Maxwell-type distribution (Equation 6.2.1, R.H.S.). The data was input to a spreadsheet and an initial most probable speed v_0 was guessed. Using Excel Solver (Microsoft), the sum of squares error term SSE was minimized by changing v_0. These values of v_0 were used to fit a Maxwell-type curve to experimental data. Method II involved a similar procedure, only the logarithm (natural) of the experimental data and the assumed Maxwell distribution were also calculated. The error between the log of experimental data and log of Maxwell distribution calculations was calculated and the SSE was minimized using the same procedure in Method I. The two methods give two different Maxwell curve fits to the data. Method I favors the higher particle fractions N/N_0 in the center while Method II favors the smaller particle fractions at larger h values. A comparison of two different curves using Method I and Method II is given

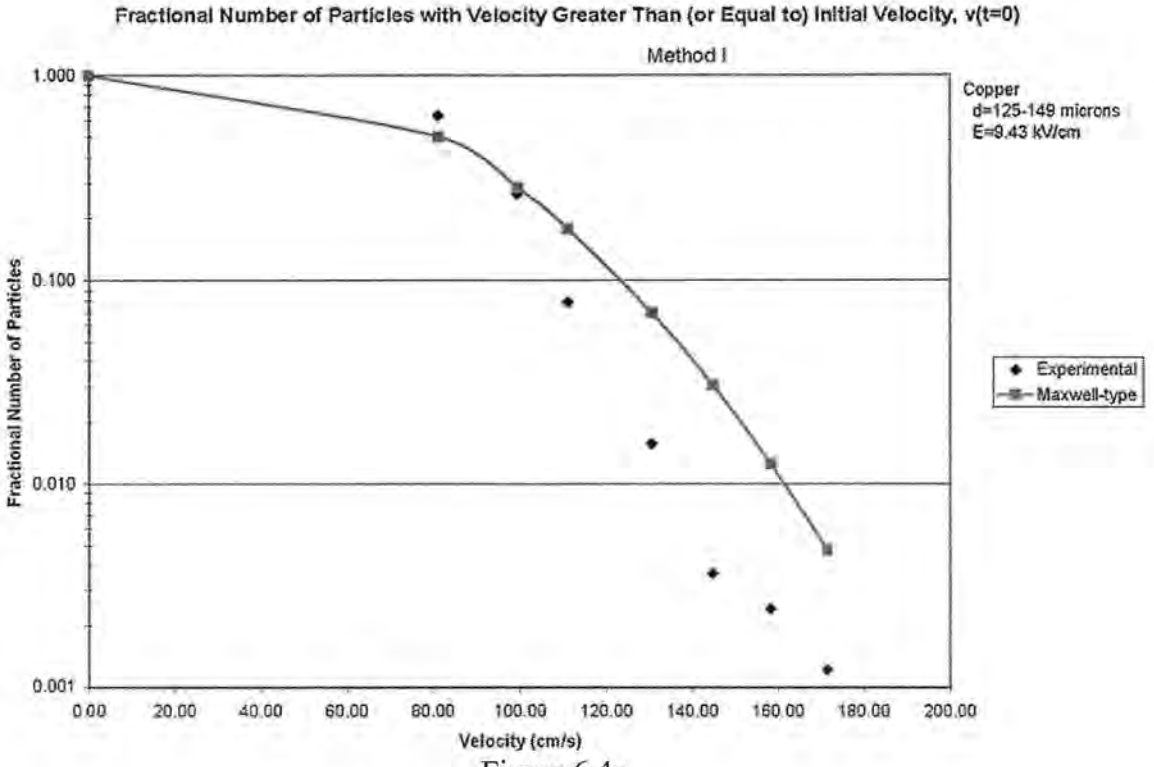

Figure 6.4a

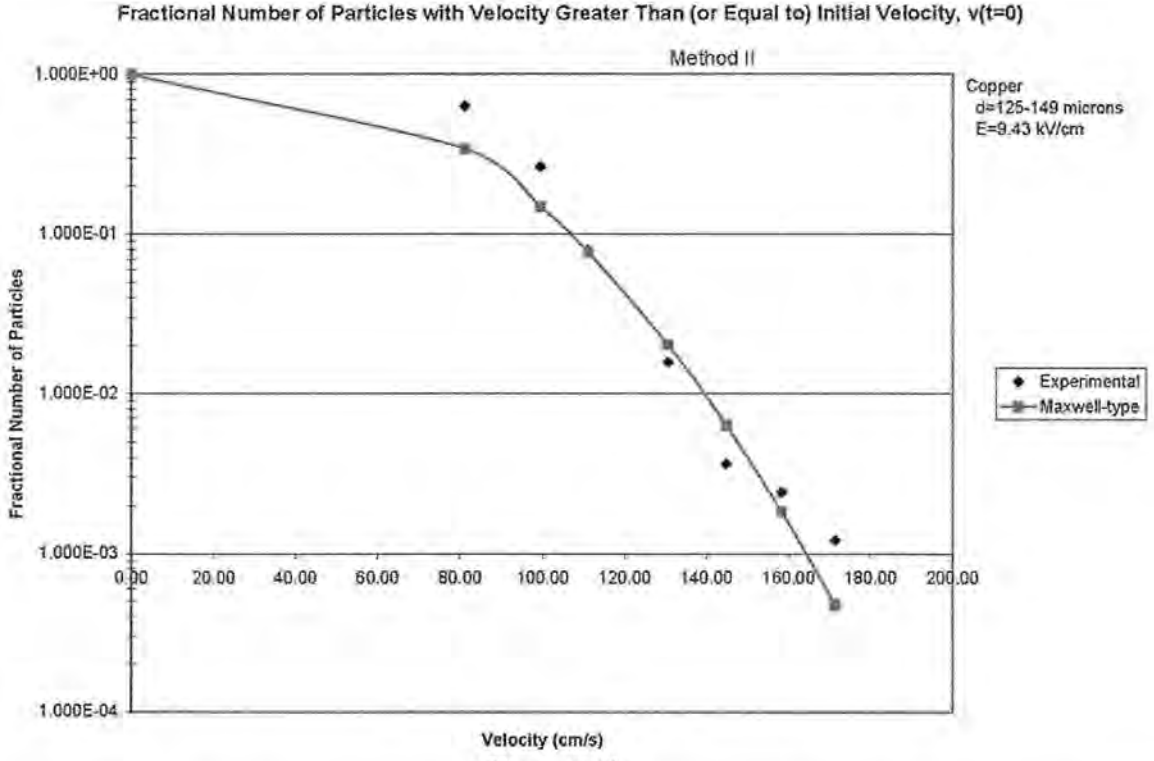

Figure 6.4b

Figure 6.4. 125-149 μm copper particles with a Maxwell curve fit using (a) Method I and (b) Method II. E=9.43 kV/cm. L=1.993 cm.

in Figures 6.4a and 6.4b for 125-149 μm copper particles. Curve fits for all data can be found in Appendix D. Generally, Method II appears to give a better Maxwell curve fit to the data. For example, copper particles (d = 63-75 μm, E = 9.43 kV/cm, L = 1.993 cm) with a Maxwell curve fit using Method II appears to give a slightly better fit than Method I. However, the sum of squares error term for Method II is higher than for Method I ($SSE_{II}>3*SSE_I$). This would imply that a greater disparity of particle speeds was experimentally observed and Method II accounts for the small fraction of particles at relatively high speeds.

A summary of different speeds for single particle (theoretical) and distributed speeds is given in Table 6.2. The average and maximum speed of a single particle, $\bar{v}_s$ and v_{max}, respectively, are theoretical values calculated using Equations 2.2.10 and Equations 2.2.11, respectively. The coefficient of restitution for the top and bottom plate (e_t and e_b, respectively) in Equation 2.2.10 was found independently by photographing the trajectory of copper spheres falling and rebounding from the bottom plate electrode used in experimentation. The shutter was set to the B setting and film remained exposed until trigger was released. By equating kinetic energy to potential energy the coefficient of restitution is found by taking the square root of the rebound height of the particle to the initial height. Values ranged from 0.47 - 0.65. The average coefficient of restitution was $e_t = 0.59$. Coefficient of restitution for the bottom plate was $e_b = 0$ due to deposition present in the test section. The most probable speed is found by experiment, and particle mean speed $\bar{v}$ and rms speed (for distribution) v_{rms} are calculated using Equation 2.4.9.

Table 6.2. Summary of characteristic particle speeds

*Speeds are in cm/s

a. Particle species
b. Particle diameter d (μm)
c. Electric field E (kV/cm)
d. Average speed v_s for single particle (Eq. 2.2.10)
e. Maximum speed v_{max} for single particle (Eq. 2.2.11)
f. Most probable speed v_0 (experimental)
g. Mean particle speed v for distribution (Eq. 2.4.9)
h. Rms speed v_{rms} for distribution (Eq. 2.4.9)

METHOD I

a. Species	b. d (μm)	c. E (kV/cm)	d. v_s	e. v_{max}	f. v_0	g. v	h. v_{rms}
Aluminum	63-75	7.58	228.6	327.76	132.2	149.2	162.0
Aluminum	63-75	12.5	373.7	540.46	120.8	136.3	148.0
Aluminum	125-149	7.45	115.7	163.55	89.9	101.5	110.1
Aluminum	125-149	13.5	205.6	296.37	84.3	95.1	103.3
Copper	63-75	6.82	117.8	162.06	68.9	77.8	84.4
Copper	63-75	9.43	158.7	224.08	77.4	87.3	94.8
Copper	63-75	13.0	215.8	308.92	74.0	83.5	90.7
Copper	125-149	7.58	95.8	127.83	61.4	69.3	75.2
Copper	125-149	9.43	115.8	159.03	62.7	70.7	76.7
Copper	125-149	13.3	158.9	224.29	58.1	65.5	71.1

METHOD II

a. Species	b. d (μm)	b. E (kV/cm)	d. v_s	e. v_{max}	f. v_0	g. v	h. v_{rms}
Aluminum	63-75	7.58	228.6	327.8	148.5	167.5	181.8
Aluminum	63-75	12.5	373.7	540.5	184.8	208.6	226.4
Aluminum	125-149	7.45	115.7	163.5	88.1	100.2	107.9
Aluminum	125-149	13.5	205.6	296.4	98.7	111.4	120.9
Copper	63-75	6.82	117.8	162.1	98.8	111.5	121.0
Copper	63-75	9.43	158.7	224.1	69.9	78.9	85.7
Copper	63-75	13.0	215.8	308.9	71.2	80.4	87.2
Copper	125-149	7.58	95.8	127.8	66.4	75.0	81.4
Copper	125-149	9.43	115.8	159.0	54.1	61.0	66.2
Copper	125-149	13.3	158.9	224.3	68.5	77.3	83.9

The theoretical average speed for a single particle is expected to be greater than for distributed mean particle speed. Viscous drag and image charge forces tend to decrease particle speed. For most samples, the single particle maximum speed was not as great as the experimental maximum speed in the distribution. This may be due to a change in particle momentum and charge accumulated through collision processes which add plus and minus velocity increments. Also, the most probable speed is expected to increase with increasing electric field strength. For the first increase in electric field for copper particles the most probable speed also increased, but decreases for the next electric field increase. Only one increase in electric field was applied to aluminum particles (due to a lack of aluminum in the laboratory) and the most probable speed decreased for increasing electric field. Mean particle speed and rms speed also show the same experimental results. This may be due to irregular data. Aluminum particles also feature a non-spherical shape which may alter dynamics of speed distribution, possibly due to inconsistent particle charging. Particle-particle collisions tend to change the charge per particle Q by charge reduction or charge neutralization of oppositely charged particles. Colver [10] showed that charge shielding (due to charge concentration in a suspension) and collision process tend to alter mass and charge flux. It should also be noted that the highest speed experimentally attained was by 63-75 μm aluminum particles traveling approximately 578 cm/s. This gives a Reynolds number of approximately 27. Therefore, the Stokes modified drag (Equation 2.2.8) is valid for calculations.

The number of particles collected was consistently lower for lower electric field. Thus, for relatively heavier copper particles only a small amount of particles could be analyzed in a

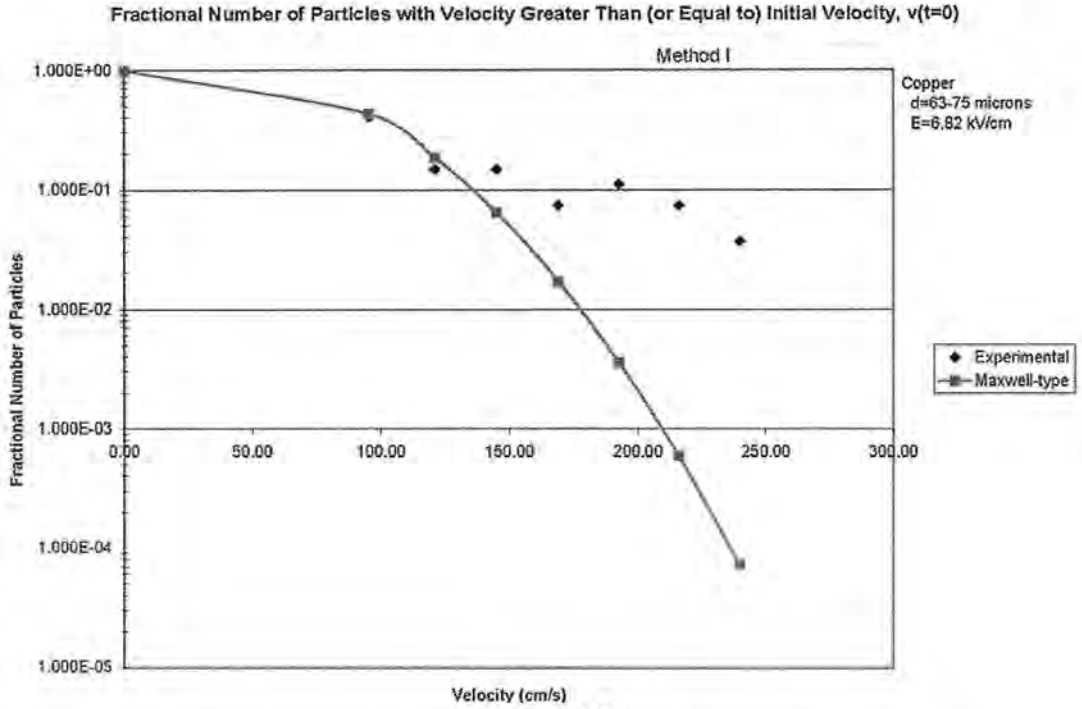

Figure 6.5a

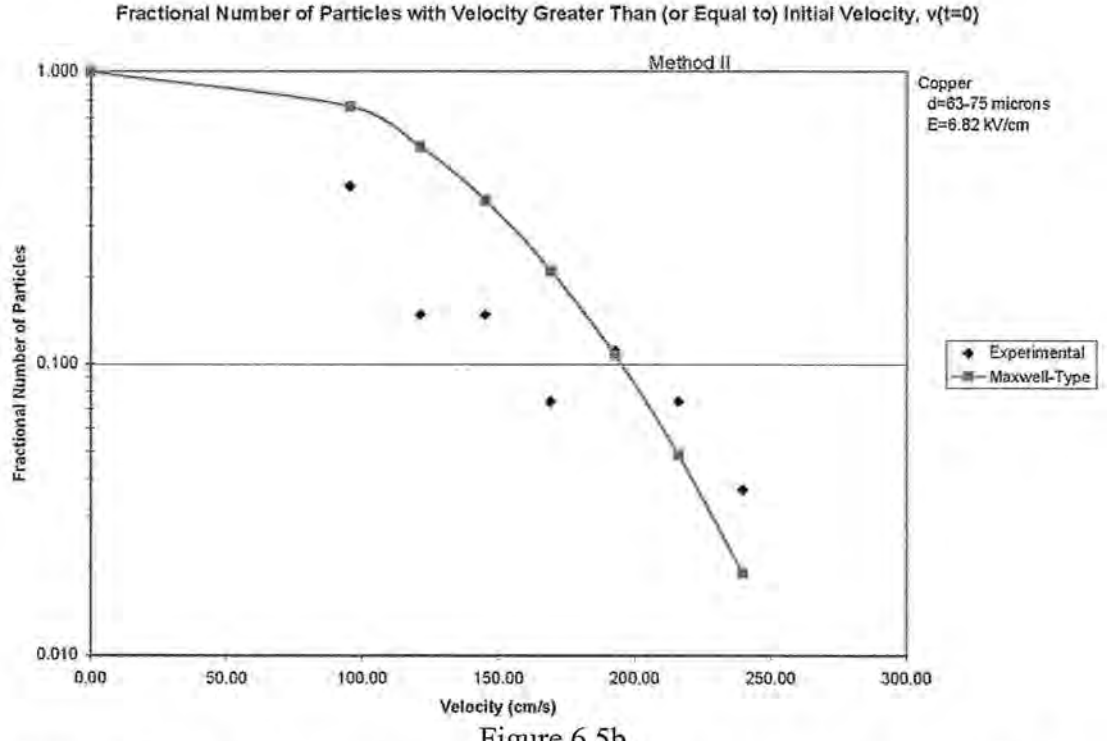

Figure 6.5b

Figure 6.5. Copper particles (d = 63-75 μm) with Maxwell curve fit (a, Method I; b, Method II) influenced by relatively low electric field strength (E = 6.82 kV/cm) yields small collection sample. Here, the total number of particles collected on 7 glass slides is $N_0 = 27$ particles.

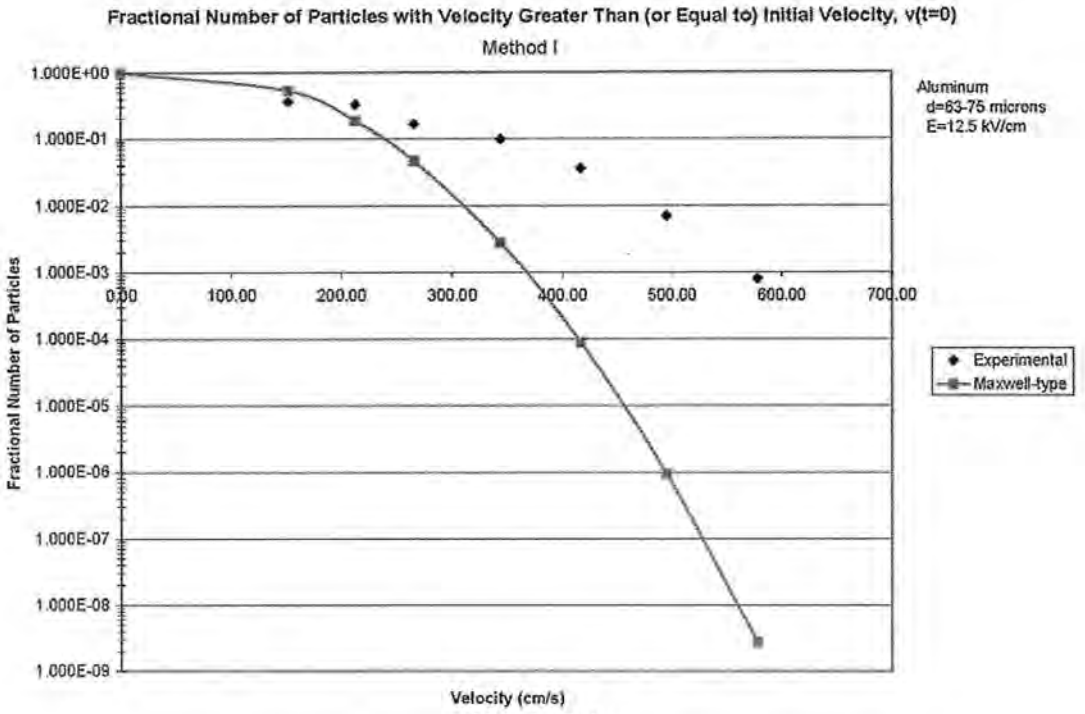

Figure 6.6a

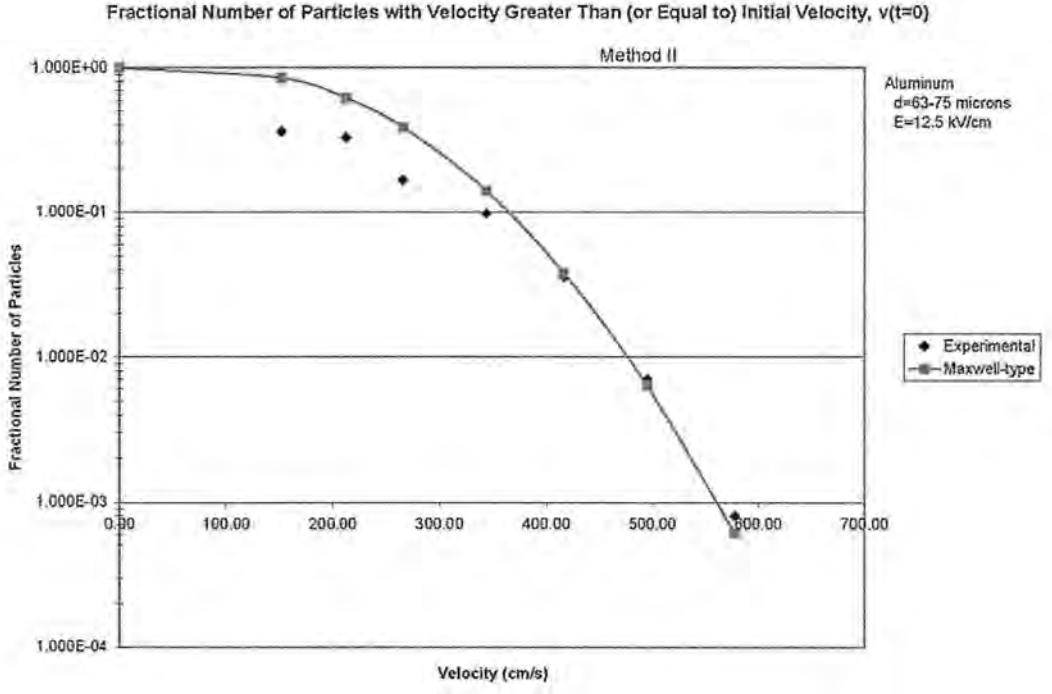

Figure 6.6b

Figure 6.6. Aluminum particles (d = 63-75 mm, E = 7.58 kV/cm, L = 1.993 cm) for a sample generally follow a Maxwell distribution for (a) Method I and (b) Method II.

particular sample and a higher (percent) error is expected. Particle speed distribution for copper particles using the lowest electric field (but large enough for particulate suspension) did not fit an assumed Maxwell curve fit (Figures 6.5a, b). This does not mean particles influenced by low electric field strength do not follow a Maxwell speed distribution. A sample of aluminum particles (d = 63-75 mm, E = 7.58 kV/cm, L = 1.993 cm) showed better results when comparing data to a Maxwell curve fit (Figures 6.6a, b). The number of aluminum particles collected for a sample should be expected to be higher compared to copper (for same electric field strength, diameter, and test section height) due to a smaller density. It should also be noted that any experimental speed distribution that resembles a Maxwellian distribution only suggests, but does not imply, that particles may have be governed by a Maxwell distribution in an electrostatic suspension.

6.3 Horizontal Speed Distribution (x-component)

Previous discussion regarding particle speed distribution has been directed at the vertical (y-component) direction of the applied electric field. The present study contributes a limited amount of analysis to horizontal (x-component) speed distribution. However, experimental evidence (observation of glass slides) suggests that a force in the direction perpendicular to the applied electric field may exist and particles traverse in this direction also in a particulate suspension. Also, particle-particle collisions or rotation of particles due to collisions could produce particle angular momentum that may allow particles to travel horizontally. The rings of the equal-area grid (Figure 5.3a) used to count particles were utilized to give a horizontal displacement of data. Individual particle horizontal displacement (leak hole being the origin) was not measured. Rather, an average displacement was assumed for a particles collected between to rings.

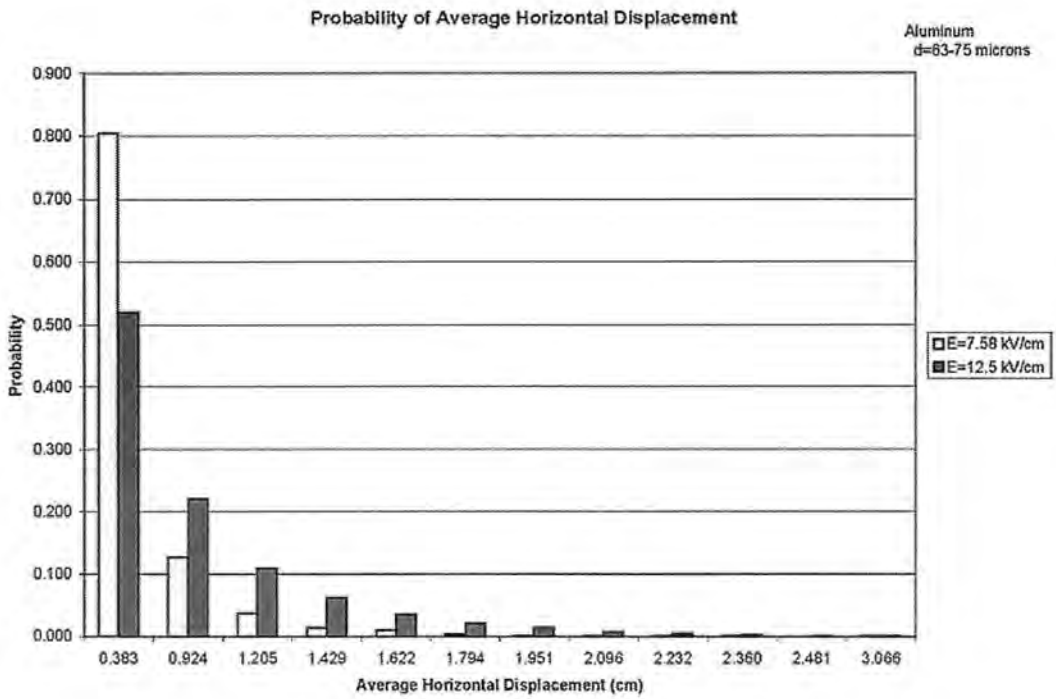

Figure 6.7a

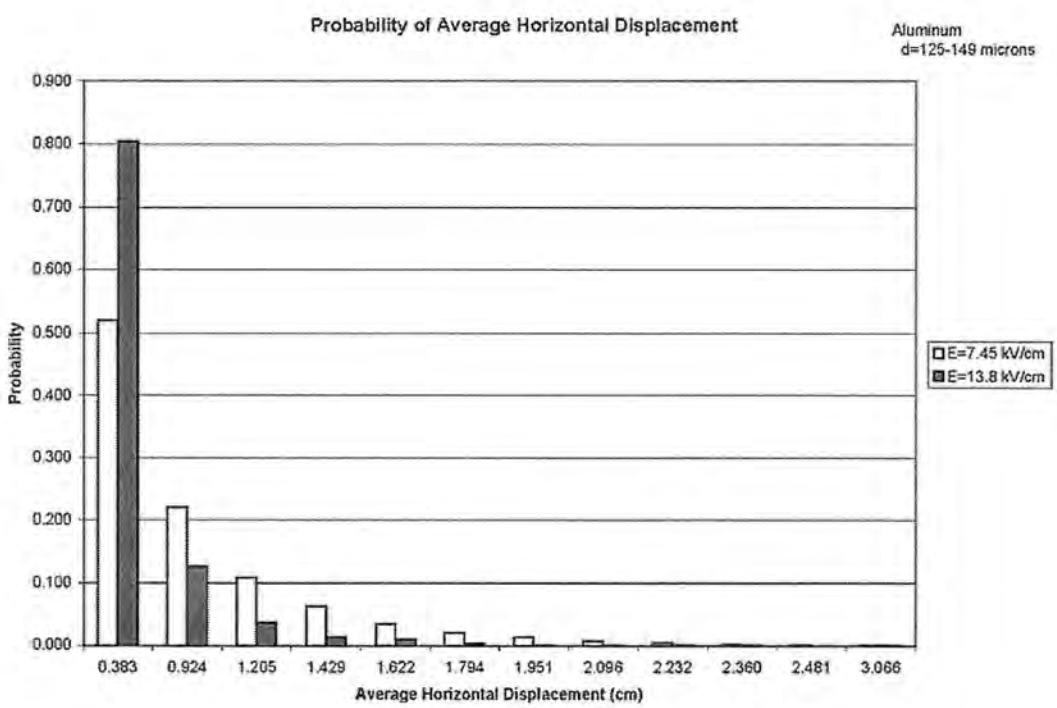

Figure 6.7b

Figure 6.7. Probability of horizontal particle displacement for aluminum particles for (a) 63-75 μm and (b) 125-149 μm particles.

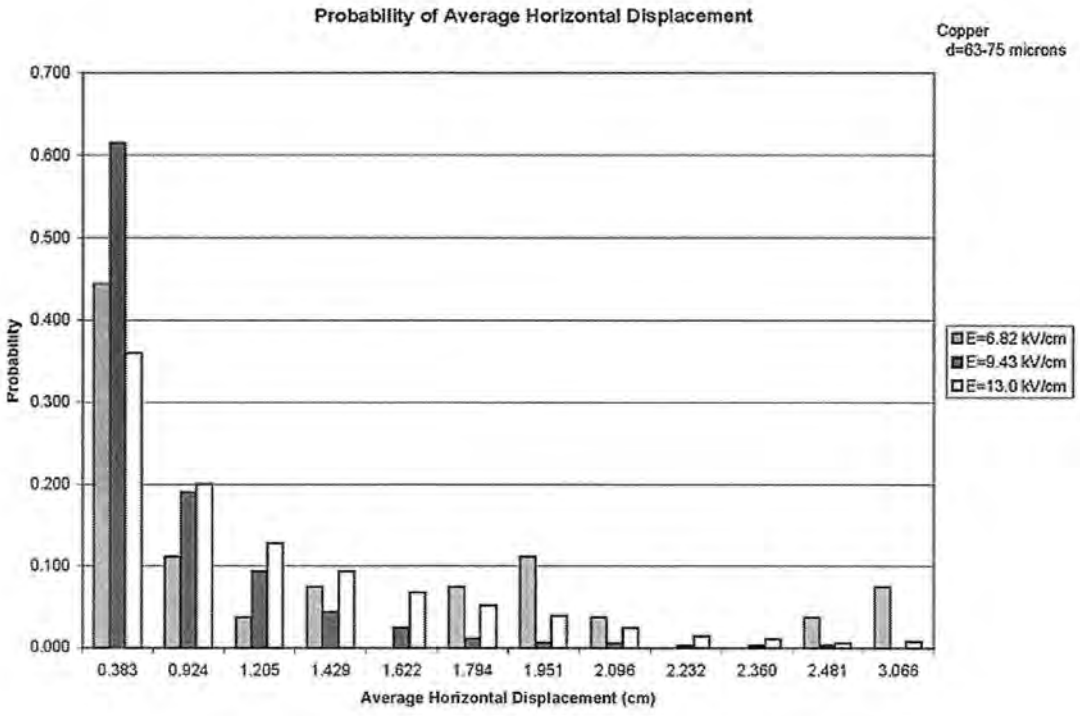

Figure 6.7c

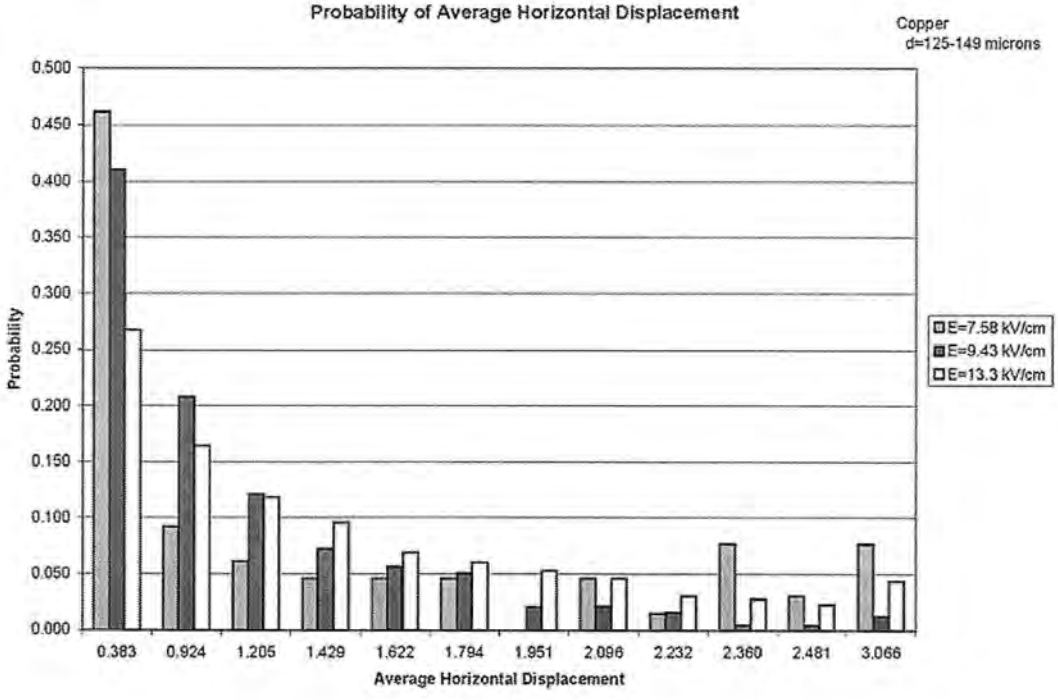

Figure 6.7d

Figure 6.7. Probability of horizontal particle displacement for copper particles for (c) 63-75 μm and (d) 125-149 μm particles.

Figures 6.7a-d are histograms showing the probability of aluminum and copper particles displaced at different horizontal distances for all samples. Experimental results show most particles lie in the first ring of average distance x = 0.766 cm. The number of particles horizontally displaced is expected to decrease for increasing horizontal displacement. This trend did not occur for all samples. Similar to the case in the vertical direction, with a smaller number of data collected, i.e. a lower applied electric field, a larger (percent) error can be expected.

6.4 Particle Number Density

Particle number density of suspended particles was calculated using the Lambert-Beer law

$$I = I_0 e^{(-nzA_p\varepsilon)}. \qquad (2.4.10)$$

The initial laser beam intensity I_0 was measured with no suspension. The beam traversed through the Pyrex cylinder to the power meter. The intensity I is expected to remain constant during particle suspension provided there is deposition in the test section. A small range of laser intensity measurements verified deposition. An independent second check on particle number density was by calculated count (weight). Small mass increments of particles were placed into the test section. Mass and current density were recorded. Deposition of particles is determined to be the point at which the first value current density remained unchanged for increased particle mass (Figure 6.8). At this point, the electric field strength could no longer suspend all particles in the test section. To accurately determine number density by count required several measurements. Deposition appeared to be more defined for some samples than others so approximations were made. Figure 6.9 shows a sample of 125-149 μm

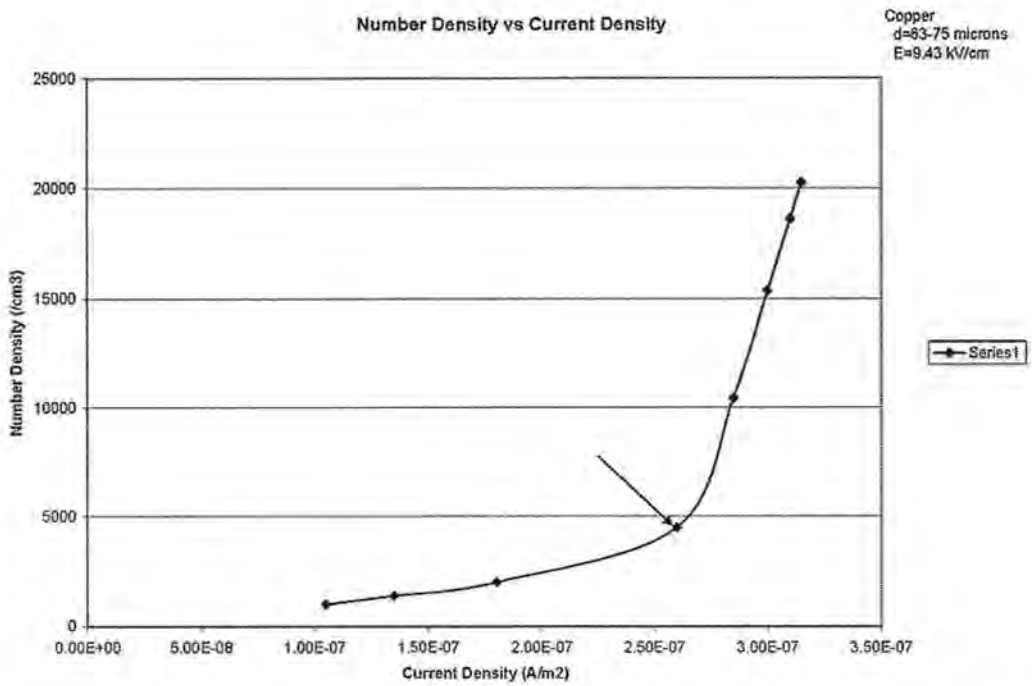

Figure 6.8. The particle number density determined by count (weight). A Graph particle mass vs. current density is shown. The data point corresponding to n = 4495 /cm3 is the particle number density with deposition.

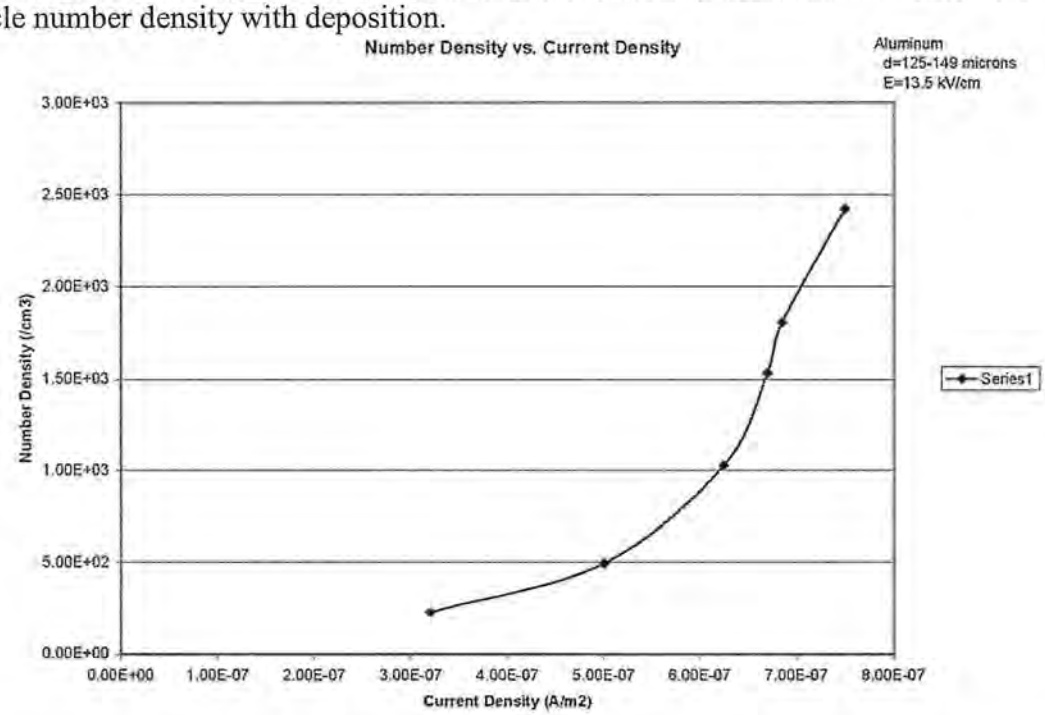

Figure 6.9. Particle number density for 125-149 μm aluminum particles by laser intensity give n = 2956 /cm^3. There were no more aluminum particles in this size range. An undetermined particle number density by count is assumed.

aluminum particles. Particle number density by count is undetermined for this sample. The electric field strengths used were the same used in Table 5.1 for each sample so as to determine particle number density during data collection. Number density calculated based on current density measurements using Equation 2.3.5 were unsuccessful (see Appendix B). This may be due to several assumptions and theoretical values used. The mean-free path for particles was also calculated using Equation 2.4.2. Requirements for the size of the sampling hole were given in Section 2.4 [2]. The ratios of the particle mean free path to sampling hole diameter to particle diameter for a 125-149 μm sample copper particles are given, respectively, $\lambda:d_{hole}:d = 96:14:1$. For 125-149 μm sample aluminum particles, $\lambda:d_{hole}:d = 101:14:1$

Table 6.3 lists calculations for number density by laser intensity and by count (weight), along with particle-particle mean-free path. Particle number density by count and by laser intensity appears to be in generally good agreement. A sample of 125-149 μm copper, however, was not in the range of particle number density predicted by laser intensity. Particle mean-free path values for some samples seem intuitively high. This may be due to experimental error, i.e. errors in measuring particle number density.

A third of determining particle number density can be calculated by measuring the particle (weight) flow rate dN/dt and equating it to

$$\frac{dN}{dt} = A_e J_n = \frac{A_e n \bar{v}}{2} \tag{2.4.6}$$

using the mean particle speed from the distribution. Recall A_e is the area of the leak hole. After data collection for each sample, the thin copper plate substituted and used as the top plate electrode. Particles were allowed to leak out of the test section for t = 5 seconds. Table

Table 6.3. Number density (laser intensity and count) and mean-free path

a. Particle species
b. Particle diameter d (μm)
c. Electric field E (kV/cm)
d. Particle number density by laser intensity (range, /cm^3)
e. Particle number density by laser intensity (average, /cm^3)
f. Particle number density by count (weight) (/cm^3)
g. Particle mean-free path λ (cm)

a. Species	b. d (μm)	c. E (kV/cm)	d. n (range)	e. n (avg.)	f. n (count)	g. λ (cm)
Aluminum	63-75	7.58	4.38-4.46*10^3	4417	4520	1.48
Aluminum	63-75	12.5	4.63-5.49*10^3	5079	5591	1.20
Aluminum	125-149	7.45	9.50-9.79*10^2	960	1217	1.39
Aluminum	125-149	13.5	2.84-3.02*10^3	2956	*N/A	0.57
Copper	63-75	6.82	2.01-2.29*10^3	2205	1753	3.81
Copper	63-75	9.43	4.55-5.12*10^3	4875	4495	1.49
Copper	63-75	13.0	6.17-8.79*10^3	7319	7082	0.94
Copper	125-149	7.58	4.55-4.67*10^2	458	665	2.55
Copper	125-149	9.43	8.21-9.71*10^2	857	857	1.98
Copper	125-149	13.3	1.01-1.13*10^3	1068	1290	1.31

*Undetermined by experiment.
Average particle number density by laser intensity used.

Table 6.4. Particle number density based on particle flow rate

a. Particle species
b. Particle diameter d (μm)
c. Electric field E (kV/cm)
d. Measured particle flow rate dN/dt (/s)
e. Particle mean speed v from Method I (cm/s)
f. Particle mean speed v from Method II (cm/s)
g. Calculated particle number density using mean speed (Method I)
h. Calculated particle number density using mean speed (Method II)
d. Particle number density by laser intensity (range, $/cm^3$)

a. Species	b. d (μm)	c. E (kV/cm)	d. dN/dt (/s)	e. v (I, cm/s)	f. v (II, cm/s)	g. n (I, $/cm^3$)	h. n (II, $/cm^3$)	d. n (range)
Aluminum	63-75	7.58	7963	149.2	167.5	3725	3318	$4.38\text{-}4.46*10^3$
Aluminum	63-75	12.5	15073	136.3	208.6	7716	5045	$4.63\text{-}5.49*10^3$
Aluminum	125-149	7.45	1433	101.5	100.2	986	998	$9.50\text{-}9.79*10^2$
Aluminum	125-149	13.5	1805	95.1	111.4	1325	1131	$2.84\text{-}3.02*10^3$
Copper	63-75	6.82	1050	77.8	111.5	942	657	$2.01\text{-}2.29*10^3$
Copper	63-75	9.43	4434	87.3	78.9	3544	3922	$4.55\text{-}5.12*10^3$
Copper	63-75	13.0	9877	83.5	80.4	8253	8578	$6.17\text{-}8.79*10^3$
Copper	125-149	7.58	256	69.3	75.0	258	239	$4.55\text{-}4.67*10^2$
Copper	125-149	9.43	536	70.7	61.0	529	613	$8.21\text{-}9.71*10^2$
Copper	125-149	13.3	802	65.5	77.3	854	724	$1.01\text{-}1.13*10^3$

6.4 gives particle number density as solved for in Equation 2.4.6. The mean particle speed from Method I and Method II are both used. The range of particle number densities for laser intensity is also listed for reference. None of the measured values in Table 6.4 are in the ranges calculated from laser intensity. Several number density values calculated from Equation 2.4.6 are on the same order of magnitude as those determined by laser intensity and count. The first two methods are not unique compared to the third method. Again, the ranges are only listed for comparison. Table 6.5 gives values of the experimental particle flow rate dN/dt and theoretical values (Equation 2.4.6). Values of particle number density n used to calculate theoretical particle flow are average values based on laser beam attenuation.

Particle mean speed $\bar{v}$ from Method I and Method II were used. Most values do not appear to agree within experimental error, although almost all values are on the same order of magnitude. Difficulties in plugging the leak hole in the copper plate can be attributed to differences in particle flow rate. Errors in particle number density based on laser beam intensity can also be attributed.

Table 6.5. Experimental and theoretical values of particle flow rate

a. Particle species
b. Particle diameter d (μm)
c. Electric field E (kV/cm)
d. Measured flow rate dN/dt (/s)
e. Particle mean speed v from Method I (cm/s)
f. Particle mean speed v from Method II (cm/s)
g. Average particle number density n using laser beam attenuation (Eq. 2.4.10)
h. Theoretical particle flow rate dN/dt (using speed v from Method I)
i. Theoretical particle flow rate dN/dt (using speed v from Method II)

a. Species	b. d (μm)	c. E (kV/cm)	d. dN/dt (/s)	e. v (I, cm/s)	f. v (II, cm/s)	g. n (/cm^3)	h. dN/dt (/s) (I)	i. dN/dt (/s) (II)
Aluminum	63-75	7.58	7963	149.2	167.5	4417	9458	10619
Aluminum	63-75	12.5	15073	136.3	208.6	5079	9938	15201
Aluminum	125-149	7.45	1433	101.5	100.2	960	1398	1380
Aluminum	125-149	13.5	1805	95.1	111.4	2956	4035	4724
Copper	63-75	6.82	1050	77.8	111.5	2205	2461	3528
Copper	63-75	9.43	4434	87.3	78.9	4875	6109	5521
Copper	63-75	13.0	9877	83.5	80.4	7319	8774	8441
Copper	125-149	7.58	256	69.3	75.0	458	455	493
Copper	125-149	9.43	536	70.7	61.0	857	870	751
Copper	125-149	13.3	802	65.5	77.3	1068	1004	1185

7. CONCLUSIONS

The speed distribution of copper and aluminum particles in an electrostatic suspension has been measured by leaking particles out of a small leak hole of a parallel plate electrode and captured above by epoxy-covered glass slides. Data has been fit with a Maxwell speed distribution curve, using two different approaches, assumed to apply in the direction of the electric field. Experimental distribution speed constants have been calculated and compared with single-particle theoretical speeds. Particle number density was calculated by three different methods: laser beam intensity, count (weight), and particle (weight) flow rate. The three methods are generally in good agreement with each other. Experimental values of article flow rate dN/dt were also compared to theoretical values.

8. RECOMMENDATIONS

The present study used a Maxwell curve fit to data. A more in-depth analysis would compare data to other distribution such as a Weibull or Log-Normal plot. A Maxwell distribution may not be unique to the data, and does not appear for some samples. A more open-minded approach is recommended. A curve fit to the data, possibly the same as the aforementioned, in the horizontal direction is also recommended for future study. A more accurate approach besides averaging should be taken to find the horizontal distance.

Most probable speeds have been found experimentally in the present study. An expression relating most probable speed to variables such as electric E, particle diameter d, and particle number density n could be experimentally found by holding two variables constant and varying the other over a range. This is also recommended for future study.

ACKNOWLEDGEMENTS

The author would like to thank the National Aeronautics and Space Administration (NASA) for its funding and support. This work is a NASA-CSA joint sponsored study between Iowa State University and McGill University (Montreal) under NASA Microgravity Combustion Science Grant NCC3-846.

The author would also like to thank Dr. Gerald Colver of Iowa State University for his great efforts in directing and assisting in this project. The author would like to thank the other two members of his POS Committee, Dr. Ron Nelson and Dr. Balaji Narasimhan, for their time and input. The author would also like to thank Dr. Michael Olsen for allowing the author use of his PIV equipment, and to Jim Dautremont for his contribution outside the laboratory. Also, the author would like to thank to Devin Schmacker for his contributions in the laboratory and to David Shoemaker and Andrew Gross for their assistance in data collection.

The author would like to extend a special thanks to Zachari and Danielle Manus for their generous hospitality.

REFERENCES

[1] S.-W. Kim. "Theoretical and experimental studies on flame propagation and quenching of powdered fuels." Thesis. Iowa State University. Department of Mechanical Engineering. 1989.

[2] G.M. Colver, L. J. Ehlinger. "Particle Speed Distribution Measurement in an Electric Particulate Suspension." IEEE Transactions on Industry Applications. Vol. 24, No. 4. July/August 1988. pp. 732-739.

[3] G.M. Colver. "Dynamics of an electric (particulate) suspension. Advances in the Mechanics and the Flow of Granular Materials." 1st Edition, Vol. 1. Trans-Tech., M. Shahinpoor, Edition, Clausthal-Zellerfeld. Federal Republic of Germany; Gulf Publishing Company, Houston. 1983. pp. 355-373.

[4] G.M. Colver, D. I. Howell. "Particle diffusion in an electric suspension. IEEE-IAS Annual Meeting." Vol. 2. Sept. 29-Oct. 3. 1980. pp. 1056-1062.

[5] G.M. Colver, J.A. Cotroneo. "Electrically Augmented Pneumatic Transport of Copper Spheres at Low Particle Reynolds Numbers." Journal of Electrostatics. Vol. 5. pp. 205-223. 1978.

[6] G.M. Colver. "Mass, Heat, and Charge Transfer in an Electric Particulate Suspension. Symposium on Heat and Mass Transfer." Department of Mechanical and Industrial Engineering. University of Illinois at Urbana-Champaign. 1987.

[7] H-C Tsai. "Particle-wall heat transfer in an electric suspension." Thesis. Iowa State University. Department of Mechanical Engineering. 1990.

[8] G.M. Colver, S.W. Kim, T-U Yu. "An electrostatic suspension method for testing spark breakdown, ignition, and quenching distance." Vol. 37. February 1996. pp. 151-172

[9] G.M Colver, C. Eimers. N. Greene. "Quenching of Combustible Dust Mixtures Using Electrostatic Particulate Suspensions (EPS): Review of a New Testing Method for Microgravity." American Institute of Aeronautics and Astronautics. 41st AIAA Aerospace Sciences Meeting and Exhibit. January 2003.

[10] G.M. Colver. "Electric Suspensions Above Fixed, Fluidized, and Acoustically Excited Beds." Journal of Powder & Bulk Solids Technology. No. 4. 2/3. 1980. pp. 21-31.

[11] G.M. Colver. "Dynamic and stationary charging of heavy metallic and dielectric particles against a conducting wall in the presence of a dc applied electric field." Journal of Applied Physics. Vol. 47, No. 11. November 1976. pp. 4839-4849.

[12] J.C. Maxwell. "A Treatise on Electricity and Magnetism." Dover Publishing. Vol.1. 3rd Edition. 1954. p. 276.

[13] N.N. Lebedev, I.P. Skal'skaya. "Force Acting on a Conducting Sphere in the Field of a Parallel Plate Condenser." Soviet Physics, Technological Physics 7. No. 3. 1962. pp. 258-270.

[14] R.M. Olsen. "Essentials of Engineering Fluid Mechanics." New York: Intext Educational. 3rd Edition. 1973. p. 422

[15] C.L. Tein, J.H. Leinhard. "Statistical Thermodynamics." Washington, D.C.: Hemisphere. Chapters 2-3. 1979.

[16] H.S. Taylor, S. Glasstone. "A Treatise on Physical Chemistry." Vol. 2: States of Matter. 3rd Edition. . New York: D. Van Nostrand Company, Inc. pp. 21-27. 1951.

[17] J.R. Hodkinson. "The optical measurement of aerosols." Aerosol Science. C. N. Davies Edition. New York: Academic Press. pp. 287-357. 1966.

[18] W. Edward Deming. "Statistical Adjustment of Data." John Wiley & Sons, Inc. Chapman & Hall, Ltd. London. pp. 38-40. 1946.

APENDIX A: ERROR ANALYSIS

Experimental error is expected during data collection when glass slides were manually exposed to particles. The 2-second time interval was chosen because (1) less error expected over a 1-second time interval and (2) a greater time interval would have increased difficulty in manually counting the particles. An automated leak-hole plug would have allowed particles to leave the test section over a more accurate interval, thus reducing the error in data collection. An automated system for measuring particle flow rate could also reduce error.

SEM photographs of both copper and aluminum show irregularities in their shape. Clearly, aluminum particles (Figures 4.3a, b) are non-spherical. Variables such as volume, mass, and charge were calculated assuming spherical aluminum particles were present. Also, the dynamics of aluminum and copper could be presumed different from each other based on shape. Copper particles (Figures 4.1a, b) have smaller satellite copper particles attached to them. These factors could have an effect on particle charging and collisions. Also, a particle size analyzer would give a better distribution of particles and reduce error in calculations by weighting particle diameter rather than averaging.

Errors in direct measuring exist due to lack of precision of the measuring instruments. This would lead to error propagation in indirect measurement. Deming [18] describes the propagation of mean square error on a relationship of a function F where F=F(x, y, z). If x, y, and z are in error by Δx, Δy, and Δz, respectively, then F has an amount of error ΔF, given as

$$\Delta F^2 = \left(F_x \Delta x\right)^2 + \left(F_y \Delta y\right)^2 + \left(F_z \Delta z\right)^2 \tag{A.1}$$

where F_x, F_y, and F_z are derivatives

$$F_x = \frac{\partial F}{\partial x}, F_y = \frac{\partial F}{\partial y}, F_z = \frac{\partial F}{\partial z} \tag{A.2}$$

An error estimate of directly measured data in the experiment is presented below:

1. The errors in measuring dimensions Pyrex height (L), Pyrex inside diameter (z), and glass slide height (h) above test section are in the order of 0.5%. Error estimates were based on accuracy of calipers used for measurement.
2. Error in measuring particle diameter (d) due to the averaging processes is on the order of 2.0%.
3. Error in measuring the total particle mass (M) using the scale is on the order of .001%.
4. Error in reading the voltage (V) from the voltmeter is on the order of 1.0%.
5. Error in measuring the leak hole (d_h) of the test section is on the order of .5%. Measurements were made using a pass/no-pass drill.

The error associated with indirect measurement can be estimated by the following:

1. The error in calculating particle mass given as

$$m = \frac{\pi d^3}{6}\rho$$

is

$$\begin{aligned}\Delta m &= \left((3\Delta d)^2\right)^{1/2} \\ &= \left((3\times.02)^2\right)^{1/2} \\ &= 6.0\%\end{aligned}$$

2. The error in calculating electric field strength given as

$$E = \frac{V}{L}$$

is

$$\begin{aligned}\Delta E &= \left((\Delta V)^2 + (\Delta L)^2\right)^{1/2} \\ &= \left((.01)^2 + (.005)^2\right)^{1/2} \\ &= 1.1\%\end{aligned}$$

3. The error in calculating the charge per particle given in Equation 2.as

$$Q = \pi\varepsilon_0 d^2 EK$$

is

$$\begin{aligned}\Delta Q &= \left((2\times\Delta d)^2 + (\Delta E)^2\right)^{1/2} \\ &= \left((2\times.02)^2 + (.011)^2\right)^{1/2} \\ &= 4.1\%\end{aligned}$$

4. The error in calculating particle number density given as

$$n = \frac{M}{\left(\frac{\pi d^3}{6}\right)\rho\left(\frac{\pi z^2}{4}\right)L}$$

is

$$\begin{aligned}\Delta n &= \left((\Delta M)^2 + (3\times\Delta d)^2 + (2\times\Delta z)^2 + (\Delta L)^2\right)^{1/2} \\ &= \left((.00001)^2 + (3\times.02)^2 + (2\times.005)^2 + (.005)^2\right)^{1/2} \\ &= 6.2\%\end{aligned}$$

5. The error in calculating the average particle velocity given in Equation 2.2.8 as

$$\bar{v} = \left[\frac{L}{8\left(1-e_t^2e_b^2\right)}\right]^{\frac{1}{2}}\left\{\begin{array}{l}\left[(1+e_t^2)\left(\frac{QE}{m}\right)+(1-e_t^2)g\right]^{\frac{1}{2}}(1+e_b)+ \\ \left[(1+e_b^2)\left(\frac{QE}{m}\right)-(1-e_b^2)g\right]^{\frac{1}{2}}(1+e_t)\end{array}\right\}$$

which can be arranged for $e_t = e_b = e$ to become

$$\bar{v} = \left[\frac{1+e}{1-e}\left(\frac{L}{2}\right)\left(\frac{QE}{m}\right)\right]^{1/2}\left\{1-\frac{1}{8}\left[\frac{1-e^2}{1+e^2}\left(\frac{mg}{QE}\right)\right]^2-\ldots\right\}$$

is approximately

$$\begin{aligned}\Delta\bar{v} &= \left(\left(\frac{1}{2}\times\Delta L\right)^2+\left(\frac{1}{2}\times\Delta Q\right)^2+\left(\frac{1}{2}\times\Delta E\right)^2+\left(\frac{1}{2}\times\Delta m\right)^2\right)^{1/2}\\ &= \left(\left(\frac{1}{2}\times.005\right)^2+\left(\frac{1}{2}\times.041\right)^2+\left(\frac{1}{2}\times.011\right)^2+\left(\frac{1}{2}\times.06\right)^2\right)^{1/2}\\ &= 3.7\%\end{aligned}$$

APPENDIX B: MATHEMATICA PROGRAMS

1. Mathematica program written to numerically solve equation of motion. The initial speed was found based on particle height. The value p is the number of points calculated. For data collection, p = 3000 to find close values for height h used in experimentation. For simplicity, p = 10 is shown.
2. Values of particle number density based on experimental values of current density were not successful. Figure B.1 shows the Mathematica program that calculated number density. Values differed by several orders of magnitude. By observation, these calculations appeared to be incorrect.

1. Mathematica progam to numerically solve equation of motion

ParticlePathwdrag.nb 1

- **Solve equations of motion for single particle in two-dimension including inertia, gravity, and particle drag given initial conditions for particle velocity & position. Time is independent variable. Numerical solution (NDSolve).**

G. Colver Sept 8, 2002
Version 2 (drag force =finite)

Nomenclature:
vz: vertical component of particle velocity
vr: horizontal component of particle velocity
m: particle mass
z: vertical distance (+ is up)
r: horizontal distance
g: acceleration of gravity
t: time

Clear all variables

```
Clear["@"]
```

Install log-log plot

```
<< Graphics`Graphics
```

Initial conditions for particle velocity and position

```
vro = 0;
vzo = 0;
ro = 0;
zo = 0;
```

Specify particle time of flight t1 (seconds) - Corrected (this is now calculated from particle diameter)

```
t0 = 0.0;
t1 = -.135;
```

Set p is number of time increments (to plot) during time of flilght t1

```
p = 10;
```

Data input: gravity, particle density, particle diameter, gas density, gas viscosity (MKS0

```
gz = 9.81;
ρ = 2.7 10^3;
d = 137 * 10^-6;
ρf = 1.2;
μ = 1.816 * 10^-5;
m = (π d^3)/6 ρ;
re[t_] := (ρf √((vz[t]^2 + vr[t]^2)) d)/μ
τ := m/(  ) (1 + 3 re[t] / 16)^-0.5;

tl = t11[d 10^6]

-0.197023
```

Numerical solve equation of motion of particle (with finite drag)

```
ss = NDSolve[{vr'[t] == -vr[t] / τ, vz'[t] == -vz[t] / τ - gz, r'[t] == vr[t], z'[t] == vz[t],
    vr[0] == vro, vz[0] == vzo, r[0] == ro, z[0] == zo}, {vr, vz, r, z}, {t, t0, tl}];
```

Extract particle velocity (versus time) and particle position (versus time) from ss

```
v[t_] = vz[t] /. ss;
zz[t_] = -z[t] /. ss;
```

Generate table of values from ss for plotting velocity versus particle height (eliminate time as a parameter)

```
table1 = Table[{First[v[t tl / p]], First[zz[t tl / p]]}, {t, 0, p}]

{{0., 0.}, {0.138827, 0.000922069}, {0.2932, 0.00381829}, {0.468031, 0.00893035},
 {0.669685, 0.0165755}, {0.90668, 0.0271704}, {1.19077, 0.0412671},
 {1.53864, 0.0596071}, {1.97474, 0.0832056}, {2.53613, 0.113486}, {3.28128, 0.152503}}
```

Linear plot - particle height (m) versus particle initial velocity (m/s)

```
ListPlot[table1]
```

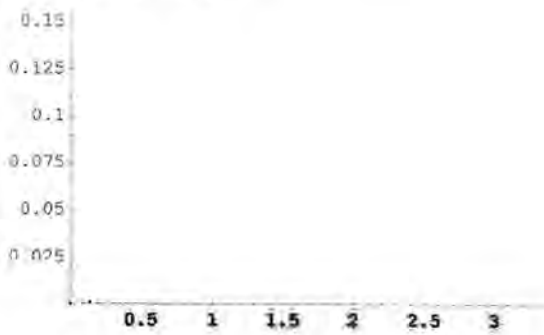


```
- Graphics -
```

Log-Log plot - particle height (m) versus particle initial velocity (m/s)

```
LogLogListPlot[table1]
```

```
LogLogListPlot[{{0., 0.}, {0.138827, 0.000922069},
  {0.2932, 0.00381829}, {0.468031, 0.00893035}, {0.669685, 0.0165755},
  {0.90668, 0.0271704}, {1.19077, 0.0412671}, {1.53864, 0.0596071},
  {1.97474, 0.0832056}, {2.53613, 0.113486}, {3.28128, 0.152503}}]
```

Linear plot - particle height (m) versus time (seconds)& particle initial velocity (m/s) versus time (seconds)

```
Plot[{v[t], zz[t]}, {t, t0, t1}]
```

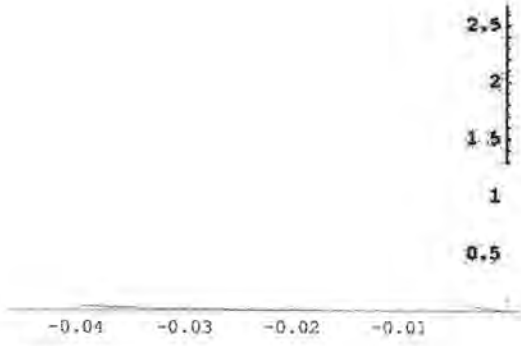


```
- Graphics -
```

2. Mathematica program to solve for number density based on current density

number density (current meas.).nb

Number density, based on current density (MKS units)

```
Q = 1.486 * 10^-13;
L = .01993;
d = 69 * 10^-6;
σ = π * d^2;
J = 8.4 * 10^-8;
v = 1.178;
```

```
Solve[J == n * Q * v * Exp[-n * σ * l], n]
```

$$\left\{\left\{n \to -\frac{\text{ProductLog}\left[-\frac{J l \sigma}{Q v}\right]}{l \sigma}\right\}\right\}$$

```
Solve[J == n * Q * v * Exp[-n * σ * l], n]
```

Approximate number density

```
J / (Q * v)
```

```
479861.
```

$$\frac{\text{ProductLog}\left[-\frac{J * l * \sigma}{Q * v}\right]}{l * \sigma}$$

```
479929
```

n = 479929 / m^3 = .479929 / cm^3

APPENDIX C: CALCULATIONS

Calculations were done using Mathematica and Excel. Any equations involving integrals was input into Mathematica and solved. Values that require no rigorous math were calculated by Excel and are listed in previous tables.

1. Tabular values for Maxwell speed distribution curve fit for Method I and Method II. Excel Solver (Microsoft) was used to calculate a most probable speed v_0 by minimizing sum of squares error SSE. Cells containing #NUM are due to calculating the logarithm (natural) of zero. Samples with relatively low electric field strength did not contain any particles.

2. Maxwell speed distribution curve-fitting data using Method I

METHOD I: Maxwell-type Speed Distribution

a. Glass slide number (4.B.1 is the first glass slide above test section)
b. Glass slide height (h) above test section
c. Initial velocity (v(t=0)) required to reach maximum height h
d. Total number of particle (N) per slide
e. Fractional number of particles (N/N_0) to reach height, h (N_0 = total number of particles)
f. Theoretical Maxwellian fractional number (N'/N_0') of particles to reach height, h (Eq. 2.4.8)
g. Error (experimental-theoretical)
h. $Error^2$
i. Sum of Squared Error terms (SSE)

Aluminum, d=63-75 μm, E=7.58 kV/cm

a. Slide #	b. h	c. v(t=0)	d. N	e. N/N_0	f. N'/N_0'	g. Error	h. $Error^2$	i. SSE
All	0.000	0.000	2664	1.000	1.000	0.000	0.000	0.001
4.C.1	2.920	151.970	1647	0.618	0.619	-0.001	0.000	
4.C.2	4.230	212.420	692	0.260	0.271	-0.011	0.000	
4.C.3	5.515	265.930	294	0.110	0.088	0.022	0.000	
4.C.4	6.845	343.950	26	0.010	0.009	0.001	0.000	
4.C.5	8.170	416.650	3	0.001	0.001	0.001	0.000	
4.C.6	9.505	494.850	2	0.001	0.000	0.001	0.000	
4.C.7	10.860	578.130	0	0.000	0.000	0.000	0.000	

Most Probable Speed

v0: 132.236 cm/s

Aluminum, d=63-75 μm, E=12.5 kV/cm

a. Slide #	b. h	c. v(t=0)	d. N	e. N/N_0	f. N'/N_0'	g. Error	h. $Error^2$	i. SSE
All	0.000	0.000	13748	1.000	1.000	0.000	0.000	0.073
4.B.1	2.920	151.970	4999	0.364	0.531	-0.167	0.028	
4.B.2	4.230	212.420	4519	0.329	0.186	0.143	0.020	
4.B.3	5.515	265.930	2279	0.166	0.046	0.120	0.014	
4.B.4	6.845	343.950	1354	0.098	0.003	0.096	0.009	
4.B.5	8.170	416.650	490	0.036	0.000	0.036	0.001	
4.B.6	9.505	494.850	96	0.007	0.000	0.007	0.000	
4.B.7	10.860	578.130	11	0.001	0.000	0.001	0.000	

Most Probable Speed

v0: 120.836 cm/s

Aluminum, d=125-149 μm, E=7.45 kV/cm

a. Slide #	b. h	c. v(t=0)	d. N	e. N/N_0	f. N'/N_0'	g. Error	h. $Error^2$	i. SSE
All	0.000	0.000	143	1.000	1.000	0.000	0.000	0.102
5.B.1	3.860	113.820	111	0.776	0.524	0.252	0.063	
5.B.2	5.170	139.070	32	0.224	0.310	-0.087	0.007	
5.B.3	6.455	163.010	0	0.000	0.160	-0.160	0.026	
5.B.4	7.785	187.590	0	0.000	0.069	-0.069	0.005	
5.B.5	9.110	212.010	0	0.000	0.025	-0.025	0.001	
5.B.6	10.445	236.770	0	0.000	0.008	-0.008	0.000	
5.B.7	11.800	262.180	0	0.000	0.002	-0.002	0.000	

Most Probable Speed

v0: 89.928 cm/s

Aluminum, d=125-149 μm, E=13.5 kV/cm

a. Slide #	b. h	c. v(t=0)	d. N	e. N/N_0	f. N'/N_0'	g. Error	h. Error^2	i. SSE
All	0.000	0.000	5413	1.000	1.000	0.000	0.000	0.015
5.C.1	3.860	113.820	2125	0.380	0.456	-0.076	0.006	
5.C.2	5.170	139.070	1509	0.270	0.245	0.025	0.001	
5.C.3	6.455	163.010	890	0.159	0.113	0.047	0.002	
5.C.4	7.785	187.590	503	0.090	0.042	0.048	0.002	
5.C.5	9.110	212.010	385	0.069	0.013	0.056	0.003	
5.C.6	10.445	236.770	0	0.031	0.003	0.028	0.001	
5.C.7	11.800	262.180	1	0.000	0.001	0.000	0.000	

Most Probable Speed

v0: 84.306 cm/s

Copper, d=63-75 μm, E=6.82 kV/cm

a. Slide #	b. h	c. v(t=0)	d. N	e. N/N_0	f. N'/N_0'	g. Error	h. Error^2	i. SSE
All	0.000	0.000	27	1.000	1.000	0.000	0.000	0.030
2.A.1	2.920	95.460	11	0.407	0.429	-0.021	0.000	
2.A.2	4.230	121.300	4	0.148	0.185	-0.037	0.001	
2.A.3	5.515	145.200	4	0.148	0.064	0.084	0.007	
2.A.4	6.845	169.150	2	0.074	0.017	0.057	0.003	
2.A.5	8.170	192.660	3	0.111	0.004	0.108	0.012	
2.A.6	9.505	216.010	2	0.074	0.001	0.073	0.005	
2.A.7	10.860	239.720	1	0.037	0.000	0.037	0.001	

Most Probable Speed

v0: 68.935 cm/s

Copper, d=63-75 μm, E=9.43 kV/cm

a. Slide #	b. h	c. v(t=0)	d. N	e. N/N_0	f. N'/N_0'	g. Error	h. Error^2	i. SSE
All	0.000	0.000	1308	1.000	1.000	0.000	0.000	0.012
2.B.1	2.920	95.460	825	0.631	0.551	0.080	0.006	
2.B.2	4.230	121.300	358	0.274	0.296	-0.023	0.001	
2.B.3	5.515	145.200	99	0.076	0.134	-0.058	0.003	
2.B.4	6.845	169.150	18	0.014	0.049	-0.035	0.001	
2.B.5	8.170	192.660	6	0.005	0.015	-0.010	0.000	
2.B.6	9.505	216.010	1	0.001	0.004	-0.003	0.000	
2.B.7	10.860	239.720	1	0.001	0.001	0.000	0.000	

Most Probable Speed

v0: 77.387 cm/s

Copper, d=63-75 μm, E=13.0 kV/cm

a. Slide #	b. h	c. v(t=0)	d. N	e. N/N_0	f. N'/N_0'	g. Error	h. Error^2	i. SSE
All	0.000	0.000	12120	1.000	1.000	0.000	0.000	0.023
2.C.1	2.920	95.460	4830	0.399	0.505	-0.106	0.011	
2.C.2	4.230	121.300	3595	0.297	0.252	0.045	0.002	
2.C.3	5.515	145.200	2143	0.177	0.104	0.073	0.005	
2.C.4	6.845	169.150	1177	0.097	0.034	0.063	0.004	
2.C.5	8.170	192.660	372	0.031	0.009	0.022	0.000	
2.C.6	9.505	216.010	1	0.000	0.002	-0.002	0.000	
2.C.7	10.860	239.720	2	0.000	0.000	0.000	0.000	

Most Probable Speed

v0: 74.036 cm/s

Copper, d=125-149 μm, E=7.58 kV/cm

a. Slide #	b. h	c. v(t=0)	d. N	e. N/N_0	f. N'/N_0'	g. Error	h. Error^2	i. SSE
All	0.000	0.000	65	1.000	1.000	0.000	0.000	0.043
3.A.1	2.920	81.150	41	0.631	0.474	0.156	0.024	
3.A.2	4.230	99.440	11	0.169	0.259	-0.090	0.008	
3.A.3	5.515	111.100	4	0.062	0.158	-0.097	0.009	
3.A.4	6.845	130.530	3	0.046	0.058	-0.012	0.000	
3.A.5	8.170	144.730	2	0.031	0.024	0.006	0.000	
3.A.6	9.505	158.320	2	0.031	0.009	0.021	0.000	
3.A.7	10.860	171.480	2	0.031	0.003	0.027	0.001	

Most Probable Speed

v0: 61.140 cm/s

Copper, d=125-149 μm, E=9.43 kV/cm

a. Slide #	b. h	c. v(t=0)	d. N	e. N/N_0	f. N'/N_0'	g. Error	h. Error^2	i. SSE
All	0.000	0.000	826	1.000	1.000	0.000	0.000	0.032
3.B.1	2.920	81.150	524	0.634	0.500	0.134	0.018	
3.B.2	4.230	99.440	218	0.264	0.284	-0.020	0.000	
3.B.3	5.515	111.100	65	0.079	0.179	-0.100	0.010	
3.B.4	6.845	130.530	13	0.016	0.070	-0.054	0.003	
3.B.5	8.170	144.730	3	0.004	0.031	-0.027	0.001	
3.B.6	9.505	158.320	2	0.002	0.012	-0.010	0.000	
3.B.7	10.860	171.480	1	0.001	0.005	-0.004	0.000	

Most Probable Speed

v0: 62.664 cm/s

Copper, d=125-149 μm, E=13.3 kV/cm

a. Slide #	b. h	c. v(t=0)	d. N	e. N/N_0	f. N'/N_0'	g. Error	h. Error^2	i. SSE
All	0.000	0.000	5039	1.000	1.000	0.000	0.000	0.021
3.C.1	2.920	81.150	1693	0.336	0.419	-0.083	0.007	
3.C.2	4.230	99.440	1197	0.238	0.209	0.028	0.001	
3.C.3	5.515	111.100	793	0.157	0.120	0.038	0.001	
3.C.4	6.845	130.530	598	0.119	0.039	0.080	0.006	
3.C.5	8.170	144.730	335	0.066	0.014	0.052	0.003	
3.C.6	9.505	158.320	241	0.048	0.005	0.043	0.002	
3.C.7	10.860	171.480	182	0.036	0.002	0.035	0.001	

Most Probable Speed

v0: 58.060 cm/s

2. Maxwell speed distribution curve-fitting data using Method II

METHOD II: Maxwell-type Speed Distribution (Method II)

a. Glass slide number (4.B.1 is the first glass slide above test section)
b. Glass slide height (h) above test section
c. Initial velocity (v(t=0)) required to reach maximum height, h
d. Total number of particle (N) per slide
e. Fractional number of particles (N/N_0) to reach height, h (N_0 = total number of particles)
f. Natural logarithm of N/N_0
g. Theoretical Maxwellian fractional number (N'/N_0') of particles to reach height, h (Eq. 2.4.8)
h. Natural logarithm of N'/N_0'
i. Error (Ln(experimental)-Ln(theoretical))
j. Error^2
k. Sum of Squared Error terms (SSE)

Aluminum, d=63-75 μm, E=7.58 kV/cm

a. Slide #	b. h	c. v(t=0)	d. N	e. N/N_0	f. $Ln(N/N_0)$	g. N'/N_0'	h. $Ln(N'/N_0')$	i. Error	j. Error^2	k. SSE
All	0.000	0.000	2664	1.000	0.000	1.000	0.000	0.000	0.000	4.844
4.B.1	2.920	151.970	1647	0.618	-0.481	0.718	-0.331	-0.150	0.023	
4.B.2	4.230	212.420	692	0.260	-1.348	0.394	-0.932	-0.416	0.173	
4.B.3	5.515	265.930	294	0.110	-2.204	0.170	-1.770	-0.434	0.188	
4.B.4	6.845	343.950	26	0.010	-4.629	0.030	-3.514	-1.115	1.244	
4.B.5	8.170	416.650	3	0.001	-6.789	0.003	-5.690	-1.099	1.209	
4.B.6	9.505	494.850	2	0.001	-7.194	0.000	-8.611	1.417	2.008	
4.B.7	10.860	578.130	0	0.000	#NUM!	0.000	-12.375	#NUM!	#NUM!	

Most Probable Speed

v0: 148.496 cm/s

Aluminum, d=63-75 μm, E=12.5 kV/cm

a. Slide #	b. h	c. v(t=0)	d. N	e. N/N_0	f. $Ln(N/N_0)$	g. N'/N_0'	h. $Ln(N'/N_0')$	i. Error	j. Error^2	k. SSE
All	0.000	0.000	13748	1.000	0.000	1.000	0.000	0.000	0.000	2.061
4.B.1	2.920	151.970	4999	0.364	-1.012	0.852	-0.160	-0.852	0.726	
4.B.2	4.230	212.420	4519	0.329	-1.113	0.619	-0.479	-0.634	0.402	
4.B.3	5.515	265.930	2279	0.166	-1.797	0.387	-0.948	-0.849	0.721	
4.B.4	6.845	343.950	1354	0.098	-2.318	0.140	-1.967	-0.351	0.123	
4.B.5	8.170	416.650	490	0.036	-3.334	0.038	-3.276	-0.058	0.003	
4.B.6	9.505	494.850	96	0.007	-4.964	0.006	-5.067	0.103	0.011	
4.B.7	10.860	578.130	11	0.001	-7.131	0.001	-7.405	0.274	0.075	

Most Probable Speed

v0: 184.84 cm/s

Aluminum, d=125-149 μm, E=7.45 kV/cm

a. Slide #	b. h	c. v(t=0)	d. N	e. N/N_0	f. $Ln(N/N_0)$	g. N'/N_0'	h. $Ln(N'/N_0')$	i. Error	j. Error^2	k. SSE
All	0.000	0.000	143	1.000	0.000	1.000	0.000	0.000	0.000	0.254
5.B.1	3.860	113.820	111	0.776	-0.253	0.503	-0.688	0.434	0.189	
5.B.2	5.170	139.070	32	0.224	-1.497	0.289	-1.242	-0.255	0.065	
5.B.3	6.455	163.010	0	0.000	#NUM!	0.144	-1.938	#NUM!	#NUM!	
5.B.4	7.785	187.590	0	0.000	#NUM!	0.059	-2.824	#NUM!	#NUM!	
5.B.5	9.110	212.010	0	0.000	#NUM!	0.021	-3.877	#NUM!	#NUM!	
5.B.6	10.445	236.770	0	0.000	#NUM!	0.006	-5.118	#NUM!	#NUM!	
5.B.7	11.800	262.180	0	0.000	#NUM!	0.001	-6.571	#NUM!	#NUM!	

Most Probable Speed

v0: 88.083 cm/s

Aluminum, d=125-149 μm, E=13.5 kV/cm

a. Slide #	b. h	c. v(t=0)	d. N	e. N/N_0	f. $Ln(N/N_0)$	g. N'/N_0'	h. $Ln(N'/N_0')$	i. Error	j. Error^2	k. SSE
All	0.000	0.000	5413	1.000	0.000	1.000	0.000	0.000	0.000	0.884
5.C.1	3.860	113.820	2125	0.380	-0.967	0.616	-0.484	-0.483	0.233	
5.C.2	5.170	139.070	1509	0.270	-1.309	0.410	-0.892	-0.417	0.174	
5.C.3	6.455	163.010	890	0.159	-1.837	0.244	-1.412	-0.425	0.181	
5.C.4	7.785	187.590	503	0.090	-2.408	0.124	-2.084	-0.324	0.105	
5.C.5	9.110	212.010	385	0.069	-2.675	0.056	-2.889	0.214	0.046	
5.C.6	10.445	236.770	0	0.031	-3.464	0.021	-3.845	0.381	0.146	
5.C.7	11.800	262.180	1	0.000	-8.628	0.007	-4.970	-3.658	13.380	

Most Probable Speed

v0: 98.694 cm/s

Copper, d=63-75 μm, E=6.82 kV/cm

a. Slide #	b. h	c. v(t=0)	d. N	e. N/N_0	f. $Ln(N/N_0)$	g. N'/N_0'	h. $Ln(N'/N_0')$	i. Error	j. Error^2	k. SSE
All	0.000	0.000	27	1.000	0.000	1.000	0.000	0.000	0.000	4.646
2.A.1	2.920	95.460	11	0.407	-0.898	0.760	-0.274	-0.624	0.389	
2.A.2	4.230	121.300	4	0.148	-1.910	0.556	-0.588	-1.322	1.747	
2.A.3	5.515	145.200	4	0.148	-1.910	0.365	-1.009	-0.901	0.812	
2.A.4	6.845	169.150	2	0.074	-2.603	0.210	-1.561	-1.042	1.085	
2.A.5	8.170	192.660	3	0.111	-2.197	0.107	-2.232	0.035	0.001	
2.A.6	9.505	216.010	2	0.074	-2.603	0.049	-3.024	0.421	0.177	
2.A.7	10.860	239.720	1	0.037	-3.296	0.019	-3.955	0.659	0.434	

Most Probable Speed

v0: 98.824 cm/s

Copper, d=63-75 μm, E=9.43 kV/cm

a. Slide #	b. h	c. v(t=0)	d. N	e. N/N_0	f. $Ln(N/N_0)$	g. N'/N_0'	h. $Ln(N'/N_0')$	i. Error	j. Error^2	k. SSE
All	0.000	0.000	1308	1.000	0.000	1.000	0.000	0.000	0.000	0.364
2.B.1	2.920	95.460	825	0.631	-0.461	0.444	-0.811	0.350	0.123	
2.B.2	4.230	121.300	358	0.274	-1.296	0.198	-1.620	0.324	0.105	
2.B.3	5.515	145.200	99	0.076	-2.581	0.071	-2.641	0.060	0.004	
2.B.4	6.845	169.150	18	0.014	-4.286	0.020	-3.926	-0.360	0.130	
2.B.5	8.170	192.660	6	0.005	-5.384	0.004	-5.438	0.054	0.003	
2.B.6	9.505	216.010	1	0.001	-7.176	0.001	-7.185	0.008	0.000	
2.B.7	10.860	239.720	1	0.001	-7.176	0.000	-9.204	2.027	4.110	

Most Probable Speed

v0: 69.936 cm/s

Copper, d=63-75 μm, E=13.0 kV/cm

a. Slide #	b. h	c. v(t=0)	d. N	e. N/N_0	f. $Ln(N/N_0)$	g. N'/N_0'	h. $Ln(N'/N_0')$	i. Error	j. Error^2	k. SSE
All	0.000	0.000	12120	1.000	0.000	1.000	0.000	0.000	0.000	12.070
2.C.1	2.920	95.460	4830	0.399	-0.920	0.464	-0.768	-0.152	0.023	
2.C.2	4.230	121.300	3595	0.297	-1.215	0.215	-1.539	0.324	0.105	
2.C.3	5.515	145.200	2143	0.177	-1.733	0.081	-2.516	0.783	0.613	
2.C.4	6.845	169.150	1177	0.097	-2.332	0.024	-3.747	1.415	2.002	
2.C.5	8.170	192.660	372	0.031	-3.484	0.006	-5.198	1.715	2.940	
2.C.6	9.505	216.010	1	0.000	-9.403	0.001	-6.876	-2.527	6.386	
2.C.7	10.860	239.720	2	0.000	-8.709	0.000	-8.816	0.106	0.011	

Most Probable Speed

v0: 71.225 cm/s

Copper, d=125-149 μm, E=7.58 kV/cm

a. Slide #	b. h	c. v(t=0)	d. N	e. N/N_0	f. $Ln(N/N_0)$	g. N'/N_0'	h. $Ln(N'/N_0')$	i. Error	j. $Error^2$	k. SSE
All	0.000	0.000	65	1.000	0.000	1.000	0.000	0.000	0.000	4.546
3.A.1	2.920	81.150	41	0.631	-0.461	0.561	-0.579	0.118	0.014	
3.A.2	4.230	99.440	11	0.169	-1.776	0.345	-1.065	-0.712	0.507	
3.A.3	5.515	111.100	4	0.062	-2.788	0.232	-1.462	-1.326	1.758	
3.A.4	6.845	130.530	3	0.046	-3.076	0.102	-2.279	-0.797	0.635	
3.A.5	8.170	144.730	2	0.031	-3.481	0.050	-2.997	-0.484	0.234	
3.A.6	9.505	158.320	2	0.031	-3.481	0.023	-3.780	0.298	0.089	
3.A.7	10.860	171.480	2	0.031	-3.481	0.010	-4.626	1.144	1.309	

Most Probable Speed

v0: 66.438 cm/s

Copper, d=125-149 μm, E=9.43 kV/cm

a. Slide #	b. h	c. v(t=0)	d. N	e. N/N_0	f. $Ln(N/N_0)$	g. N'/N_0'	h. $Ln(N'/N_0')$	i. Error	j. $Error^2$	k. SSE
All	0.000	0.000	826	1.000	0.000	1.000	0.000	0.000	0.000	1.161
3.B.1	2.920	81.150	524	0.634	-0.455	0.342	-1.072	0.617	0.381	
3.B.2	4.230	99.440	218	0.264	-1.332	0.149	-1.903	0.571	0.326	
3.B.3	5.515	111.100	65	0.079	-2.542	0.077	-2.567	0.025	0.001	
3.B.4	6.845	130.530	13	0.016	-4.152	0.020	-3.904	-0.248	0.061	
3.B.5	8.170	144.730	3	0.004	-5.618	0.006	-5.061	-0.557	0.310	
3.B.6	9.505	158.320	2	0.002	-6.023	0.002	-6.310	0.286	0.082	
3.B.7	10.860	171.480	1	0.001	-6.717	0.000	-7.649	0.933	0.870	

Most Probable Speed

v0: 54.087 cm/s

Copper, d=125-149 μm, E=13.3 kV/cm

a. Slide #	b. h	c. v(t=0)	d. N	e. N/N_0	f. $Ln(N/N_0)$	g. N'/N_0'	h. $Ln(N'/N_0')$	i. Error	j. $Error^2$	k. SSE
All	0.000	0.000	5039	1.000	0.000	1.000	0.000	0.000	0.000	1.002
3.B.1	2.920	81.150	1693	0.336	-1.091	0.591	-0.526	-0.565	0.319	
3.B.2	4.230	99.440	1197	0.238	-1.437	0.378	-0.972	-0.466	0.217	
3.B.3	5.515	111.100	793	0.157	-1.849	0.262	-1.339	-0.510	0.260	
3.B.4	6.845	130.530	598	0.119	-2.131	0.123	-2.095	-0.037	0.001	
3.B.5	8.170	144.730	335	0.066	-2.711	0.063	-2.761	0.051	0.003	
3.B.6	9.505	158.320	241	0.048	-3.040	0.031	-3.489	0.449	0.202	
3.B.7	10.860	171.480	182	0.036	-3.321	0.014	-4.277	0.956	0.914	

Most Probable Speed

v0: 68.542 cm/s

APPENDIX D. GRAPHS

1. Graphs of number of particles vs. particles height and corresponding number of particles vs. initial velocity for d = 63-75 μm aluminum particles, 125-149 μm aluminum particles, 63-75 μm copper particles, and 125-149 μm copper particles.
2. Graphical comparisons of Maxwell curve fit for Method I and Method II from values in C.2.

1. d = 63-75 μm aluminum particles

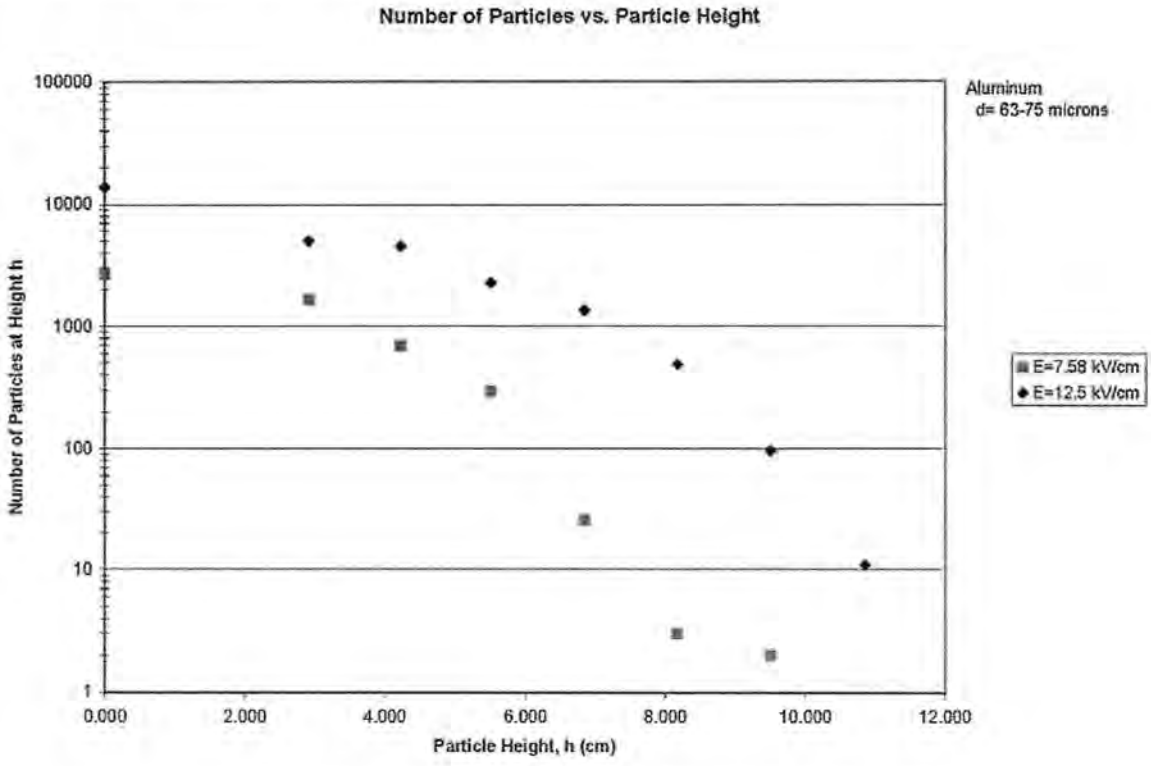

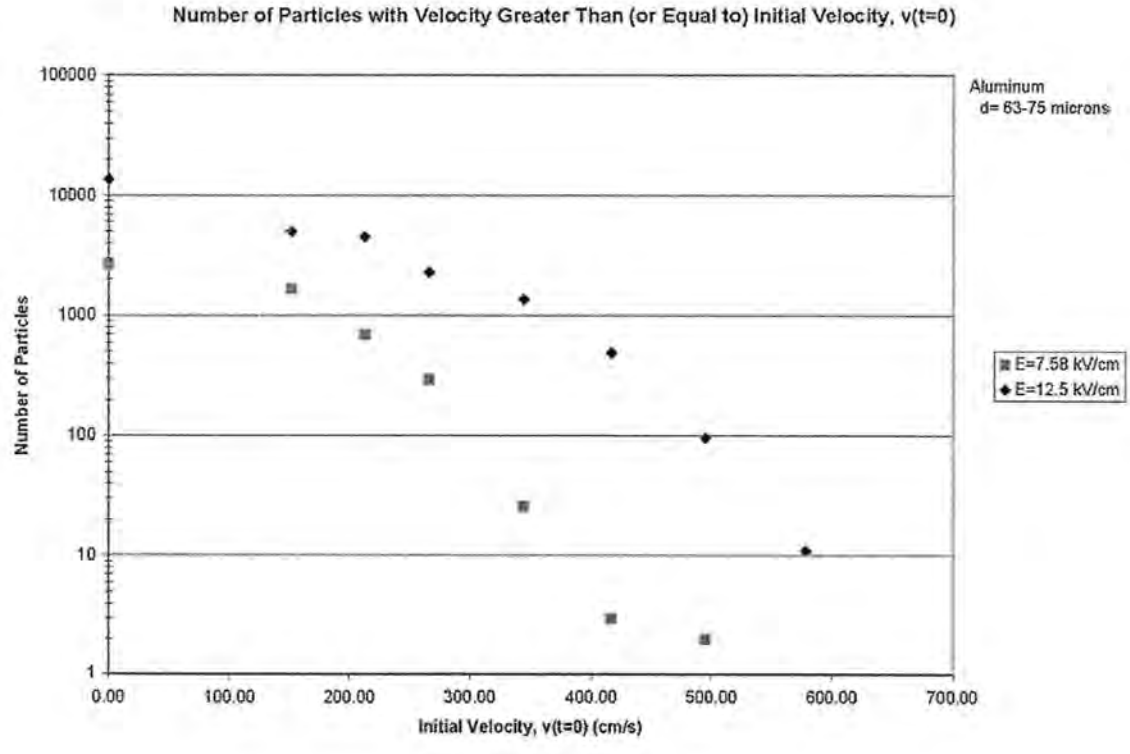

1. d = 125-149 μm aluminum particles

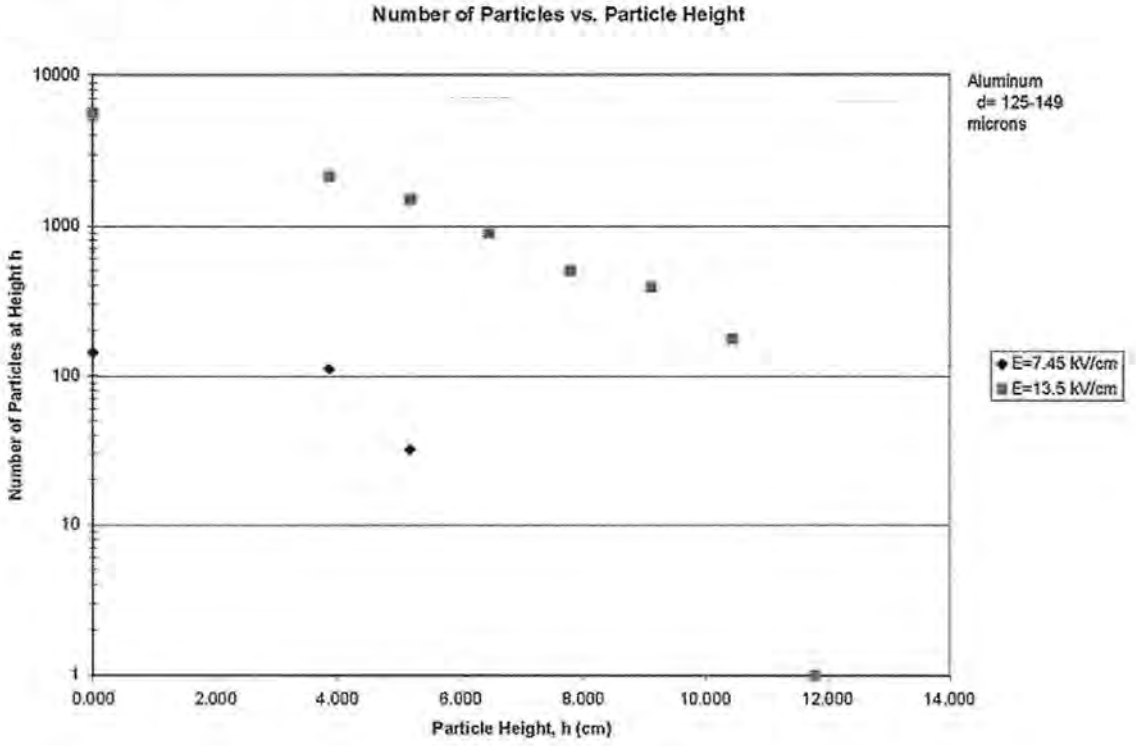

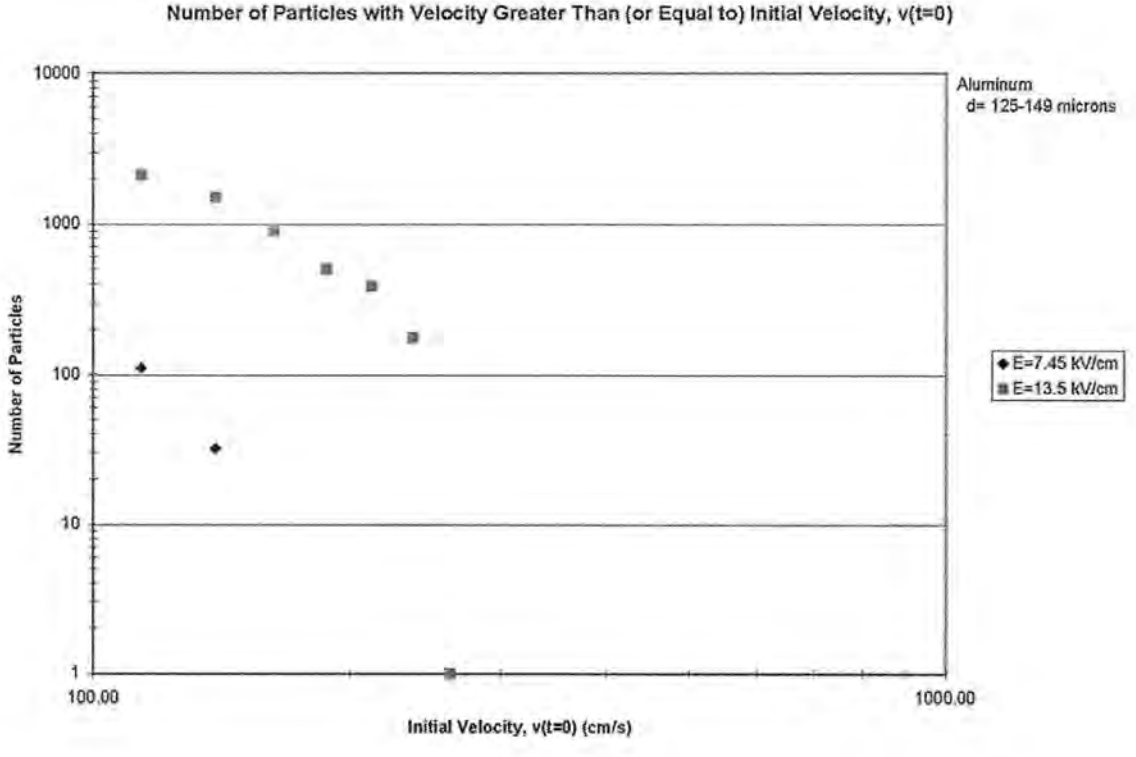

1. d = 63-75 μm copper particles

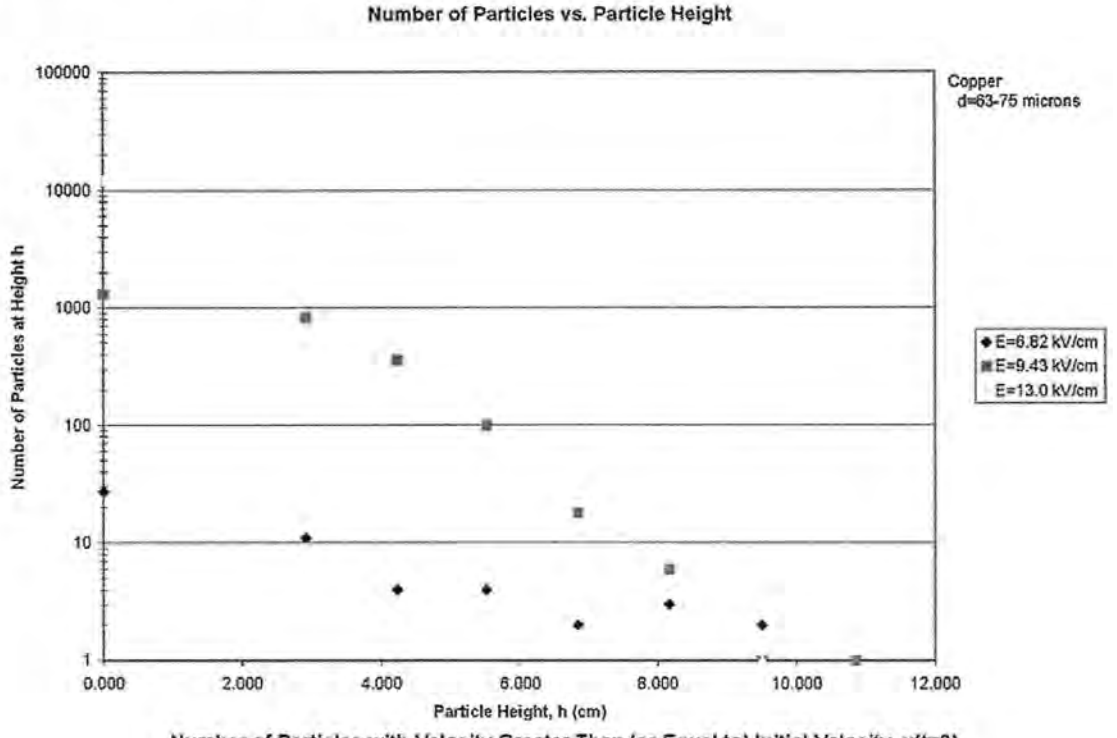

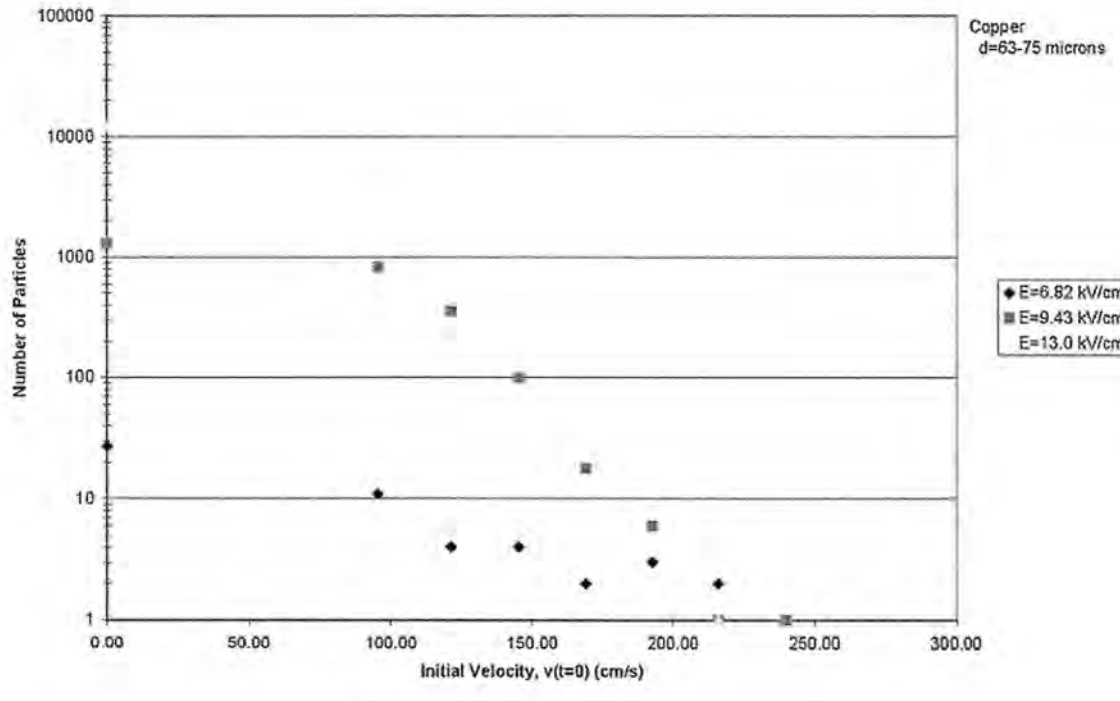

1. d = 125-149 μm copper particle

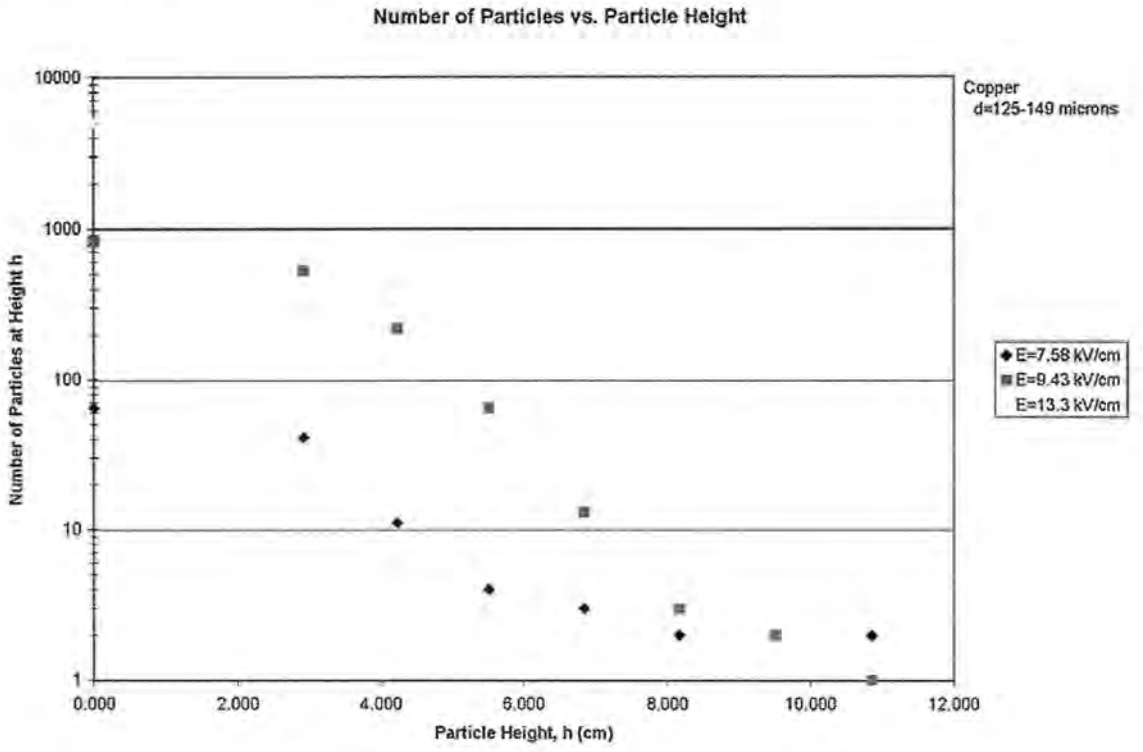

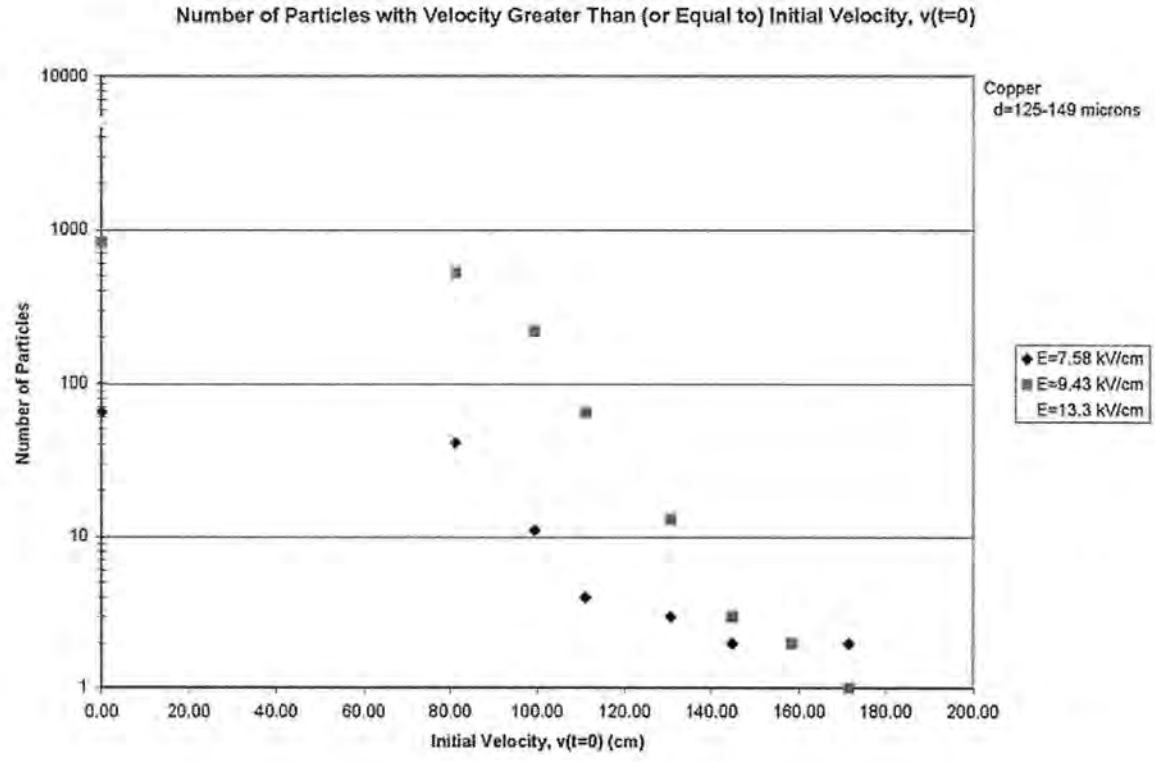

2. Comparison of Method I and Method II for aluminum particles.
   d = 63-75 μm, E = 7.58 kV/cm, L = 1.993 cm.

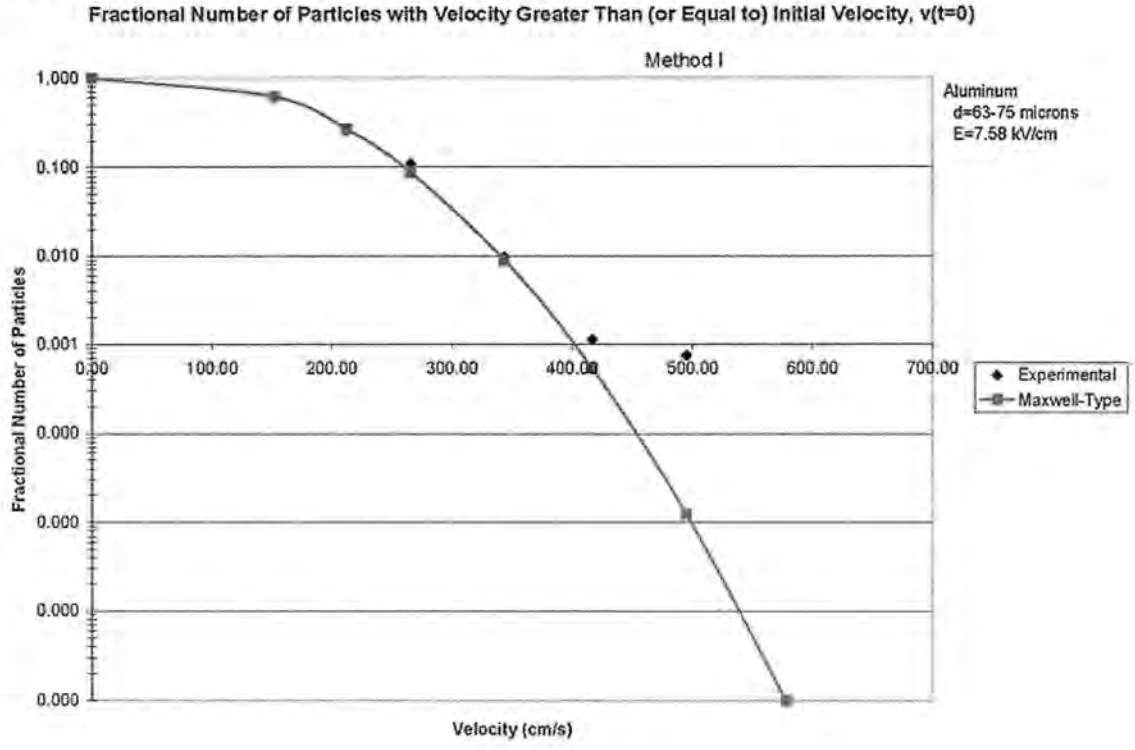

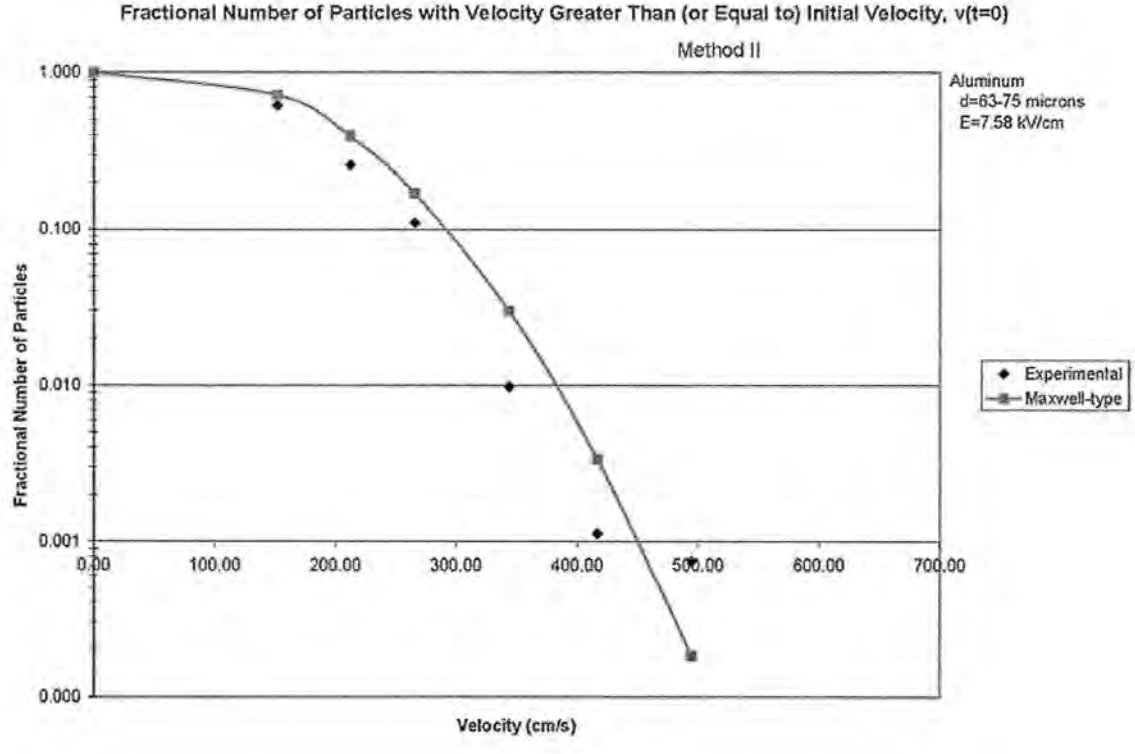

2. Comparison of Method I and Method II for aluminum particles.
   d = 63-75 μm, E = 12.5 kV/cm, L = 1.993 cm.

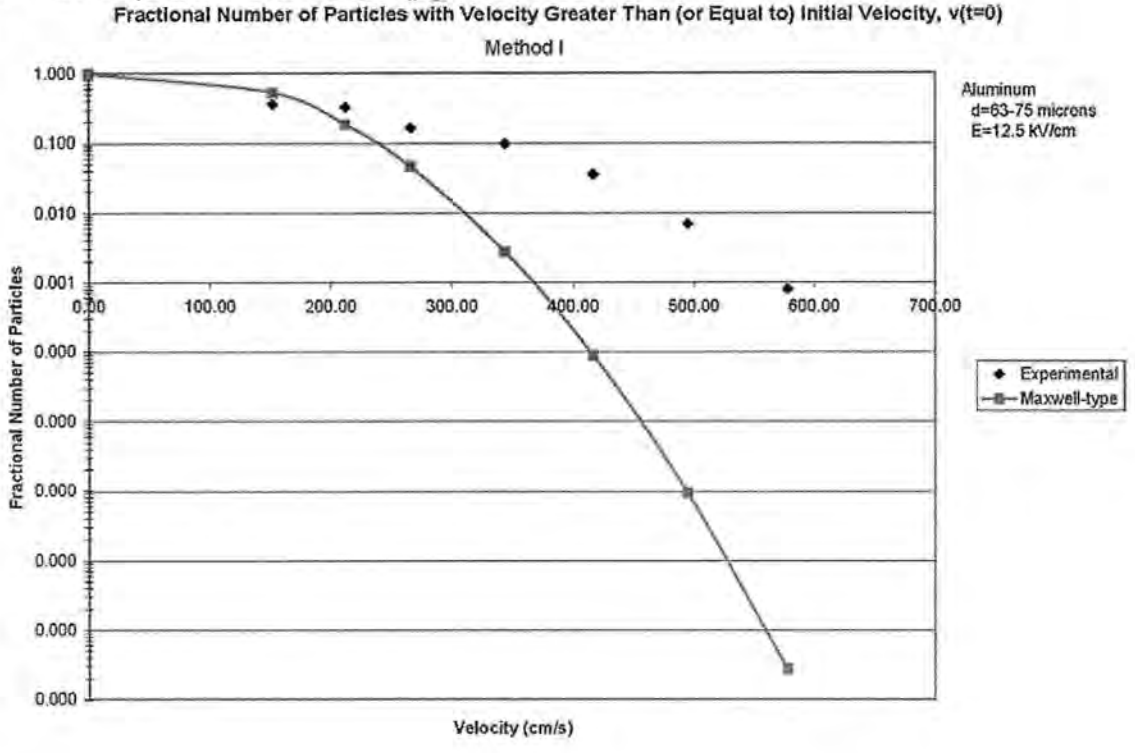

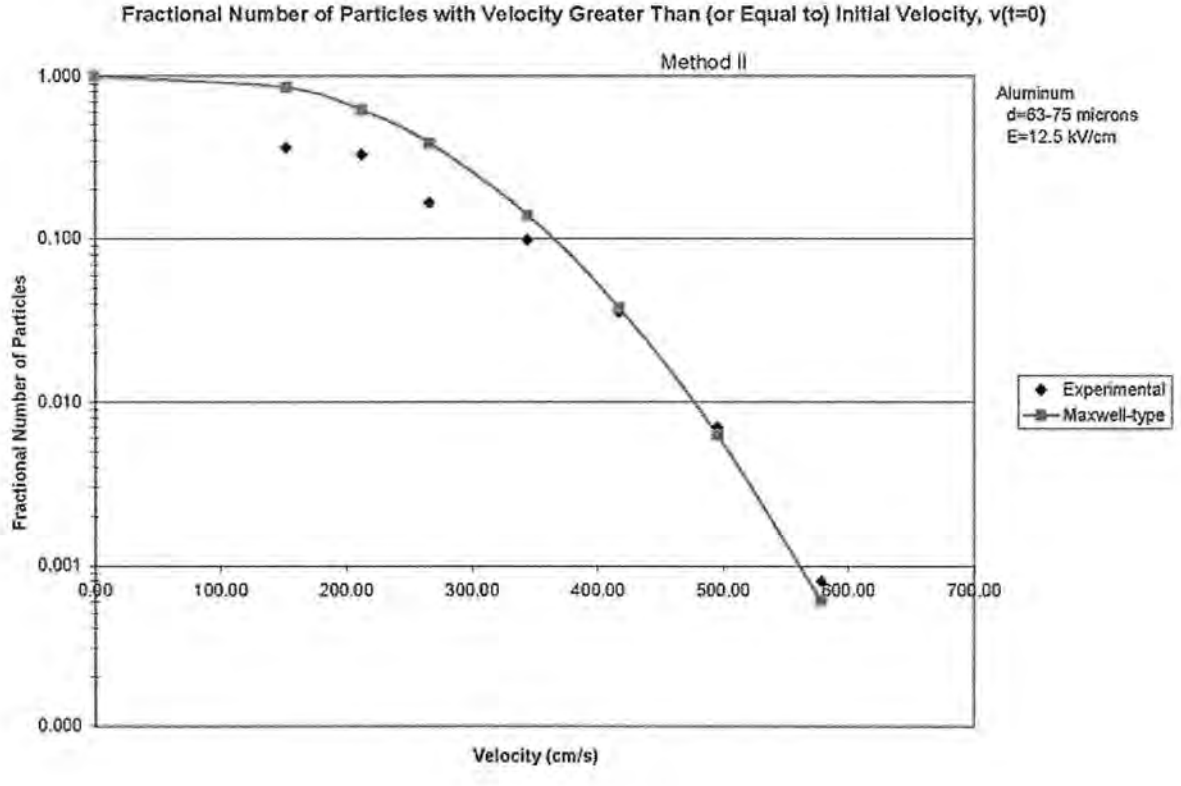

2. Comparison of Method I and Method II for aluminum particles.
   d = 125-149 μm, E = 7.45 kV/cm. L = 1.020 cm.

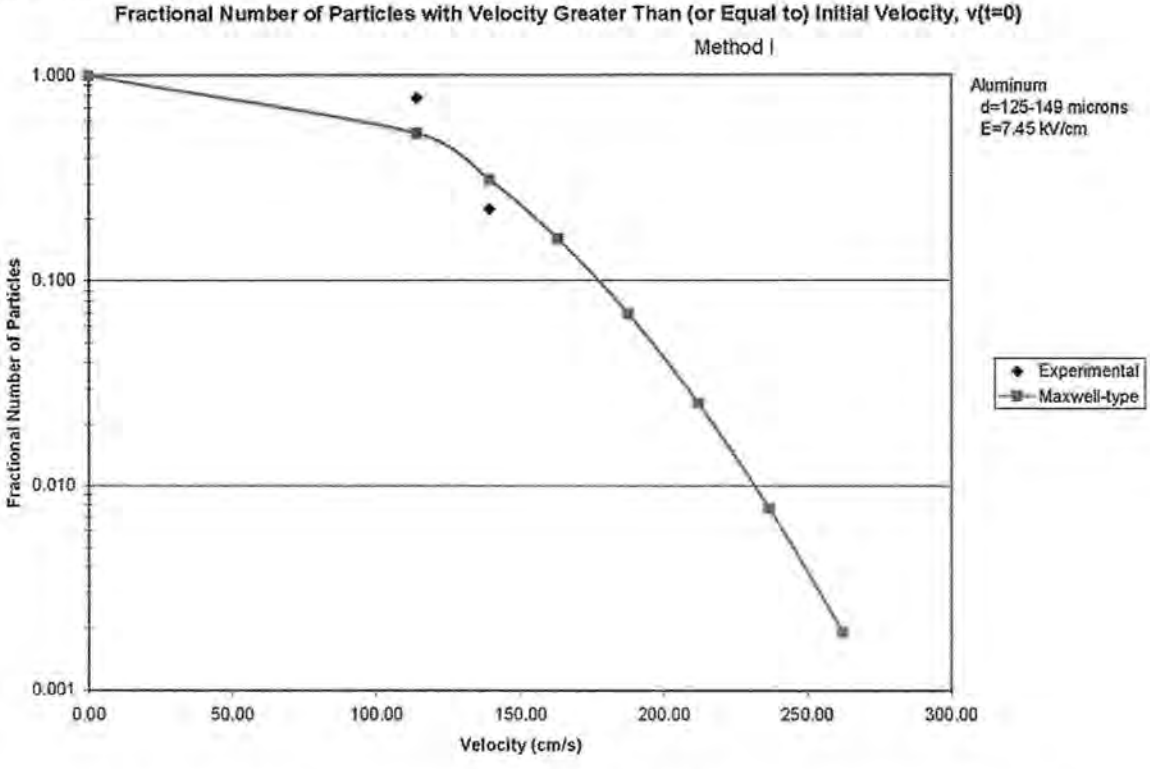

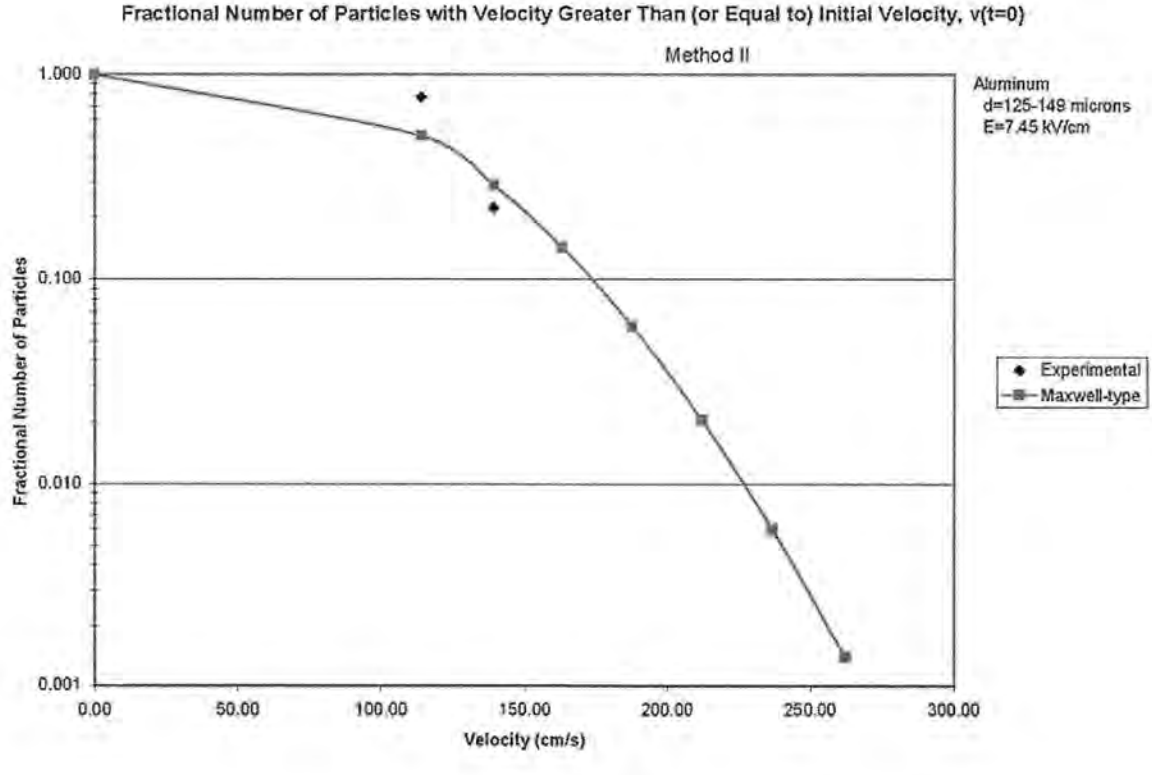

2. Comparison of Method I and Method II for aluminum particles.
   d = 125-149 μm, E = 13.5 kV/cm. L = 1.020 cm.

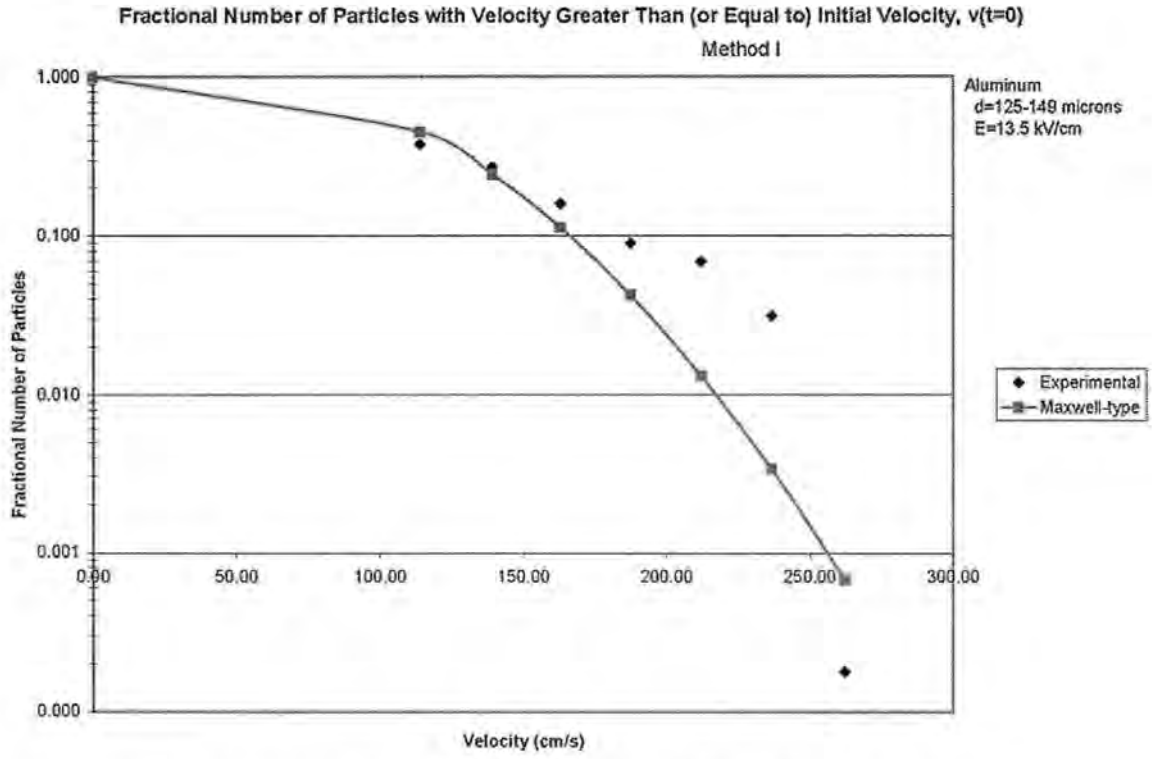

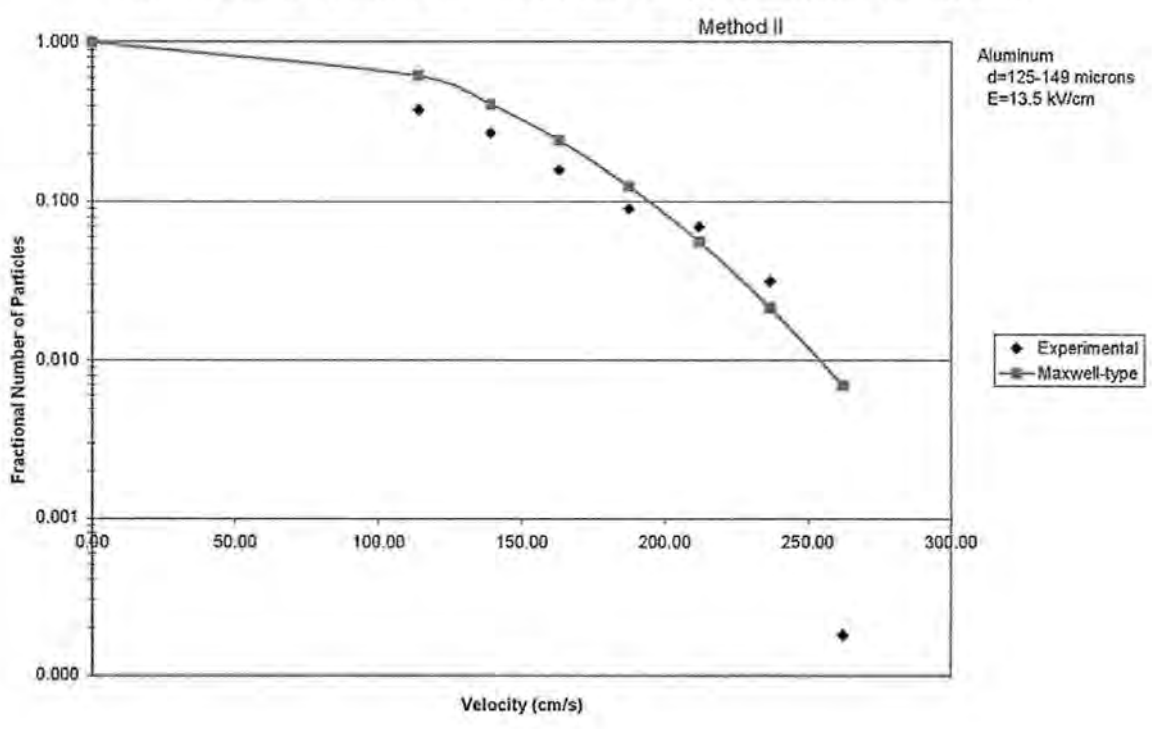

2. Comparison of Method I and Method II for copper particles.
   d = 63-74 μm, E = 6.82 kV/cm. L = 1.993 cm.

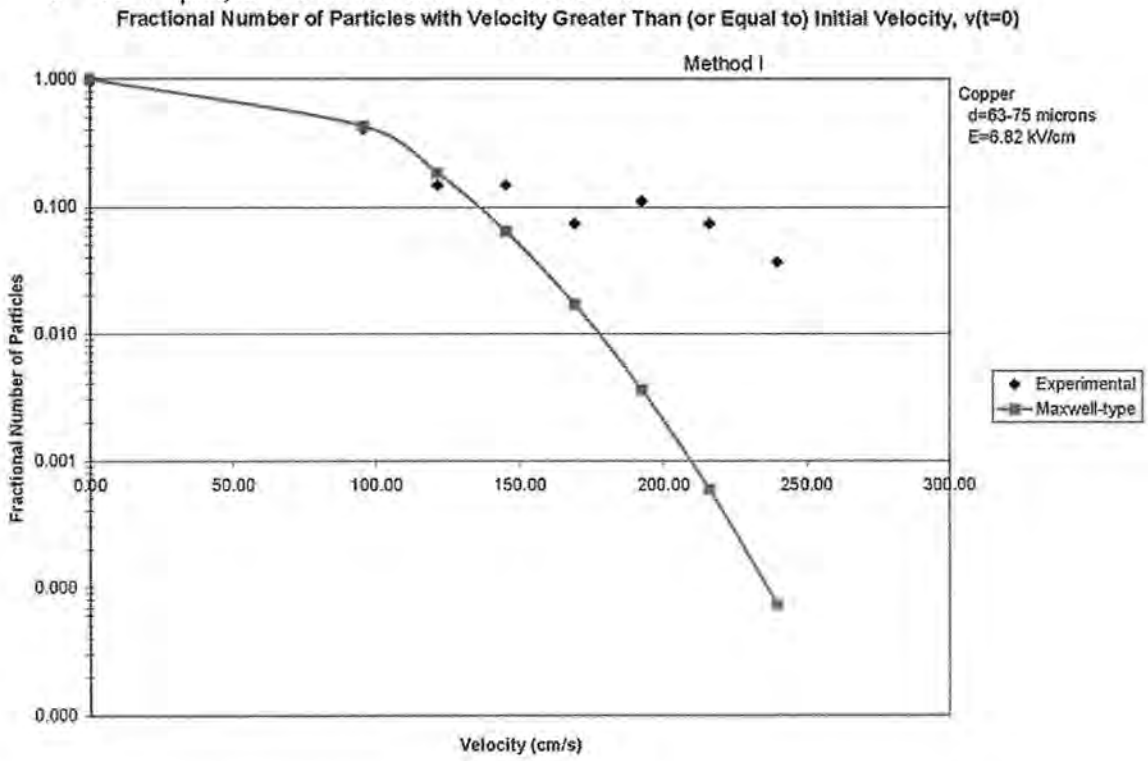

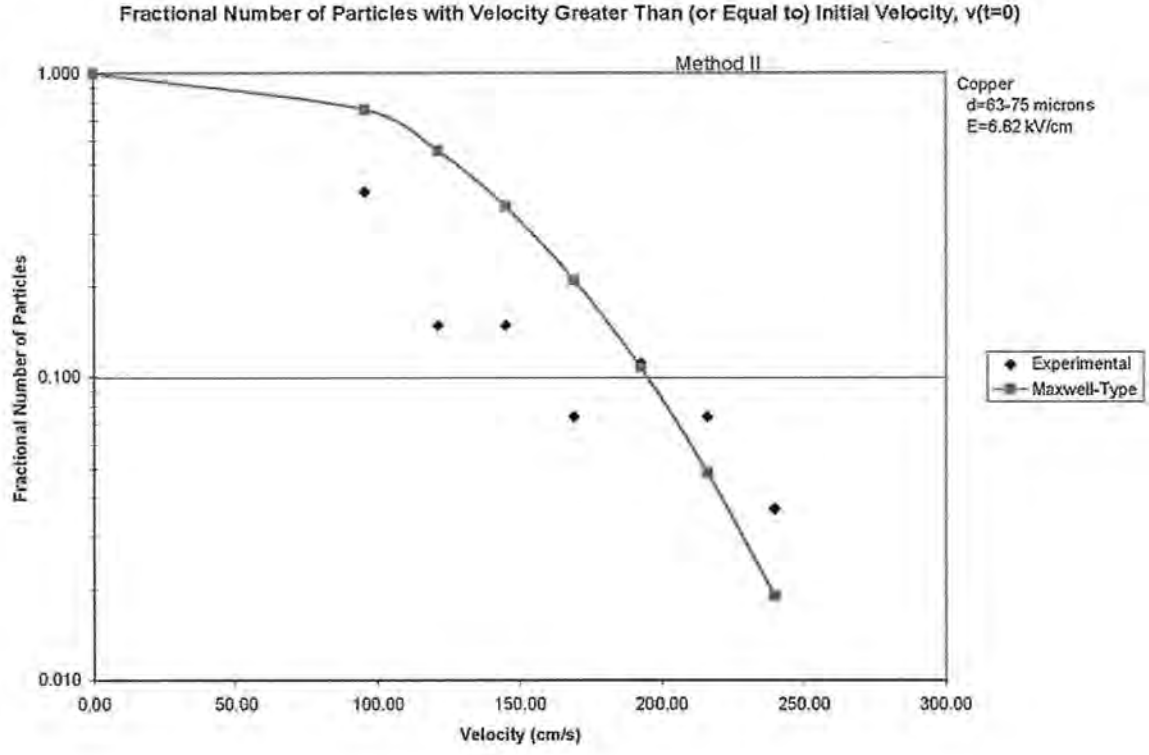

2. Comparison of Method I and Method II for copper particles.
   d = 63-74 μm, E = 9.43 kV/cm. L = 1.993 cm.

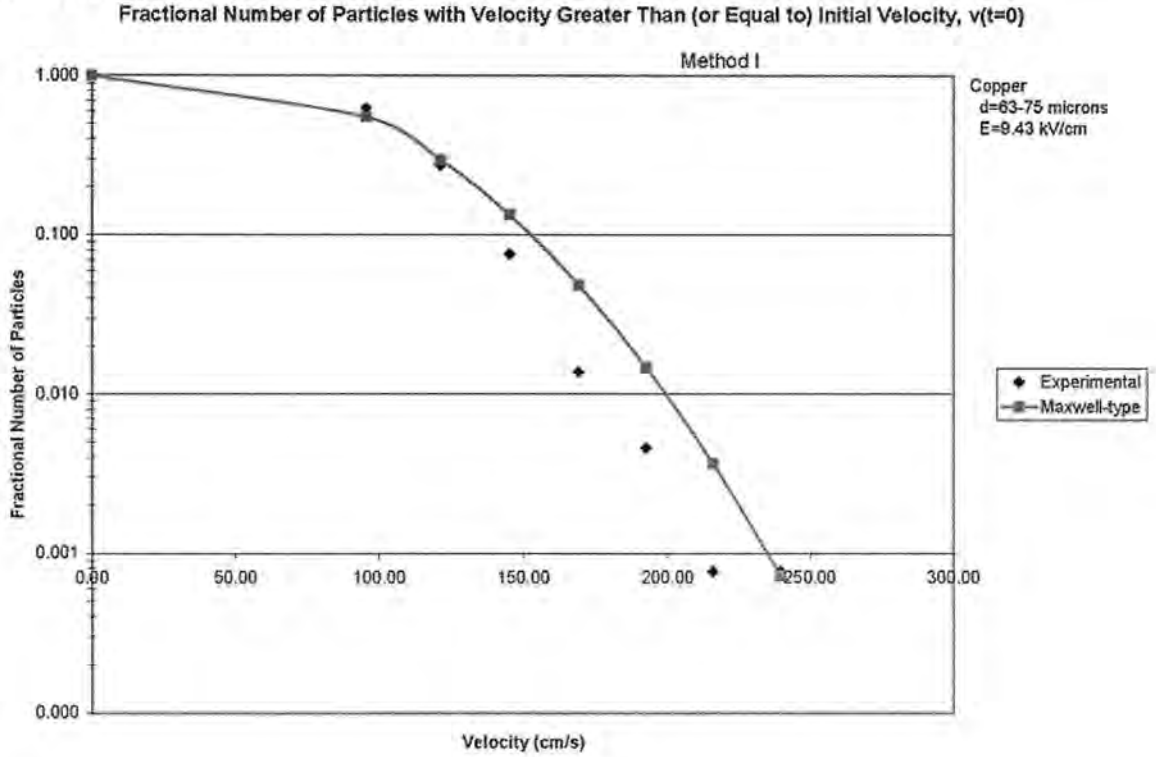

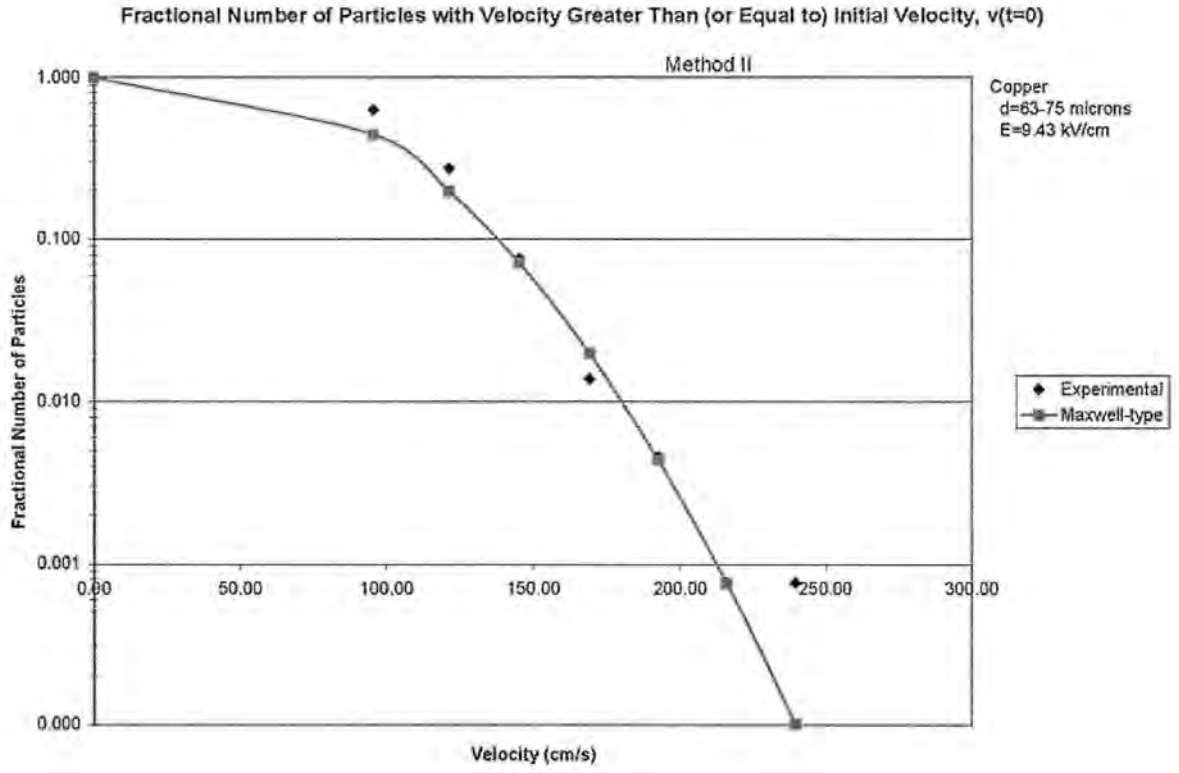

2. Comparison of Method I and Method II for copper particles.
   d = 63-74 μm, E = 13.0 kV/cm. L = 1.993 cm.

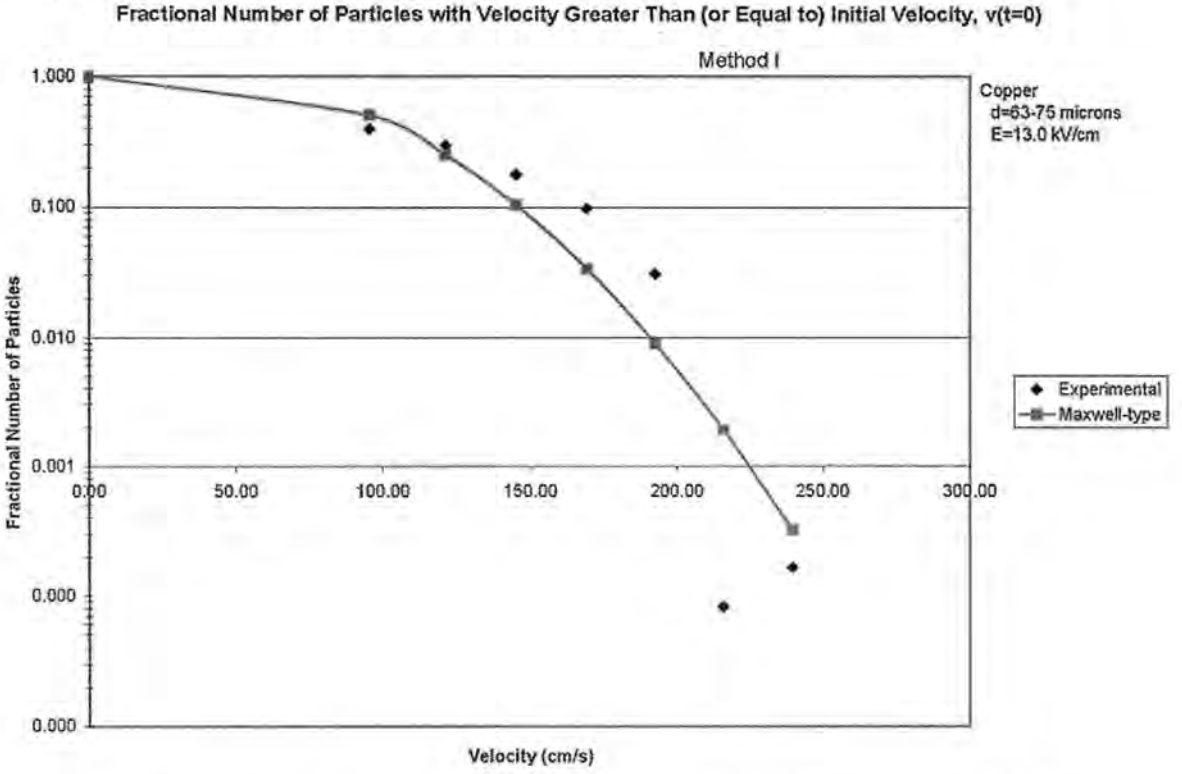

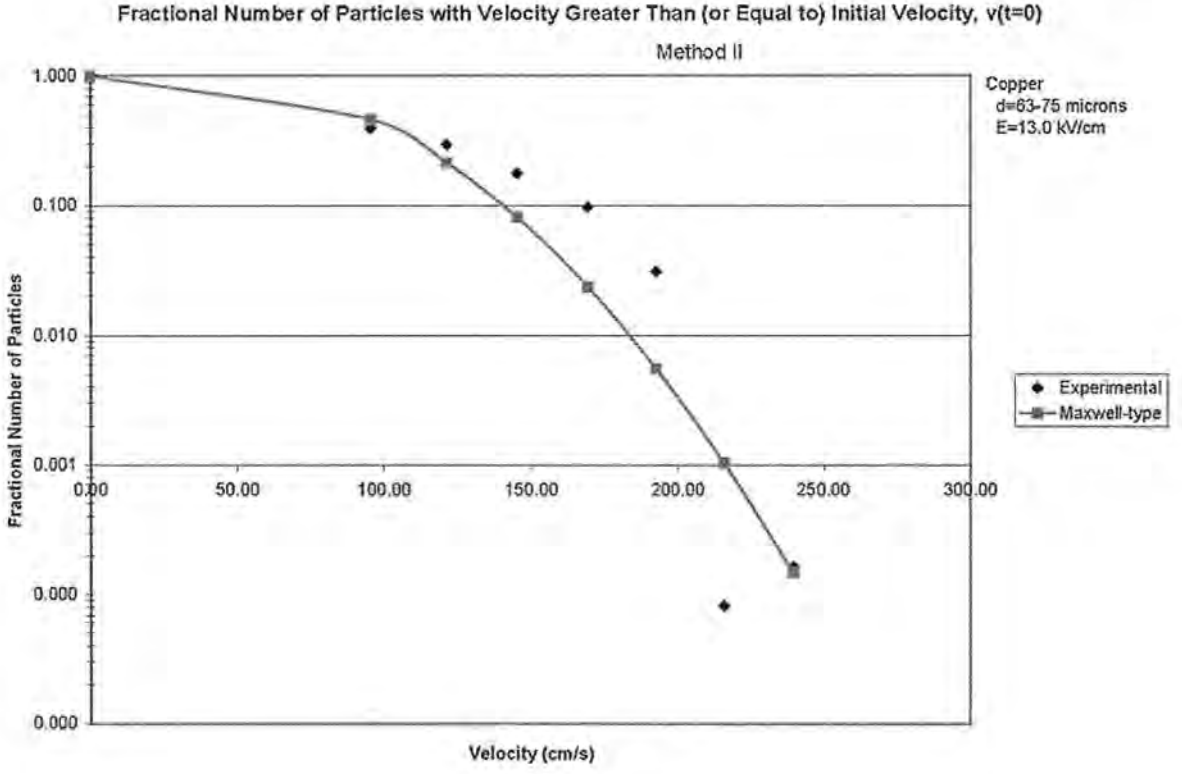

2. Comparison of Method I and Method II for copper particles.
   d = 125-149 μm, E = 7.58 kV/cm. L = 1.993 cm.

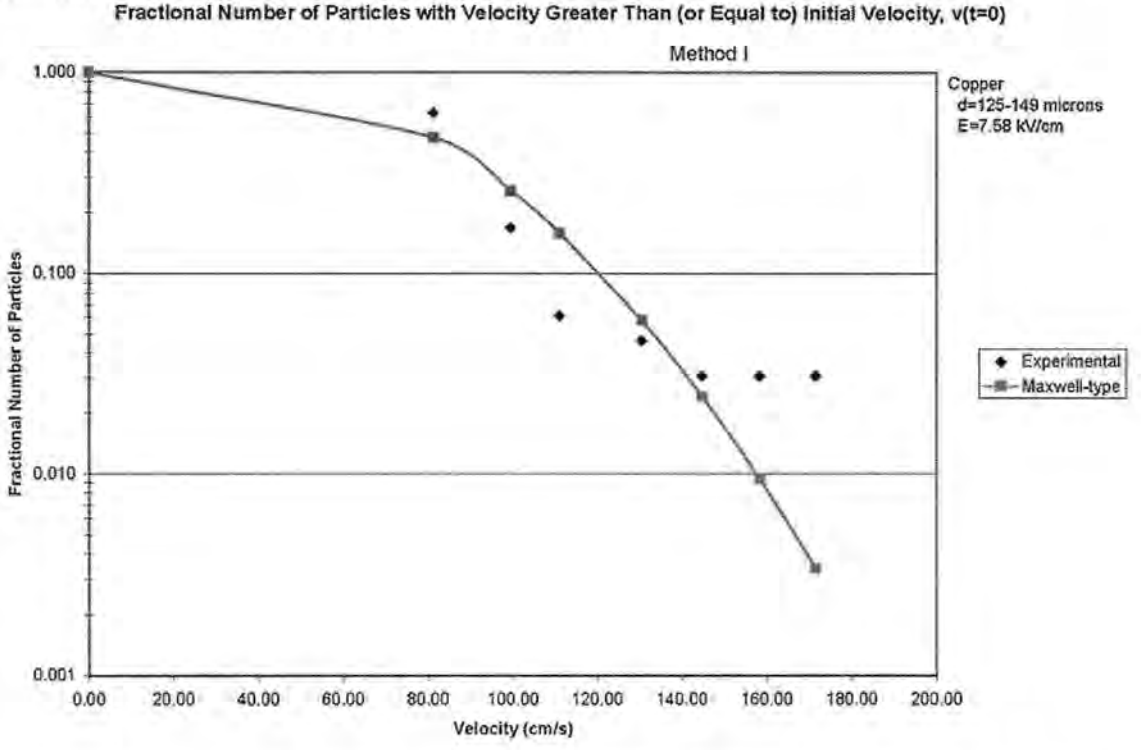

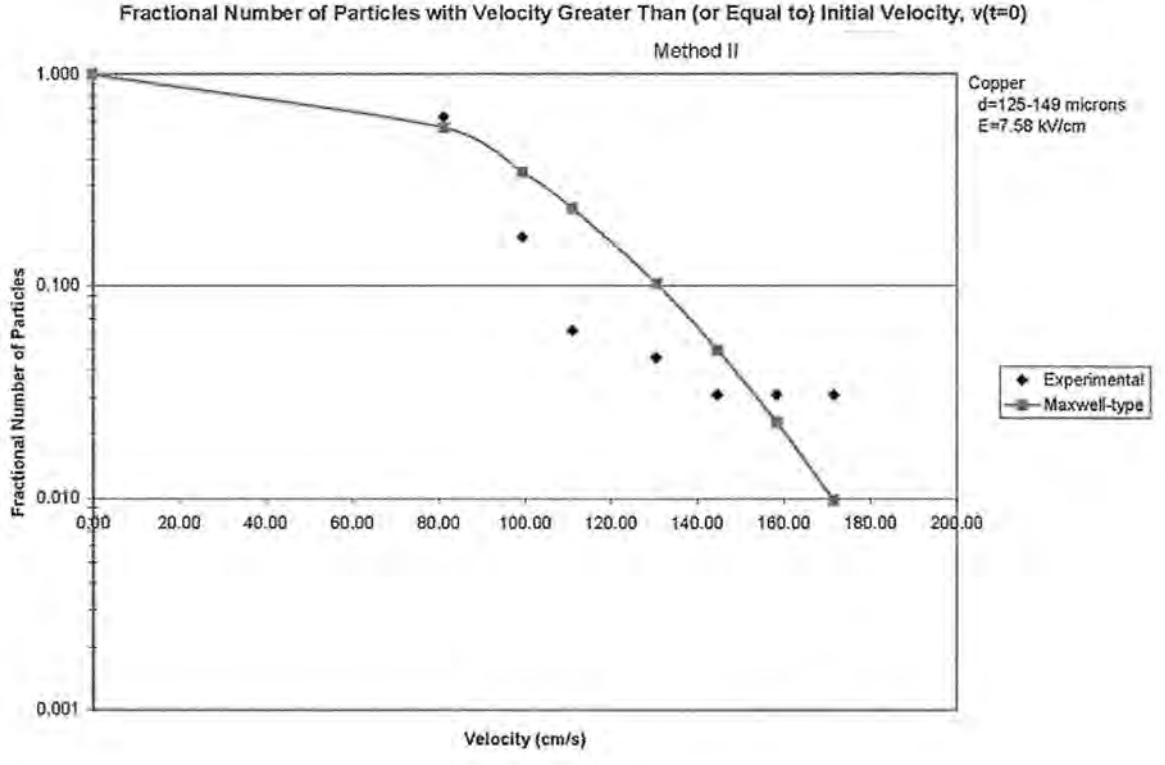

2. Comparison of Method I and Method II for copper particles.
   d = 125-149 μm, E = 9.43 kV/cm. L = 1.993 cm.

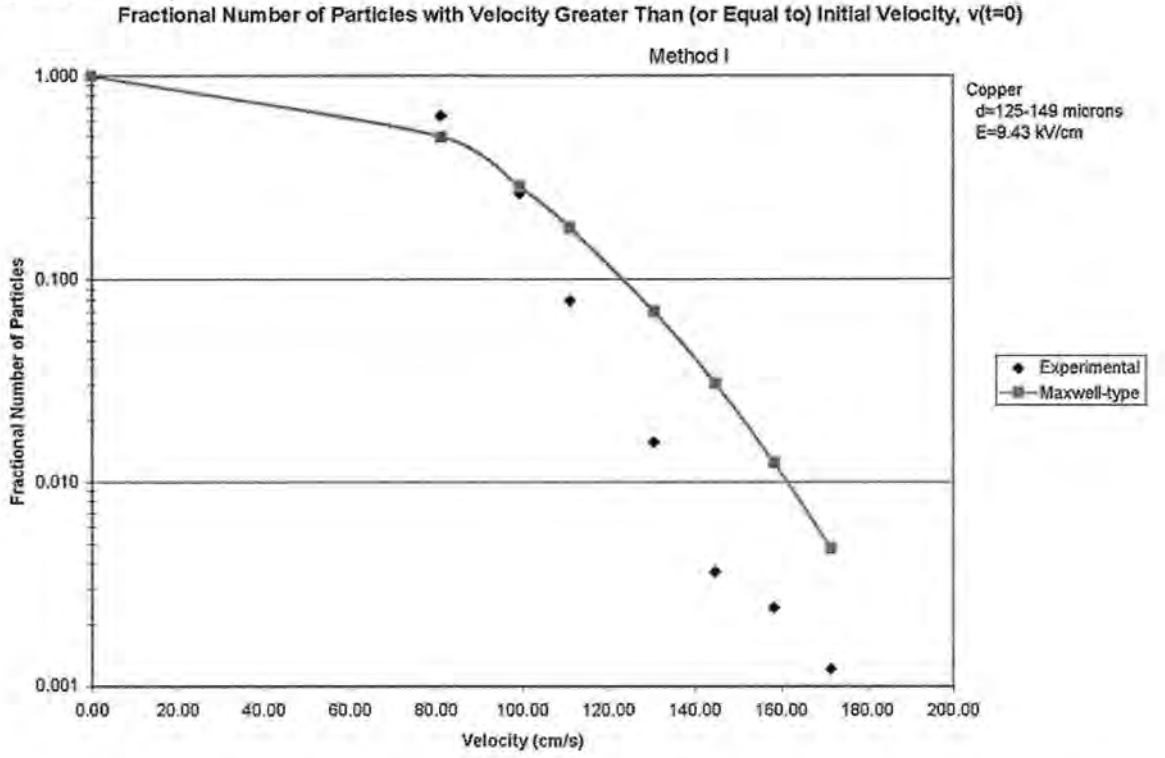

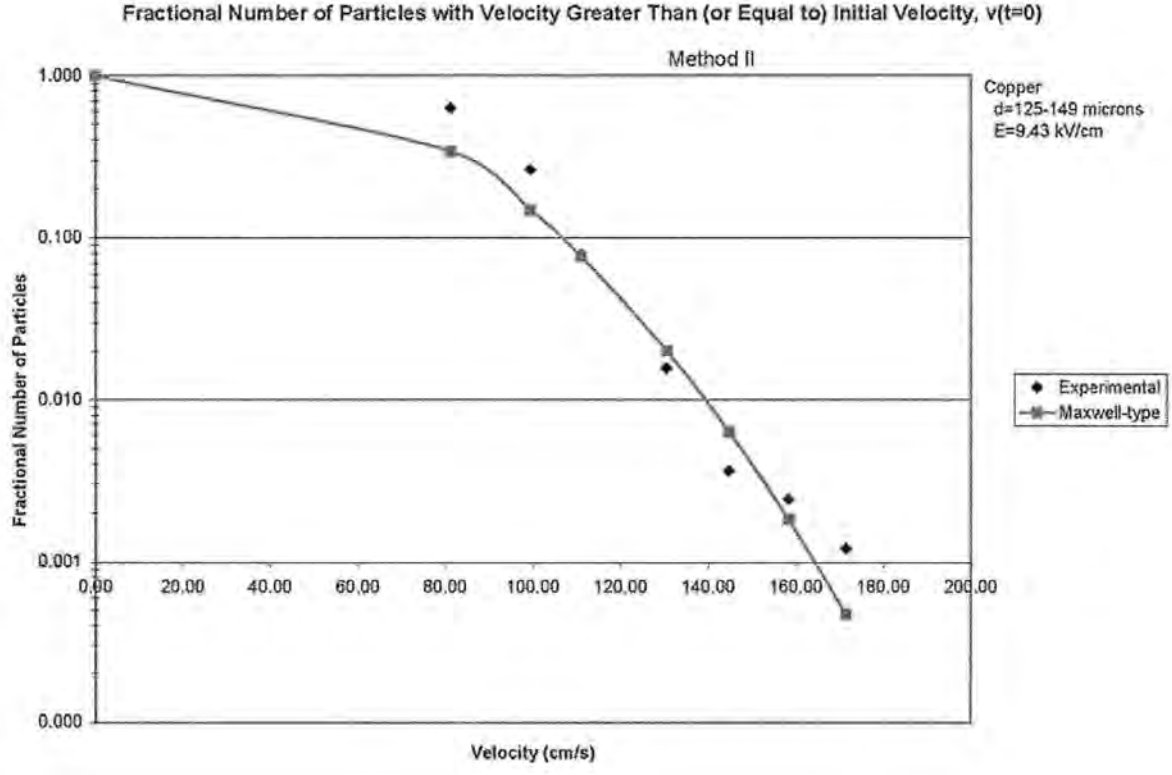

2. Comparison of Method I and Method II for copper particles.
   d = 125-149 μm, E = 13.3 kV/cm. L = 1.993 cm.